Development of Phage/Antibody Immobilized Magnetostrictive Biosensors

by

Liling Fu

A dissertation submitted to the Graduate Faculty of
Auburn University
in partial fulfillment of the
requirements for the Degree of
Doctor of Philosophy

Auburn, Alabama
May 14, 2010

Keywords: magnetostrictive milli/micro cantilever, resonance behavior, biosensors, bio-detection, phage/antibody immobilization, nonspecific adsorption

Approved by

Zhongyang Cheng, Chair, Associate Professor of Materials Engineering
Jeffrey W. Fergus, Professor of Materials Engineering
Barton C. Prorok, Associate Professor of Materials Engineering
Curtis G. Shannon, Professor of Chemistry and Biochemistry

Abstract

There is an urgent need for biosensors that are able to detect and quantify the presence of a small amount of pathogens in a real-time manner accurately and quickly to guide prevention efforts and assay food and water quality. Acoustic wave (AW) devices, whose performance is defined by mass sensitivity (S_m) and quality factor (Q value), have been extensively studied as high performance biosensor platforms. However, current AW devices still face some challenges such as the difficulty to be employed in liquid and low Q value in practical applications. The objective of this research is to develop magnetostrictive sensors which include milli/microcantilever type (MSMC) and particle type (MSP).

Compared to other AW devices, MSMC exhibits the following advantages: 1) wireless/remote driving and sensing; 2) easy to fabricate; 3) works well in liquid; 4) exhibits a high Q value (> 500 in air). The fundamental study of the damping effect on MSMCs from the surrounding media including air and liquids were conducted to improve the Q value of MSMCs. The experiment results show that the Q value is dependent on the properties of surrounding media (e.g. viscosity, density), the geometry of the MSMCs, and the harmonic mode on the resonance behavior of MSMCs, etc.

The phage-coated MSMC has high specificity and sensitivity even while used in water with a low concentration of targeted bacteria. Two currently developed phages, JRB7 and E2, respectively respond to *Bacillus anthracis* spores and *Salmonella*

typhimurium, were employed as bio-recognition elements in this research. The phage-immobilized MSMC biosensors exhibited high performance and detection of limit was 5 x 10^4 cfu/ml for the MSMC in size of 1.4 x 0.8 x 0.035 mm. The MSMC-based biosensors were indicated as a very potential method for *in-situ* monitoring of the biological quality in water.

The MSP combine antibody was used to detect *Staphylococcus aureus* in this experiment. The interface between MSPs and antibody was modified using Traut's Reagent by introducing the sulfhydryl group. To improve the mass sensitivity of magnetostrictive biosensors, several blocking agents were used to resist the nonspecific adsorption of *S. aureus* on the surface of the magnetostrictive biosensors and the blocking effects were studied by using ELISA and SEM. The results showed casein was one of the best blocking agents to resist the nonspecific binding in this experiment. Casein blocked antibody immobilized MSP biosensors exhibited high sensitivity and the limit of detection is 10^2 cfu/ml.

Acknowledgements

I would like to express my sincere gratitude to Dr. Z. -Y. Cheng for his expert guidance, support and persistent encouragement during my graduate studies at Auburn University. I would like to emphasize that his influence on me was not only in acquiring scientific knowledge but also as a person.

I would like to give my appreciation and sincere thanks to Dr. Barton C. Prorok, Dr. Curtis G. Shannon, Dr. Jeffrey W. Fergus for serving on my committee and for their generous guidance and kind support, to Dr. Byran A. Chin for providing the bio-safety laboratory, and to Dr. Tung-shi Huang for his helpful discussions and insightful suggestions. Thanks are also due to Ms. I-Hsuan Chen for her help in the biological sample preparations; Mr. L.C. Mathison and Mr. Roy Howard for the general technical support; and Ms. Alison Mitchell for the writing/formatting corrections of the papers and dissertation.

Thanks also go to my colleague and friends, Dr. Suiqiong Li, Dr. Xiaobing Shan, Levar Odum, Kewei Zhang, Peixuan Wu, Lin Zhang, Xu Lu, Dr. Anxue Zhang, Dr. Jing Hu, Yuhong Wang, Dr. Yuming Hzou, Shichu Huang, Shin Horikawa, Wen Shen, Michael L. Johnson, Dr. Liwei Wang, and Dr. Dongna Shen for all their help and suggestions.

The author would also like to thank her parents and her family for their love, constant emotional support and encouragement during her studies.

Table of Contents

List of Figures

List of Tables

CHAPTER 1

INTRODUCTION

1.1 Background

Bacteria are unicellular microorganisms and thousands of types of bacteria are naturally present in our environment. Some types of bacteria are used beneficially in making foods such as cheese and yogurt. Other bacteria, pathogens, cause disease in humans, animals, and plants. In food industry, when certain pathogens enter the food supply, they can cause food-borne illness. Only a few types (i.e. *Salmonella* and *Escherichia coli*) cause millions of cases of food-borne illness each year. Most of the bacteria cause the foodborne illness undetectably since they cause the flu-like symptoms and have no odor and do not change the color or texture of the food. Therefore, it would be fairly easy to result in an epidemic in a fairly large population by using a bacteria infection. It has been suggested that 1.5 billion people around the world are infected by bacteria each year, and that 70% of these infections are food-borne [1]. Furthermore, the number of illness caused by food-borne bacteria in the United States is 33 million annually, with the mortality rate being approximately 10, 000 people [1]. Illnesses caused by these organisms cost the U.S. economy $9.3-12.8 billion every year. Bacteria present in animals at slaughter can also lead to human illness.

In the U.S., it is estimated that 1% of the beef carcasses, 8.7% of the swine carcasses, and 20% of poultry carcasses are contaminated with *Salmonella* (U.S. Food and Drug Administration 2002).

Another type of bacteria, caused human diseases or death, is biological threat agent. There are a number of different types of biological agents that could be used in an attack. Some cause diseases that can be spread by infected people, such as smallpox, while others are only dangerous when a person comes into direct contact with the biological agent, such as anthrax. Since the biological terrorism attack on September 2001, the anthrax bacillus, *Bacillus anthracis* has come into insight and attracted the attention of biological researchers.

Prevention of microbial diseases depends on an effective and rapid detection of various pathogenic micro-organisms in food, clinic medicine and the environment. Therefore, analytical technologies for detecting and quantifying the presence of a small amount of biological threat agents in a real-time manner are urgently needed in food safety, medical diagnostics, environmental monitoring, and in public safety/security areas.

1.2 Bacteria

1.2.1 *Salmonella*

Salmonella species are a leading cause of foodborne bacterial illnesses in humans. *Salmonella* species are common, naturally occurring bacteria found in the intestinal tracts of many animals and birds. Human salmonellosis is generally increasing worldwide. Most people infected will develop diarrhea, fever and abdominal cramps within a few days of infection, and their illness can last up to a week. Poultry, beef and eggs are the predominant reservoirs of *Salmonella* species with other foods (fruits and vegetables) as potential vehicles for infection.

The recent S*almonella* outbreak in Sept. 2008 was caused at least 388 people infection and cover 42 states in United States [2]. Additionally, various strains of S*almonella* have been linked to previous outbreaks, caused by contaminated eggs, meat, poultry, vegetables, pet food and even peanut butter. For example, from August 2006 to May 2007, 628 cases of salmonellosis linked to peanut butter were occurred at the plant. Fall 2006, S*almonella* outbreak related to contaminated tomatoes cause at least 183 people's sickness (e.g. diarrhea, and fever) in 21 states of United States. In April 2005, USDA linked cases of *Salmonella* infections in people to stuffed frozen chicken products sold in Minnesota and Michigan. In 2004, several outbreaks of *Salmonella* were linked to consumption of uncooked Roma tomatoes. These outbreaks resulted in over 500 cases of illness. It is believed that the implicated tomatoes were contaminated in either the field or the packing house.

1.2.2 *Bacillus anthracis* spores

Biological warfare is the use of viruses, bacteria, other microorganisms, or toxins derived from living organism to cause death or disease in humans, animals or plants [3]. Biological warfare agents are more problematic to use as a weapon of mass destruction and could kill more people than a nuclear or chemical attack. It poses a serious global threat to military and civilian populations. Biological warfare aerosols are usually invisible, odor- and taste-free and are difficult to detect due to condensation of liquids droplets on the skin or uniform. Unlike a chemical agent attack, a biological attack does not cause an immediate reaction.

Research and development of technologies for detecting weapons of mass destruction have intensified since 1991 when chemical and biological weapons were discovered in Iraq's arsenal. Currently, 17 countries are suspected of having an offensive biological weapons program. In 1992, 20 people were administered

chemoprophylaxis after a Virginia man sprayed his roommates with a substance that he claimed was anthrax. In 1994, a Japanese sect of the Aum Shinrikyo cult attempted an aerosolized release of anthrax from the top of building in Tokyo [4]. In 1995, 2 members of a Minnesota militia group were convicted of possession of ricin, which they had produced themselves for use in retaliation against local government officials. In 1996, Ohio man was able to obtain bubonic plague cultures through the mail.

In 1997, the Defense Against Weapons of Mass Destruction Act directed the Department of National Head of the Home Security Office and Defense to establish a domestic preparedness program to improve the ability of local, state, and federal agencies to respond to biological incidents. During 1998 and 1999, multiple hoaxes occurred involving the threatened release of anthrax in the United States that resulted in decontamination and antibiotic prophylaxis for the intended victims. Nearly 6000 persons across the United States have been affected by these threats. According to a study by the Centers for Disease Control and Prevention (CDC), an intentional release of anthrax by a bioterrorist in a major US city would result in an economic impact of $ 477.8 million to $ 26.2 billion per 100, 000 persons exposed.

Concentrated anthrax spores, used for bioterrorism in the 2001 anthrax attacks in the United States, were delivered by mailing postal letters containing a few grams of spores. From then to November 2001, a total of 23 confirmed or suspected cases of bioterrorism-related anthrax (10 inhalation, 13 cutaneous) occurred in the United States [5]. Most cases involved postal workers in New Jersey and Washington DC, and the rest occurred at media companies in New York and Florida, where letters contaminated with anthrax were handled or opened. As a result of these cases, approximately 32,000 persons with potential exposures initiated antibiotic prophylaxis to prevent anthrax infections.

1.2.3 *Staphylococcus aureus*

Staphylococcus aureus is a common cause of foodborne illness which is excluded in some epidemiologic surveillance programs [6]. By producing the heat-stable staphylococcal toxins, some strains of *S. aureus* can result in staphylococcal food poisoning. The common symptoms include nausea, vomiting, abdominal cramps, prostration and diarrhea. This kind of symptoms can last 30 minutes to seven hours after consumption of foods contained staphylococcal toxins. *S. aureus* also would cause skin abscesses, pneumonia, bacteremia, endocarditis and toxic shock syndrome, which is not from the foodborne source. Thus, it requires the treatment with antibiotics and hospitalization.

The spread of *S. aureus* could be through human-human contact, domesticated animals (e.g. pets) [7]. Another important source of *S. aureus* is the nosocomial infection, especially nosocomial pheumonia, surgical wound infection, and bloodstream infection [8]. For example, Methicillin-resistant *S. aureus* (MRSA) was recognized in the United States in 60s' the last century [9-12].

1.3 Research objectives

The goal of this research is to develop a methodology to in-situ detect the target bacteria using phage/antibody immobilized magnetostrictive sensors. The objectives are:

1) The fundamental study of resonance behavior of magnetostrictive milli/micro cantilevers (MSMC) including the resonant frequency and Q value in various surrounding media such as air and liquids. Study the damping effect from surrounding media, and investigate size effect of MSMC device such as the scale and harmonic mode, on the Q value and resonance frequency of MSMC in surrounding media.

2) Establish bacteria binding test system in real-time manner.

3) Demonstration of the in-situ detection of several targeted bacteria including *B. anthracis* spores, and *S. typhimurium* via static system and dynamic system using phage-immobilized MSMC biosensors; study the size effect on the mass sensitivity and limit of detection.

4) Antibody modification by using Traut's reagent. Study the effect of the molar extra fold of Traut's reagent on the thiolation of antibody (e.g. sulfhydryls per antibody).

5) Characterization of blocking agent to resist the nonspecific adsorption of *S. aureus* on the magnetostrictive biosensors. Study the influence of blocking agents on the mass sensitivity of magnetostrictive biosensors.

1.4 Dissertation organization

The first chapter introduces the background and the research objective. The second chapter reviews the current microbial detection techniques including the conventional methods, molecular methods and biosensors. A new biosensor combined the magnetostrictive micro/milli cantilever (MSMC) with phage is introduced. The third chapter gives the operation principle of MSMC based biosensors and the determination of several important parameters. The fourth chapter discusses the damping effect from the surrounding media and size effect on the resonance behaviors of the MSMCs including the resonance frequency and the Q value. The fifth chapter demonstrates the performance of phage-coated MSMCs to in-situ detect the targeted bacteria including *B. anthracis* spores and *S. typhimurium* in water via static system and dynamic system. The sixth chapter studies the interface between antibody and gold coated magnetostrictive biosensors by using Traut's reagent. The resistance of the nonspecific adsorption of *S. aureus* on the sensor's surface by using various

blocking agents with different concentrations is studied in Chapter 7. Chapter 8 gives the prospect of MSMCs with smaller size by the microfabrication techniques and antibody immobilization by difference methods.

References

1. Envirotainer. 2001. Available from http://www.envirotainer.com
2. http://www.cnn.com/2009/HEALTH/01/08/salmonella.outbreak.cdc/index.html
3. North Atlantic Treaty Organization, NATO Handbook on the Medical Aspects of NBC Defensive Operations, Part II, Biological NATO Amed P-6(B), 1996.
4. G.W. Christopher, T.J. Cieslak, J.A. Pavlin, E.M. Eitzen, Jr., Biological warfare. A historical perspective, J. Am. Med. Assoc. 278 (1997) 412-417.
5. http://www.themoldsource.com/archives/bw.html
6. http://www.ecolab.com/PublicHealth/Saureus.asp
7. J.C. Seguin, R.D. Walker, J.P. Caron, W.E. Kloos, C.G. George, R.J. Hollis, R.N. Jones, M.A. Pfaller, Methicillin-resistant *Staphylococcus aureus* outbreak in a veterinary teaching hospital: potential human-to animal transmission, J. Clin. Microbio. 37 (5) (1999) 1459-1463.
8. D.S. Schaberg, D. Culver, R. Gaynes, Major trends in the microbial etiology of nosocomial infection, Am. J. Med. 91 (3B) (1991) 72s-75s.
9. F.E. Barrett, R.P. McGehee, M. Finland, Methicillin-resitant *Staphylococcus aureus* at Boston City Hospital, N. Engl. J. Med. 279 (1968) 441- 448.
10. R.W. Haley, A.W. Hightower, R.F. Khabbaz, The emergence of methicilin-resistant *Staphylococcus aureus* infections in United States hospitals: possible role of the house staff-patient transfer circuit, Ann. Intern. Med. 97 (1982) 297-308.

11. F.H. Kavser, T.M. Mak, Methicillin-resistant staphylococci, Am. J. Med. Sci. 264 (1972) 197-205.
12. 12. R.D. O'Toole, I. Drew, B.J. Dahlgren, H.N. Beatv, An outbreak of methicillin-resistant *Staphylococcus aureus* infection, JAMA 213 (1970) 257-263.

CHAPTER 2

LITERATURE REVIEW

In this chapter, the current microbial techniques for detecting the bio-threaten agents and food-borne pathogens were reviewed. The current microbial detection methods include conventional culture methods, molecular recognition techniques including nucleic acid-based and immunological based detection, and biosensors. The biosensors are divided into three types according to the detection transductions: electrochemical biosensors, optical biosensors, and acoustic wave devices. Several important acoustic wave sensors especially microcantilevers and their operating principle were described.

2.1 Conventional culture methods

The conventional culture method for bacterial detection is by putting bacteria sample onto agar culture plates and incubating these plates at optimal temperatures (e.g. 37^{o}C) for 1-2 days; then the bacteria are counted based on formation of colonies on the agar surface. Some bacteria require a variety of agar media to detect them. Culture methods are the most reliable tools for detection and identification of bacteria, viruses and the like, however, they are laborious and time-consuming, which is not suitable for the in-field test [1].

2.2 Molecular recognition methods

Molecular recognition systems that can be used for rapid identification can improve response time and thus avert or reduce the number of casualties associated with food contamination, a potential bioterrorism or biowarfare event [2].

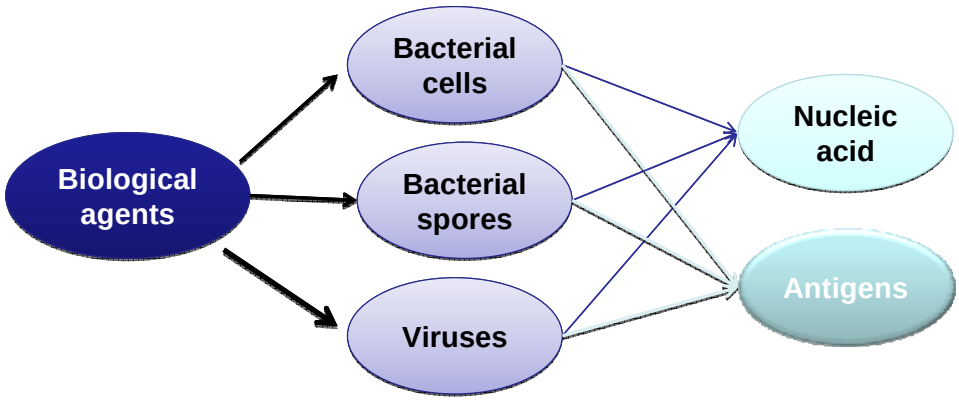

Figure 2-1. The schematic of biological agent detection: targeting at molecular level.

According to the molecular level of biological agents (see Figure 2-1), molecular recognition methods can be divided into two types: nucleic acid-based detection and immunological-based detection. Molecular recognition methods have been widely applied in food testing, clinical diagnostics and environmental monitoring by the identification of bacteria, viruses and their products (e.g. antigens and toxins). Generally, immunological detection is faster, more reliable and more robust than nucleic acid-based detection, but the latter is more specific and sensitive.

2.2.1 Nucleic acid-based detection (PCR)

By definition, virtually any self-replicating biological entity can be separated based on the nucleic acid sequences unique to the particular organism except prions because of the absence of nucleic acid in these protein particles. Nucleic acid-based detection can be broadly classified into two categories: direct target probing with signal

amplification and target amplification. Polymerase Chain Reaction (PCR) is a typical assay based on target amplification. Direct DNA hybridization is better than PCR to quantify target, however, the latter is more sensitive.

As a typical molecular based method, PCR is a technique widely used in molecular biology, microbiology, genetics, diagnostics, clinical laboratories, environmental science, and many other applications [3-5]. PCR so called comes from the DNA polymerase used to amplify a targeted DNA or DNA region by in vitro enzymatic replication. The "chain reaction" means the original DNA template such as a single piece of DNA, or a very small number of pieces of DNA exponentially amplified.

The PCR is one of the most sensitive existing rapid methods to detect microbial pathogens in clinical specimens, especially for those specific pathogens that are difficult to culture in vitro or require a long cultivation period. However, the application of PCR to clinical specimens still has many potential problems due to the susceptibility of PCR to inhibitors, contamination and experimental conditions. For example, the sensitivity and specificity of a PCR assay is dependent on target genes, primer sequences, PCR techniques, DNA extraction procedures, and PCR product detection methods. Even though the basic protocols of a PCR assay have been well-established, which include DNA extraction and preparation as well as the amplification and detection of amplicons, PCR detection of bacteria in clinical samples (e.g. cerebrospinal fluid) has not yet been reviewed.

2.2.2 Immunological-based detection (ELISA)

Immunological-based assay is a laboratory technique that makes use of the immunological binding between an antigen and its homologous antibody to identify and

quantify the specific antigen or antibody in a blood or body fluid sample. Antibody-based immunoassay is one of the most successful techniques which are employed to detect bacterial cells, spores and viruses. An antibody is a protein (immunoglobulin) which produced by B-lymphocytes in response to stimulation by an antigen. Quantitative detection of antibody/antigen can be obtained by a variety of methods. Labeling the antigen/antibody is one of the most common methods. The label may be an enzyme, radioisotope, magnetic label or fluorescence. Recently, immunological detection has been extensively developed for the bacterial detection. One is Enzyme-Linked ImmunoSorbent Assay (ELISA). ELISA is an excellent method which was used to detect bacteria in food successfully [6-7]. The ELISA test is based on the concept that a molecule (e.g. antibody or antigen) is immobilized to a plate. There are three frequently-used forms of ELISA test: sandwich assays, indirect assays, and competitive assays as shown in Figure 2-2. The form selected is case-dependent, which means the availability of reagents and the dynamic range required for a certain assay should be considered. Usually, sandwich assays are more sensitive and robust and therefore are used frequently. In sandwich assays, the primary antibody, which is highly specific to the antigen, is firstly immobilized onto a plate (shown in Figure 2-2(a)). Then, the antigen and the secondary antibody as the detection antibody are added consequently to form 'sandwich' structure between the two antibodies. Usually, an enzyme is attached to the detection antibody to generate a different epitope. Finally, the substrate is added to react under the enzyme and produce a colorimetric readout as the detection signal, which is proportional to the amount of target antigen.

The indirect assays involve the antigen attached to a plate firstly, as shown in

Figure 2-2(b). Then the primary antibody specific to the antigen is added into the plate. A species-specific antibody (secondary antibody) labeled with enzyme is added next. The same as the sandwich assay, the substrate is added to produce the signal. The signal is directly indicate the amount of an antibody to a specific antigen.

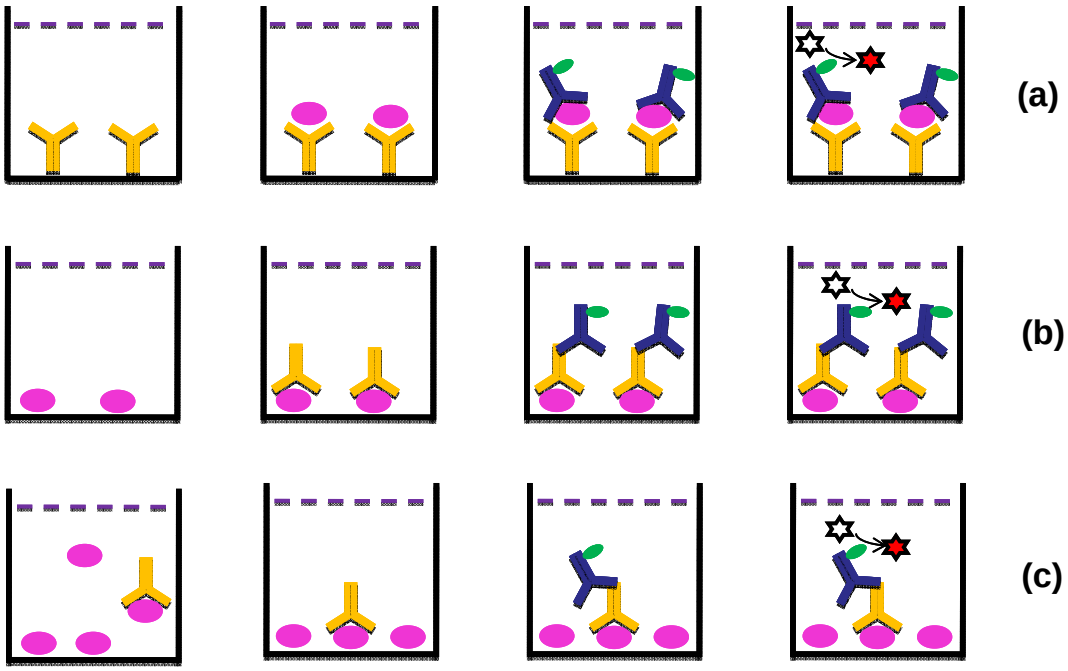

Figure 2-2. The schematics of three types of ELISA assays. (a) Sandwich assays; (b) Indirect assays; and (c) Competitive assays.

Competitive assays (Figure 2-2(c)) are based on the competition of labeled and unlabeled ligand for a limited number of antibody/antigen binding sites. This method usually is used to measure small analytes, or while the primary antibodies and secondary antibodies to the antigen do not exist. Only one antibody is used in this assay due to the steric hindrance from two antibodies binding to a very small analyte. The steps for competitive ELISA assay are somewhat different with the above two assays. To quantify the small analytes, a fixed amount of labeled antigen and variable amount of unlabeled

antigen are added into the antibody-coated plate. The more unlabeled antigen, the less labeled antigen bound to the antibody. Then the secondary antibody specific to labeled antigen is added to generate the signal. For competitive ELISA, the more the unlabeled antigen in the sample, the weaker the eventual signal.

However, most of these molecular methods are laborious and require the well-skilled personnel. It still needed to develop robust molecular based in-field test.

2.3 Biosensors

A biosensor is an analytical device incorporating a biological sensing element (probe/receptor) to a transducer (platform) system. The schematic of a typical biosensor is shown in Figure 2-3. The bio-recognition element, such as antibody, is highly specific to the target species [9-10]. The reaction between the target species and the bio-recognition unit would result in some changes in the physical/chemical properties of the recognition unit. These changes are measured by using a transducer. According to the transduction methods, the biosensors can be classified into three main types: electrochemical biosensors [11], optical biosensors [12], acoustic wave (AW) devices [13-15]. The first biosensor, the “enzyme-electrode” was demonstrated by Clark and Lyons in 1962 [8], which was used to measure glucose concentration in solution. The novel discoveries in optics (e.g. the evanescent wave phenomenon) and the use of piezoelectric-based acoustic wave devices were contributed to the development of biosensors. AW sensors attracted a great deal of attentions since it can offer many advantages such as real-time detection, simplicity of structure, ease to be miniaturize and cost effectiveness.

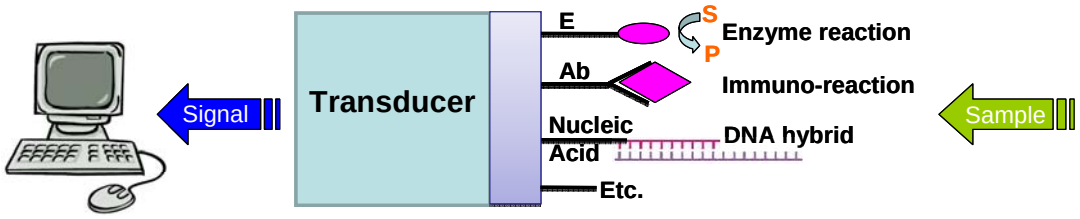

Figure 2-3. Schematic diagram of a typical biosensor. E and Ab represent enzyme and antibody respectively.

2.3.1 Electrochemical sensors

Electrochemical biosensors are the most common type of biosensors which coupled a biological recognition element to an electrode transducer. In this process, an electrochemical species (e.g. electrons) are consumed or generated to produce a useful electrochemical signal, which can be measured by an electrochemical detector. According to the electrochemical property measured by a detector, electrochemical biosensors may be classified into conductometric, potentiometric, and amperometric biosensors. Conductometric biosensors measure the changes in the conductance of the biological component arising between a pair of metal electrodes [16-18]. Potentiometric and amperometric biosensors are the most commonly used in conjunction with electrochemical biosensors. In potentiometric biosensors, the analytical signal is obtained by converting the biorecognition process into a potential signal and the potential difference between an indicator and a reference electrode was measured. They function under equilibrium conditions and monitor the accumulation of charge at zero current, created by selecting binding at the electrode surface [19-20]. Amperometric biosensors monitor the current resulted from the electrochemical oxidation/reduction of an electroactive species which involved in the recognition process at a constant applied potential. It usually performed by maintaining a constant-potential at a Pt, Au or C based

working electrode or an array of electrodes with respect to a reference electrode. Amperometric biosensors are more attractive because of its high sensitivity, rapid response, wide linear range and low cost [21]. The advantage of linear concentration dependence of amperometry makes it well suited for bacterial assay. Amperometric sensors aimed at microbial analysis have been reported [22-24].

It was reported that the detect limit is 10^4~10^5 cfu/ml of *Staphylococcus aureus* by using amperometric biosensors [22]. The limitation of this method was the variation in the signal produced by different strains of bacteria.

Despite of the large number of published reports on electrochemical biosensors capable of detecting microorganisms, it is still a challenge to create electrochemical biosensors with the necessary properties for reliable and effective determination of microorganism in real samples. A biosensor must be able to provide a lower detection limit with a rapid analysis time at a relatively low cost. Biosensor development facing some technical problems that include the interaction of matrix components, methods of sensor calibration, the requirements for reliable and low maintenance functioning over extended periods of time, sterilization, reproducible fabrication of numerous sensors, the ability to manufacture the biosensor at a competitive cost, disposable format, and a clearly identified market. The next generation of battlefield detection devices will most likely be stand-alone, multi-analyte, remote sensing, fully automated devices with integrated sample preparation and biosensing elements.

2.3.2 Optical sensors

Optical sensor is based on the measurement of photons, rather than the electrons in electrochemical sensors, especially measurement of absorbance, reflectance, or

fluorescence emissions occurred in the ultraviolet (UV), visible, or near-infrared (NIR). So far fluorescence is the detection method most often applied and comes into a variety of schemes. In fluorescence biosensing, the detection parameters include the intensity, decay time, anisotropy, quenching efficiency, luminescence energy transfer, and so on. According to the detection parameter, the fluorescence biosensing can be divided into three types: direct sensing, which the molecule being detected before and after a change/reaction; indirect biosensing, where a dye is added to optically transduce in the presence of an analyte [25]; and fluorescence energy transfer (FRET), which an energy transfer during the reaction. Optical layouts include plain sensor foils and also waveguide optical systems, capillary sensors, and arrays. The advantage of optical biosensors is that their results are either real time or close to real time. As the molecule being detected comes into contact with the biologic or biological sensing element an optical change occurs that the biorecognition element detects. The only limitation is the rate at which the instrument processes the data and therein displays the information to its operator.

Optical sensors based on the excitation of surface plasmons are called surface plasmon resonance (SPR). SPR biosensors were well developed by different companies in the last more than 15 years. The geometrical setup of SPR biosensors is mostly in the easy-to-build *Kretschmann* configuration as shown in Figure 2-4. In general, an SPR is comprised of an optical system, a medium and an electronic system. SPR detects a change in the propagation constant (e.g. coupling angle, coupling wavelength, intensity, and phase) of the surface plasmon caused by a change in the refractive index of the dielectric through coupling condition. Accordingly to the measured characteristics of the light wave modulated by a surface plasmon, SPR sensors can be classified as sensors

with angular, wavelength, intensity, or phase modulation [26]. In SPR sensors with angular modulation, a surface plasmon was excited by a monochromatic light wave. The strength of coupling between the incident wave and the surface plasmon is observed at multiple angles of incidence, typically by employing a convergent light beam. The excitation of surface plasmons is found as a dip in the angular spectrum of reflected light. The angle of incidence yielding the strongest coupling is detected and used a sensor output [27]. In SPR sensors with wavelength modulation, a collimated light wave containing multiple wavelengths was used to excite a surface plasmon, typically a beam of polychromatic light. The excitation of surface plasmons is observed as a dip in the wavelength spectrum of reflected light. The wavelength yielding the strongest coupling is acted as a sensor output [28]. Intensity modulation is based on the measurement of the strength of the coupling between the light wave and the surface plasmon at a single angle of incidence and wavelength, and the intensity of light wave used as a sensor output [29]. In SPR sensors with phase modulation the shift in phase of the light wave coupled to the surface plasmon is measured at a single angle of incidence and wavelength of the light wave and served as a sensor output [30].

In the last decades, various pathogens in food including *Escherichia coli* O157:H7, *Salmonella typhimurium*, and the like have been studied by SPR biosensors. By using SPR, *Escherichia coli* O157:H7 was first detected by Fratamico et al. in 1998 [31]. After that, numerous SPR biosensors for detecting of *Escherichia coli* O157:H7 have been reported. Choi's group combined Multiskop (Optrel GBR, Germany), a commercial SPR sensor, with monoclonal antibodies immobilized on a protein G-coated sensor surface. The sensor was capable to directly detect *Escherichia coli* O157:H7 and the limit of

detection (LOD) was at 10^4 cells/ml [32]. To improve the sensor performance, by conjunction with the immobilization of antibodies via a mixed SAM of alkanethiolates, they used the same SPR instrument which can detect *Escherichia coli* O157:H7 down to 10^2 cells/ml [33]. Additionally, Choi's group also demonstrated the detection of *Salmonella typhimurium* in buffer by using the same instrument and monoclonal antibodies immobilized via protein G attached to an alkanethiolate SAM on the sensor surface. The LOD was found at the concentration of 10^2 cells/ml [34]. It was reported that the LOD for *Salmonella typhimurium* in milk was at 10^5 cells/ml [35].

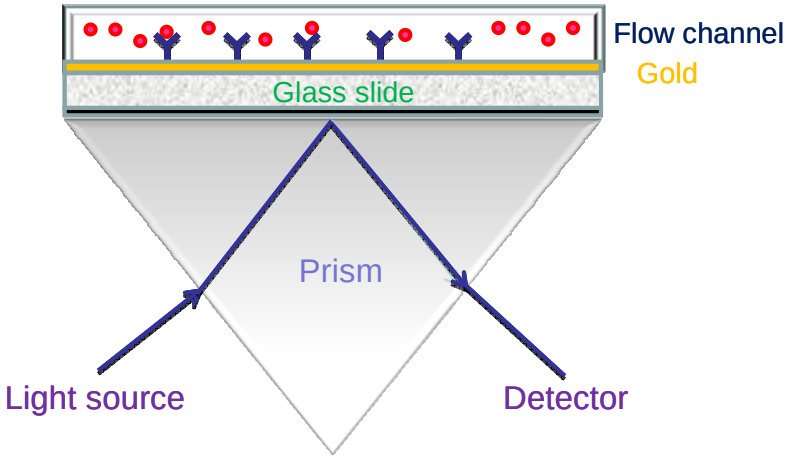

Figure 2-4. Schematic of SPR based biosensors.

In the past 5 years, the performance of SPR biosensors has been improved in terms of sensor hardware and biospecific coatings. However, SPR sensors still face some challenges regarding certain measurements: (1) refractive index is the only signal measured by SPR; (2) surface chemistry is limited by the obligatory noble surface (e.g. gold); (3) the SPR signal (e.g. the refractive index) is influenced by physical side effects, which means the instruments should be calibrated in different buffers. Thus, advanced SPR sensor platforms in combination with novel biospecific surface is still urgently

needed for rapid, sensitive and specific detection of bacteria in food and environment.

2.3.3 Acoustic wave devices

Acoustic wave (AW) devices are operated based on acoustics – the use of elastic/mechanical waves at frequencies well above the audible range propagating in specially designed solid sensing structures. AW devices have been commercially used for more than 60 years. For example, the surface acoustic wave devices acted as bandpass filters are successfully used in transceiver electronics. Additionally, AW devices are also used as torque and tire pressure sensors in automotive industry, chemical sensors in medical applications, and the sensors to measure vapor, humidity, temperature and mass in environment. AW devices are low cost, inherently rugged, very sensitive, and intrinsically reliable. Some are also capable of being passively and wirelessly interrogated (no sensor power source required).

2.3.3.1 Classification of AW devices

Usually AW devices use a piezoelectric material to generate the acoustic wave. When the acoustic wave propagates through or on the surface of the piezoelectric material, a change of the characteristics of the propagation path gets rise to a change of the velocity/amplitude of the wave, which can be monitored by measuring the frequency/phase characteristics of the device. A wave propagating through the substrate is called a bulk wave which including the Thickness-Shear Mode (TSM) resonator and Shear-Horizontal Acoustic-Plate-Mode (SH-APM). If the wave propagates on the surface of the substrate, it is called a surface wave. The most commonly used surface wave devices are Surface-Acoustic-Wave (SAW) sensor and Shear-Horizontal Surface Acoustic Wave (SH-SAW) sensor. One of the other AW devices is base on

Flexural-Plate-Wave (FPW). The schematics of these several main AW devices were shown in Figure 2-5 and their advantages and disadvantages were listed in Table 2-1.

TSM (Figure 2-5(b)) typically consists of a thin disk of AT-cut quartz with circular electrodes patterned on both sides. Usually TSM resonator uses a piezoelectric substrate material in which the electric field generated between electrodes couples to mechanical resonances. Therefore, in a practical sensor, changes in resonance frequency of the device are measured electrically (e.g. electrical admittance).

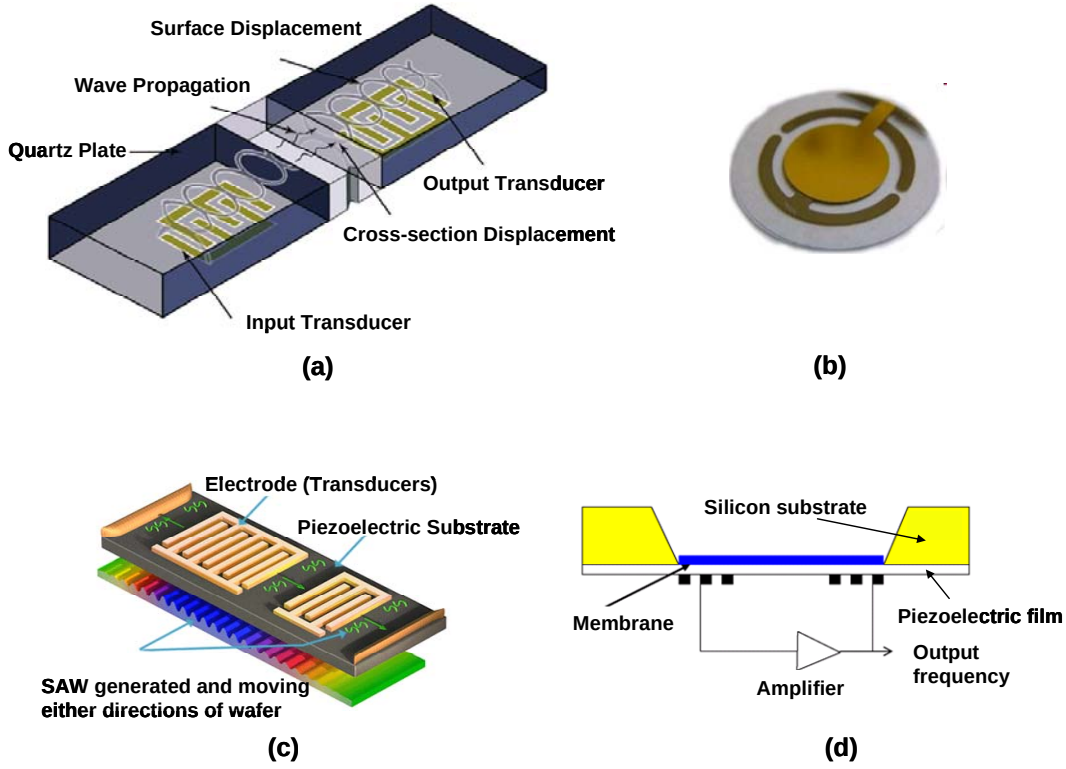

Figure 2-5. The schematics of several important AW devices: (a) SH-APW; (b) TSM; (c) SAW, and (d) FPW. [36-39]

SAW devices (Figure 2-5(c)) are based on stress-free boundary imposed by the surface of a crystal gives rises to a unique acoustic mode whose propagation is confined to the surface and therefore known as a surface acoustic wave. SAW is most conveniently

excited on a piezoelectric crystal using an interdigitated electrode pattern, or interdigital transducer (IDT). For an IDT, the transducer operates most efficiently when the SAW wavelength matches the transducer periodicity. This occurs when the transducer is excited at the synchronous frequency, defined by the product of the SAW propagation velocity over the transducer periodicity. When SAW devices are used for sensors or thin-film characterization, the interactions between surface waves and a perturbation give rise to wave velocity and attenuation response. This surface wave is very sensitive to the surface perturbation. Therefore, SAW sensors exhibit a much higher sensitivity than TSM. However, the presence of the surface-normal displacement component makes the SAW poorly suited for liquid sensing application.

SH-APW sensors use a thin piezoelectric substrate/plate which is functionalized as an acoustic waveguide confining the energy between the upper and lower surfaces of the plate (shown in Figure 2-5(a)). Therefore, both faces of the crystal undergo displacement, so that detection can occur on either surface of the device. SH mode has particle displacements predominantly parallel to the device surfaces and normal to the direction of propagation. The absence of a surface-normal component of displacement allows SH plate mode to propagate in contact with a liquid without coupling excessive amounts of acoustic energy into the liquid, which makes it suit for liquid sensing application. The sensitivity of the SH-APM depends on the thickness of the substrate.

SH-APM sensors are more sensitive than TSM resonator, but less sensitive than SAW sensors. There are two reasons: one is the sensitivity to mass loading and other perturbations is substrate thickness reversal dependent, which means sensitivity increasing as the device is thinned and the minimum thickness is constrained by

manufacturing processes. The other one is that in SH-APM sensor, the wave energy is not maximized at the surface, which reduces sensitivity since the sensitivity is proportional to the amount of energy in the propagation path.

Table 2-1. Review of AW devices.

Techniques	Advantages	Disadvantages
TSM resonator Thickness Shear Mode QCM (quartz crystal microbalance)[13-14]	High sensitivity; Easy to use; Cost effectiveness.	The sensitive material has to be brought onto one of these electrodes; Need an external voltage source to generate the signal.
SAW device [40] (Surface Acoustic wave)	more sensitive, low cost and better reliability than TSM	Restricted to crystal surface; Not work well in liquid since the acoustic wave got damped severely.
FPW device [14] (Flexural Plate Wave)	Higher sensitivity in low frequency range than SAW	Difficult to fabricate
MC [15, 41] (Microcantilever)	Compact size; Easy integration with analysis circuit; Higher sensitivity than other AW devices	The amplitude of the resonant peak and Q value reduce significantly in a viscous environment such as air or liquid
MSMC[42] Magnetostrictive microcantilever	Rapid response; Easy to operate; Wireless sensed Low-cost production	Q value and amplitude need to be increased when exposed to liquid system

In a FPW device (Figure 2-5(d)), an acoustic wave is excited in a thin plate, whose thickness is a fraction of the acoustic wavelength. FPW can be dimensioned so that its phase velocity is lower than that of most liquids, when the FPW device contacts or is immersed in such a liquid, a slow mode of propagation exists in which there is no radiation from the plate. FPW device works well in a liquid environment. FPW device has a very high sensitivity due to its very small thickness.

2.3.3.2 Operation principle

An AW device is an acoustic resonator and mostly works as a mass sensor. That is, the reaction between the bio-recognition component and the target species results in a change in the mass load of the transducer/resonator, which shifts the resonance frequency. Thus, by monitoring the resonance frequency of an AW device, the reaction between the bio-recognition unit and the target species, such as captured bacterium cells by antibody/phage, can be determined. An AW device as a transducer used in biosensors is characterized using two critical parameters: mass sensitivity ($S_m = -\frac{df}{dm}$) and quality merit factor (or Q value). The mass sensitivity is defined as the shift in resonance frequency due to the attachment of a unit mass, while the Q value reflects the mechanical loss of the devices and characterizes the sharpness of the resonance peak in the amplitude/phase versus frequency plot. A higher S_m means a more sensitive device, while a higher Q value represents a capability to determine a smaller change in resonance frequency (i.e. a higher resolution in determining resonance frequency). Therefore, it is highly desirable for an AW device to have a higher S_m and a larger Q value. Among all AW devices, micro/nano-cantilever exhibits extremely high sensitivity primarily due to its small mass [41, 43-44]. For example, the detection of a mass as small as 10^{-18} g using cantilever has been demonstrated. Therefore, a great deal of efforts has been spent on the development of micro/nano-cantilever based biosensors. However, the current cantilever used in liquid exhibits a small Q value, which makes the cantilevers work poorly in liquid. For example, the Q value of these cantilevers in liquid is barely more than 10 [15, 45]. This is really a challenge for cantilever-based biosensors since most of the samples to be tested are liquids.

2.3.3.3 A typical AW device - QCM

A quartz crystal microbalance (QCM), a type of TSM resonator, is a piezoelectric based mass sensor which can be used in different environments (e.g. vacuum and liquid). A QCM is a gold-coated quartz crystal as shown in Figure 2-6. As a sensitive surface mass sensor, QCM has been also extensively studied as transducer for biosensors due to its simplicity, convenience and real time response [48-49]. The schematic of QCM as biosensor is shown in Figure 2-6. The QCM sensors generally measure the immune reactions in liquid between immobilized and target molecules (e.g. antibody and antigen) [50-51]. It is also effective at determining the affinity of molecules (e.g. protein) to surfaces functionalized with recognition sites. The detection limit and response time for QCM reported by Hao et al., on 2009 is about 10^3 cfu/ml and less than 30 min respectively for detecting of *Bacillus anthracis* spores and vegetative cells [52].

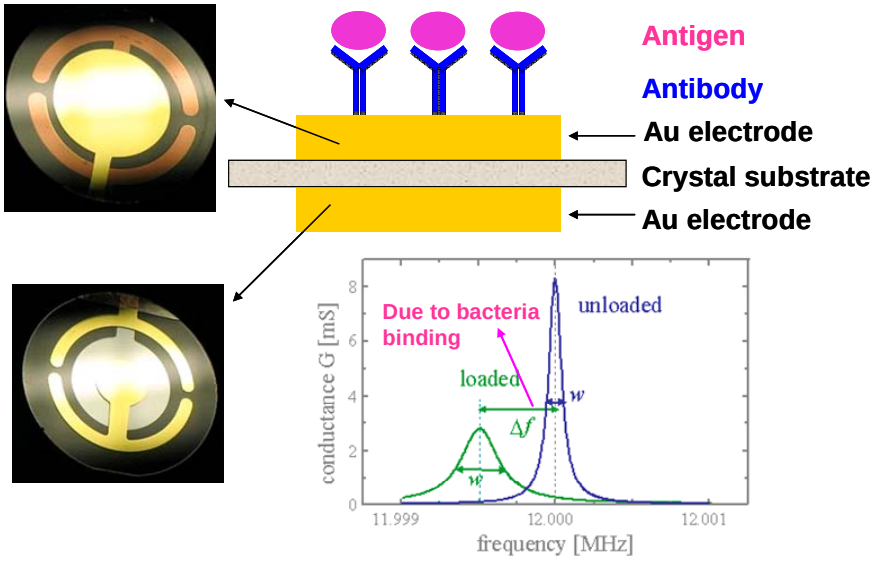

Figure 2-6. Construction of a QCM biosensor and its principle.

2.3.4 Microcantilever based biosensors

2.3.4.1 Operation mode

Recently, micro- and nanometer scale cantilevers have been studied as sensor platforms using physical principles that are similar to those found in atomic force microscopy. In terms of actuating and sensing technologies, Microcantilevers (MCs) can be operated based on three different principles: static, heat, and dynamic modes [53-55]. The static deflection mode [56-58] is based on that the binding on one side of a cantilever causes unbalanced surface stress resulting in a measurable deflection up or down (shown in Figure 2-7(a)). In this mode, the target molecules should be only bound on one side of the cantilever, otherwise the additional stress from the opposing surface would cancel and the cantilever will not bend. The deflections of about 10nm for the cantilever sensors were caused by surface stresses of several 10^{-3} N/m [59].

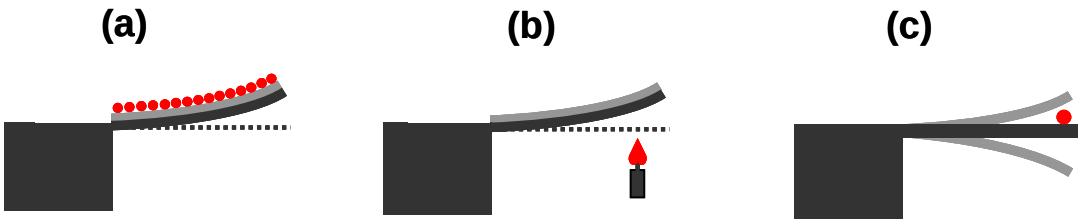

Figure 2-7. Cantilever sensor modes of operation: (a) static mode, where asymmetric molecular binding to the cantilever's top surface leads to an overall cantilever bending, (b) heat mode detecting temperature changes by a static bending due to different thermal expansion of the metal layer and silicon cantilever, and (c) dynamic mode detecting mass changes on the cantilever by changes in resonance frequency. [60]

In heat (bimetallic) mode [53, 55], the cantilevers are coated by a thin metal layer. Thus, heating up or cooling down metal-silicon cantilever structure will result in the

difference in the thermal expansions of these two materials and thus bending of the cantilever as shown in Figure 2-7(b). It can be measured the cantilever deflections of several nanometers while the temperature changes of 10^{-5}K.

In dynamic mode [61-62] the cantilever is an oscillator as shown in Figure 2-7(c); the binding on the cantilever increases mass and thus lowers the resonant frequency, much like quartz crystal microbalances. It can be detected that a change of 1 Hz in resonance frequency roughly corresponds to a mass change of 1 pg for the cantilever [62]. MCs based on the dynamic mode have many advantages over those based on the static mode, such that both surfaces of the device can be used for sensing and no preferable orientation of cantilever beam (in static mode, the cantilever beam has to be horizontal). Dynamic MCs investigated so far can be classified into two types [15, 45]: passive and active. The passive MCs, e.g. silicon-based MCs [46], require a mechanical system to actuate the device oscillation and an optical system to measure the vibration of the device. On the other side, the active MCs, e.g. piezoelectric MCs [63], can be actuated by simply applying an electric field, and the vibration of active MCs can be easily monitored (e.g. impedance for piezoelectric MCs).

2.3.4.2 Cantilever arrays

Disregarding of the operating mode of MCs, it is always of advantage to use several cantilevers in parallel, so called array, as indicated in Figure 2-8. It is evident that more information from a single experiment can be obtained by using sensor arrays. A lot of concerns in biological detection have risen since the biological systems are normally more complex and more unique than physical systems and their properties are actual environment dependent. We have already known that cantilevers are

temperature-sensitive sensors and might also respond to changes in buffer composition. In addition, not only the target molecules, also several other molecules in the sample might interact with the sensor. To eliminate the noise signal for measurement environment, the cantilever array, which was composed several physically identical cantilevers only covered with different surface coatings is as a substitute alternative of single cantilever. The physical identity should be checked before an experiment by either recording the thermal responses of the cantilevers by a well defined heat pulse or by measuring the resonance frequencies. Up to now, cantilever arrays of up to eight cantilevers in parallel were preformed in complex biological samples.

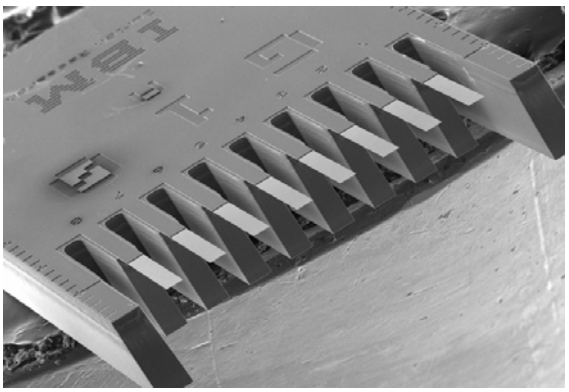

Figure 2-8. Scanning electron micrograph of a cantilever sensor array. [64]

2.3.4.3 Surface functionalization

In order to recognize and identify the complex biological systems, the surface of cantilevers should be changed to an intelligent sensor surface. Therefore, it is an important issue for sensor applications to coat or functionalize the sensor surface with the recognition layer which can define the application and performance of a sensor. One of the major challenges in sensor application is how to tailor biosensor coatings so that the biological recognition elements are tightly bound to the sensor surface but are still functional as in their natural environment [65].

Cantilever biosensors in the surface stress mode, only one side of a cantilever need coat biological receptors for the target molecules, whereas the other side should prevent any specific or non-specific adsorption of sample molecules. Surface coatings have to be reliable, and they should be robust against changes in buffer and temperature and ideally withstand repetitive detection and cleaning cycles. Cantilever sensors, interactions on top of the sensing layer should be fully transferred to the underlying substrate favoring a dense and covalent surface functionalization with receptor molecules close the surface.

Up to date, usually cantilevers show two distinct surfaces including silicon based and gold based surface. Therefore, silane and thiol chemistry can be used to respectively modify the silicon and gold surface with different receptor layer or inert coatings. Based on the high affinity between gold and sulfur groups, the gold surface can be modified by thio-labeled nucleic acids/proteins exposing cysteines at the surface [66]. Additionally, thiolated poly(ethylene glycol)s can act as inert layers which prevent molecular adsorption on the cantilever surface. For the silicon based surface, it can be modified by amino- or mercapto-silane monolayers since its end groups can be further cross-linked to receptor molecules [67]. On the other hand, the negatively charged silicon dioxide can electrostatically absorb the highly positively charged molecules. But there are different sophisticated methods for surface modification for different biosensing applications.

2.3.4.4 Biological applications

Cantilever-based devices as highly versatile sensors have already shown an impressive performance by using mechanical, optical, electrostatic, and electromagnetic methods to actuate/sense cantilever motion and a move to more advanced applications

(e.g. gases, chemicals, or biological organisms). Cantilever sensors can be operated in various environments including vacuum, air, or liquids. The major advantages are the wide field of applications, that they are small size and label-free, and provide fast response time, high sensitivity, can be microfabricated, and need only small sample volumes for their operation. The response of cantilever is, to date, comparable with other established label-free biosensing methods and a general setup can be easily modified to detect a variety of different parameters and substances such as temperature, mass, gases, biomolecules or cells.

2.4 MSMC-based biosensors

Silicon-based MCs have been much more widely investigated than active MCs because of the availability of microfabrication techniques for silicon-based materials and devices. Additionally, silicon-based MCs exhibit a larger Q value and a higher S_m than piezoelectric-based MCs [42]. However, it is still a big challenge for current MC-based biosensors operating in liquids. For example, the Q value of these cantilevers in liquid is barely more than 10 [15, 45].

Table 2-2. Comparison MSMC with Current MCs.

Characteristics	Silicon based MCs	Piezo based MCs	MSMCs
Transduction	Optical (separated bulk system)	Electrical (on broad circuit)	Magnetically (wireless, no connection)
Operate in air	Yes	Yes	Yes
Operate in liquid	Difficult	Very difficult	Works well
Q value	High (>100 in air)	Low (<100 in air)	Very high (>200 in air)
Structure	Simplest	Complicated	Simpler
Fabrication	Easy	Difficult	Easy
Overall sensitivity	High	Low	High

Magnetostrictive materials have been widely used in the development of actuators and sensors due to their low cost and robustness [68-74]. By using magnetostrictive materials, a new type of active cantilever, magnetostrictive cantilever, was introduced recently as a biosensor platform. Magnetostrictive milli/micro cantilevers (MSMCs) can be easily actuated and sensed. More importantly, they exhibit a high Q value, ~500 in air and ~30 in water, respectively [42]. The comparison of three cantilevers was reviewed in Table 2-2. Thus, MSMC exhibits the potential application as the sensor platform in the biological detection.

References

1. R. Kumar, P.K. Surendran, N. Thampuran, Evaluation of culture, ELISA and PCR assays for the detection of Salmonella in seafood, Letters in Applied Microbiology 46 (2008) 221-226.
2. S.S. Iqbal, M.W. Mayo, J.G. Bruno, B.V. Bronk, C.A. Batt, J.P. Chambers, A review of molecular recognition technologies for detection of biological threat agents, Biosensors and Bioelectronics 15 (2000) 549-578.
3. S.G. Pathmanathan, N. Cardona-Castro, M.M. Sanchez-Jimenez, M.M. Correa-Ochoa, S.D. Puthucheary, K.L. Thong, Simple and rapid detection of Salmonella strains by direct PCR amplification of the hilA gene, Journal of Medical Microbiology 52 (2003) 773-776.
4. L.T. Daum, W.J. Barnes, J.C. McAvin, M.S. Neidert, L.A. Cooper, W.B. Huff, L. Gaul, W.S. Riggins, S. Morris, A. Salmen, K.L. Lohman, Real-time PCR detection of Salmonella in suspect foods from a gastroenteritis outbreak in Kerr County, Texas, Journal of Clinical Microbiology 40(8) (2002) 3050-3052.

5. Y. Kim, T.R. Flynn, R.B. Donoff, D.W. Wong, R. Todd, The gene: The polymerase chain reaction and its clinical application Journal of Oral and Maxillofacial Surgery 60 (2002) 808-815.
6. S. Piletsky, E. Piletska, A. Bossi, K. Karim, P. Lowe, A. Turner, Substitution of antibodies and receptors with molecularly imprinted polymers in enzyme-linked and fluorescent assays, Biosensors and Bioelectronics 16 (2001) 701-707.
7. G.S. Nunes, I.A. Toscano, D. Barceló, Analysis of pesticides in food and environmental samples by enzyme-linked immunosorbent assays, Trends in Analytical Chemistry 17 (2) (1998) 79-87.
8. L.C. Clark, C. Lyons, Electrode systems for continuous monitoring in cardiovascular surgery, Ann. N. Y. Acad. Sci. 102 (1962) 29-45.
9. Kim, R. Rogers; Mulchandani, A. Affinity biosensors: techniques and protocols; Totowa, N. J.: Humana Press, 1998.
10. F. He, Q. Geng, W. Zhu, L. Nie, S. Yao, C. Meifeng, Rapid detection for E. coli using a separated electrode piezoelectric crystal sensor. Analytic Chimica Acta 289 (1994) 313-319.
11. L.D. Mello, L T. Kubota, Review of the use of biosensors as analytical tools in the food and drink industries, Food Chemistry 77 (2002) 237-256.
12. D. Ivnitski, I. Abdel-Hamid, P. Atanasov, E. Wilkins, Biosensors for detection of pathogenic bacteria, Biosensors & Bioelectronics 14 (1999) 599-624.
13. J.W. Grate, S.J. Martin, R.M. White, Acoustic-Wave Microsensors, Analytical Chemistry 65 (1993) A940-A948.
14. D.S. Ballantine, R.M. White, S.J. Martin, A.J. Ricco, G.C. Frye, E.T. Zellers, H.

Wohltjen, Acoustic wave sensors: theory, design and physico-chemical applications: Academic Press, 1997.

15. N.V. Lavrik, M.J. Sepaniak, P.G. Datskos, Cantilever transducers as a platform for chemical and biological sensors, Review of Scientific Instruments 75 (7) (2004) 2229-2253.
16. S. Sukeerthi, A. Q. Contractor, Applications of conducting polymers as sensors, Indian Journal of Chemistry 33A (1994) 565-571.
17. M. Gerard, A. Chaubey, B. D. Malhotra, Application of conducting polymers to biosensors, Biosensors and Bioelectronics 17 (5) (2002) 345-359.
18. D.C. Cullen, R.S. Sethi, C.R. Lowe, Multi-analyte miniature conductance biosensors, Analytica Chimica Acta 231 (1990) 33-40.
19. M. Mascini, Potentiometry: Enzyme electrodes, Encyclopedia of Analytical Science (1995) 4112-4118.
20. R. Koncki, A. Radomska, S. Glab, Potentiometric determination of dialysate urea nitrogen, Talanta 52 (1) (2000) 13-17.
21. A. L. Ghindilis, P. Atanasov, M. Wilkins, E. Wilkins, Immunosensors: electrochemical sensing and other engineering approaches, Biosensors and Bioelectronics 13 (1998) 113-131.
22. J. L. Brooks, B. Mirhabibollahi, R.G. Kroll, Sensitive enzyme-amplified electrical immunoassay for protein A-bearing *Staphylococcus aureus* in foods, Applied and Environmental Microbiology 56 (11) (1990) 3278-3284.
23. N. Nakamura, A. Shigematsu, T. Matsunaga, Electrochemical detection of viable bacteria in urine and antibiotic selection, Biosensors and Bioelectronics 6 (1991)

575-580.

24. J. L. Brook, B. Mirhabibollahi, R. G. Kroll, Experimental enzyme-linked amperometric immunosensors for the detection of Salmonellas in foods, Journal of Applied Bacteriology 73 (1992) 189-196.
25. P.N. Prasad, Introduction to biophotonics, John Wiley & Sons, Inc., 2003.
26. J. Homola, Surface plasmon resonance based sensors; Springer: Berlin, Germany, 2006.
27. K. Matsubara, S. Kawata, S. Minami, A compact surface plasmon resonance sensor for measurement of water in process, Applied Spectroscopy 42 (1988) 1375-1379.
28. L.M. Zhang, D. Uttamchandan, Optical chemical sensing employing surface plasmon resonance, Electronics Letters 24 (1988) 1469-1470.
29. C. Nylander, B. Liedberg, T. Lind, Gas detection by means of surface Plasmon resonance, Sensors and Actuators 3 (1982) 79-88.
30. J.M. Brockman, B.P. Nelson, R.M. Corn, Surface plasmon resonance imaging measurements of ultrathin organic films, Annual Review Physical Chemistry 51 (2000) 41-63.
31. P.M. Fratamico, T.P. Strobaugh, M.B. Medina, A.G. Gehring, Detection of *E. coli* O157:H7 using a surface-plasmon resonance biosensor, Biotechnology Techniques 12 (1998) 571-576.
32. B.K. Oh, Y.K. Kim, Y.M. Bae, W.H. Lee, J.W. Choi, Detection of *Escherichia coli* O157:H7 using immunosensor based on surface plasmon resonance, Journal of Microbiology and Biotechnology 12 (2002) 780-786.

33. B.K. Oh, W. Lee, W.H. Lee, J.W. Choi, Nano-scale probe fabrication using self-assembly technique and application to detection of *Escherichia coli* O157:H7 Biotechnology and Bioprocess Engineering 8 (2003) 227-232.
34. B.K. Oh, Y.K. Kim, K.W. Park, W.H. Lee, J.W. Choi, Surface plasmon resonance immunosensor for the detection of *Salmonella typhimurium*, Biosensors and Bioelectronics 19 (11) (2004) 1497-1504.
35. S.D. Mazumdar, M. Hartmann, P. Kämpfer, M. Keusgen, Rapid method for detection of *Salmonella* in milk by surface plasmon resonance (SPR), Biosensors and Bioelectronics 22 (9-10) (2007) 2040-2046.
36. http://www.techbriefs.com/images/stories/techbriefs/2006/10958-121-fig1.png
37. http://www.ifw-dresden.de/institutes/iff/research/surfdyn/SAW/blood-coagulation/TSM.JPG/image_mini
38. http://www.itf.co.kr/tech/image/sub3_2.GIF
39. http://spie.org/Images/Graphics/Newsroom/Imported/1468/1468_fig1.jpg
40. D.W. Galipeau, P. R. Story, K.A. Vetelino, R.D. Mileham, Surface acoustic wave microsensors and applications, Smart Materials & Structures 6 (1997) 658-667.
41. R. Raiteri, M. Grattarola, H.J. Butt, P. Skladal, Micromechanical cantilever-based biosensors. Sensors and Actuators, B: Chemical 79 (2-3) (2001) 115-126.
42. S. Li, L. Orona, Z. Li, Z.-Y. Cheng, Biosensor based on magnetostrictive microcantilever, Applied Physics Letters 88(7) (2006) 073507.
43. L.G. Carrascosa, M. Moreno, M. Alvarez, L.M. Lechaga, Nanomechanical biosensors: A new sensing tool, Trends in Analytical Chemistry 25 (3) (2006) 196-206.

44. T.P. Burg, M. Godin, S.M. Knudsen, W. Shen, G. Carlson, J.S. Foster, K. Babcock, S.R. Manalis, Weighing of biomolecules, single cells and single nanoparticles in fluid, Nature 446 (7139) (2007) 1066-1069.
45. C. Ziegler, Cantilever-based biosensors, Analytical and Bioanalytical Chemistry 379 (7-8) (2004) 946-959.
46. B. Ilic, H.G. Craighead, Attogram detection using nanoelectromechanical oscillators, Journal of Applied Physics 95(7) (2004) 3694-3703.
47. G.A. Campbell, M.B. Medina, R. Mutharasan, Detection of *Staphylococcus enterotoxin* B at pictogram levels using piezoelectric-excited millimeter-sized cantilever sensors, Sensors and Actuators B: Chemical 126 (2) (2007) 354-360.
48. Liu Y., Tang X., Liu F., Li K., Selection of ligands for affinity chromatography using quartz crystal biosensor. Analytical Chemistry 77 (13) (2005) 4248-4256.
49. Yang. D.H., Bae A.H., Koumoto K., Lee S.W., Sakurai K., Shinkai S., In situ monitoring of polysaccharide - polynucleotide interaction using a schizophyllan - immobilized QCM device, Sensors and Actuators B: Chemical 105 (2005) 490-494.
50. X. Su, Y. Li, A QCM immunosensor for *Salmonella* detection with simultaneous measurements of resonant frequency and motional resistance, Biosensors and Bioelectronics 21 (2005) 840-848.
51. S. Lee, D.D. Stubbs, J. Cairney, W.D. Hunt, Rapid detection of bacterial spores using a quartz crystal microbalance (QCM) immunoassay, IEEE Sensors Journal 5 (4) (2005) 1-7.
52. R. Hao, D. Wang, X. Zhang, G. Zuo, H. Wei, R. Yang, Z. Zhang, Z. Cheng, Y.

Guo, Z. Cui, Y. Zhou, Rapid detection of *Bacillus anthracis* using monoclonal antibody functionalized QCM sensor, Biosensors and Bioelectronics 24(5) (2009) 1330-1335.

53. R. Berger, Ch. Gerber, H.P. Lang, J.K. Gimzewski, Micromechanics: A toolbox for femtoscale science: "Towards a laboratory on a tip", Microelectronic Engineering 35 (1-4) (1997) 373-379.
54. H.P. Lang, M. Hegner, E. Meyer, Ch. Gerber, Nanomechanical from atomic resolution to molecular recognition based on atomic force microscopy technology, Nanotechnology 13(5) (2002) R29-R36.
55. R. Berger, H.P. Lang, Ch. Gerber, J.K. Gimzewski, J.H. Fabian, L. Scandella, E. Meyer, H.-J. Güntherodt, Micromechanical thermogravimetry, Chemical Physics Letters 294(4-5) (1998) 363-369.
56. R. Berger, E. Delamarche, H.P. Lang, C. Gerber, J.K. Gimzewski, E. Meyer, H.-J. Güntherodt, Surface stress in the self-assembly of alkanethiols on gold, Science 276 (5321) (1997) 2021-2024.
57. J. Fritz, M.K. Baller, H.P. Lang, H. Rothuizen, P. Vettiger, E. Meyer, H.-J. Güntherodt, Ch. Gerber, J.K. Gimzeski, Translating biomolecular recognition into nanomechanics, Science 288 (5464) (2000) 316-318.
58. J. Fritz, M.K. Baller, H.P. Lang, T. Strunz, E. Meyer, H.-J. Güntherodt, E. Delamarche, Ch. Gerber, J.K. Gimzewski, Stress at the solid-liquid interface of self-assembled monolayers on gold investigated with a nanomechanical sensor, Langmuir 16(25) (2000) 9694-9696.
59. R. McKendry, J. Zhang, Y. Arntz, T. Strunz, M. Hegner, H.P. Lang, M.K. Baller,

U. Certa, E. Meyer, H.-J. Güntherodt, C. Gerber, Multiple label-free biodetection and quantitative DNA-binding assays on a nanomechanical cantilever array, Proceeding of the National Academy Sciences of the United States of America 99(15) (2002) 9783-9788.

60. J. Fritz, Cantilever biosensors, The Analyst 133 (2008) 855-863.
61. T. Thundat, R.J. Warmack, G.Y. Chen, D.P. Allison, Thermal and ambient-induced deflections of scanning force microscope cantilevers, Applied Physics Letters 64 (21) (1994) 2894-2896.
62. F.M. Battiston, J.P. Ramseyer, H.P. Lang, M.K. Baller, Ch. Gerber, J.K. Gimzewski, E. Meyer, H.J. Güntherodt, A chemical sensor based on a microfabricated cantilever array with simultaneous resonance-frequency and bending readout, Sensors and Actuators B: Chemical 77(1-2) (2001) 122-131.
63. J.W. Yi, W.Y. Shih, W.H. Shih, Effect of length, width, and mode on the mass detection sensitivity of piezoelectric unimorph cantilevers, Journal of applied physics 91(2002) 1680-1686.
64. http://www.nccr-nano.org/nccr/media/nanonews/nanonews_05/highlights/highlight_03/highlight-3-3.jpg
65. B. Kasemo, Biological surface science, Surface Science 500 (1-3) (2002) 656-677.
66. J.C. Love, L.A. Estroff, J.K. Kriebel, R.G. Nuzzo, G.M. Whitesides, Self-assembled monolayers of thiolates on metals as a form of nanotechnology, Chemical Review 105(4) (2005) 1103-1169.
67. S.J. Oh, S.J. Cho, C.O. Kim, J.W. Park, Characteristics of DNA microarrays

fabricated on various aminosilane layers, Langmuir 18(5) (2002) 1764-1769.

68. C.A. Grimes, D. Kouzoudis, K.G. Ong, R. Crump, Thin-film magnetoelastic microsensors for remote query biomedical monitoring, Biomedical Microdevices 2(1) (1999) 51-60.
69. Q. Cai, C.A. Grimes, A remote query magnetoelastic pH sensor, Sensors and Actuators B 71 (1) (2000) 112-117.
70. L. Puckett, G. Barrett, D. Kouzoudis, C. Grimes, L. Bachas, Monitoring blood coagulation with magnetoelastic sensors, Biosensors and Bioelectronics 18 (5-6) (2003) 675-681.
71. C. Ruan, K. Zeng, O.K. Varghese, C.A. Grimes, Magnetoelastic immunosensors: amplified mass immunosorbent assay for detection of *Escherichia coli* O157:H7, Analytical Chemistry 75 (23) (2003) 6494-6498.
72. K. Zeng, C.A. Grimes, Wireless magnetoelastic physical, chemical, and biological sensors, IEEE Transactions on Magnetics 43 (6) (2007) 2358-2363.
73. M.L. Johnson, J. Wan, S. Huang, Z.-Y. Cheng, V.A. Petrenko, D.-J. Kim, I.-H. Chen, J.M. Barbaree, J.W. Hong, B.A. Chin, A wireless biosensor using microfabricated phage-interfaced magnetoelastic particles, Sensors & Actuators A: Physical 144(1) (2008) 38-47.
74. R. Guntupalli, J. Hu, R.S. Lakshmanan, T.S. Huang, J.M. Barbaree, B.A. Chin, A magnetoelastic resonance biosensor immobilized with polyclonal antibody for the detection of *Salmonella typhimurium*, Biosensors and Bioelectronics 22 (7) (2007) 1474-1479.

CHAPTER 3

SENSOR PLATFORM – MSMC

3.1 Configuration of MSMC

The MSMCs used in this research are unimorph type cantilevers. A cantilever beam consists of two layers: an active layer and an inactive layer. The configuration of MSMC is shown in Figure 3-1. The active layer used here is an amorphous magnetostrictive alloy, Metglas^{TM} 2826 ribbon (Honeywell, Morristown, NJ); the inactive layer is Cu thin film sputtered on the Metglas using magnetron DC sputtering system.

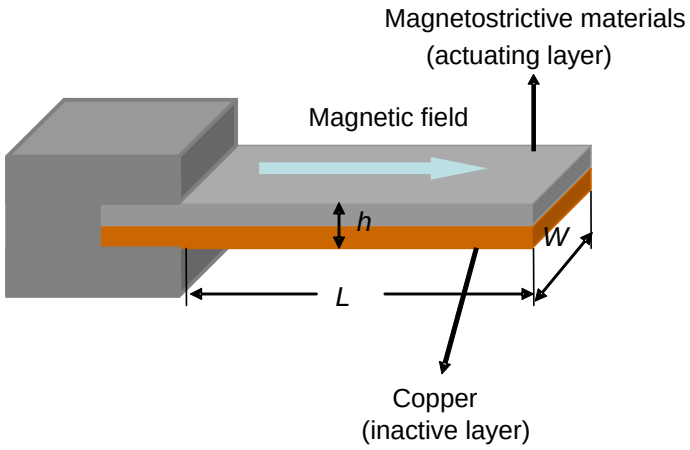

Figure 3-1. The schematic of Magnetostrictive cantilever.

The properties of cantilever beam such as density, Young's modulus, and Poisson's ratio are listed in Table 3-1. The thickness is 20 μm and 15 μm for the active layer and the inactive layer, respectively. Since these two layers have the same length and

width, the volume of these two layers is only thickness dependent. Thus, the average density calculated from the Metglas™ 2826 alloy and Cu can be used as the density of the MSMC.

In fabrication of MSMCs, firstly the Metglas™ 2826MB ribbon was polished to about 20μm of the thickness by using 2000# polish paper and then cleaned with acetone in a Cole Parmer 8891 ultrasonic cleaner for ten minutes. The copper layer (~15 μm in thickness) was sputtered on the polished Metglas thin film. Prior to the deposition of copper layer, a chromium thin film of 100 nm in thickness was deposited on the Metglas to enhance the bonding between Metglas layer and copper layer. The copper/Metglas bilayer was then cut into rectangles (strips) in different sizes. The bilayer strip was clamped at one end using a PMMA plastic holder to form the cantilever or MSMC. The cantilever was then coated with a gold layer (~ 130 nm in thickness) by magnetron sputtering. The gold layer is employed to prevent the corrosion of the cantilever and to promote the immobilization of the bio-recognition element. Prior to the gold deposition, a thin layer of chromium with a thickness of 100 nm was sputtered on the cantilever as the adhesion layer. The Denton Sputtering System was employed in all the sputtering steps.

Table 3-1. The effective material properties of Metglas™ 2826, Cu thin film, and cantilever beam.

Materials	Density g/cm^3	Young's Modulus GPa	Thickness μm	Poisson's Ratio
Metglas™ 2826 [1]	7.9	100-110	20	0.5 or 0.33 [3]
Copper thin film [2]	8.9	110	15	0.36
Metglas™ /Cu bilayer	8.32	110	35	0.5

3.2 Operation principle

The operation principle of all acoustic wave devices based sensor platforms are the same: a change in the mass load on the sensor shifts the resonance frequency, which can be measured and recorded by using computer-based output system. The sensing principle of the MSMC platform is shown in Figure 3-2. An MSMC consists of two layers: magnetostrictive/active layer and inactive layer as shown in Figure 3-2 (a). Due to the magnetostrictive effect, the length of the active layer would change under magnetic field. Meanwhile, the inactive layer, bonded together with the active layer, restricts the length change, which would result in the bending of the MSMC. If a time-varying (ac) magnetic field (see Figure 3-2 (b)) is applied, a bending/flexural oscillation of the MSMC would be induced. Due to the magnetic nature, the bending/flexural oscillation of the MSMC results in an emission of a magnetic flux, which can be detected using a pick-up coil (see Figure 3-2 (c)). The output oscillating signal (e.g. phase signal) of the pick-up coil is shown in Figure 3-2 (d).

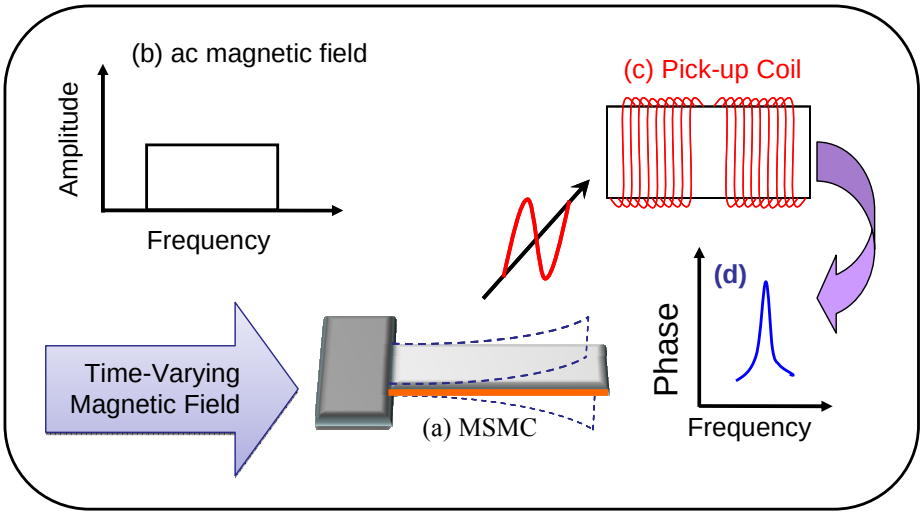

Figure 3-2. Schematic illustration of the principle of MSMC as a transducer for biosensors.

If the time-varying magnetic field is a sine wave, the bending vibration of an MSMC would also be a sine function of time. Since the magnetostrictive strain response (λ) is an even function of the driving magnetic field (H), as shown in Figure 3-3, the MSMC is usually actuated using a small ac signal imposing on a large dc bias. As revealed in Figure 3-3, if only a small ac magnetic signal is applied, the strain response in the material is in a quadratic function of the driving magnetic field. As a result, the strain response is small and at a frequency that is the double of the frequency of the driving ac field. On the other hand, if the small ac field is imposed on a dc bias, a larger ac stain response is observed at the same frequency as, and is proportional to, the ac driving field. Therefore, an MSMC is usually operated by imposing a small ac magnetic field on a dc bias.

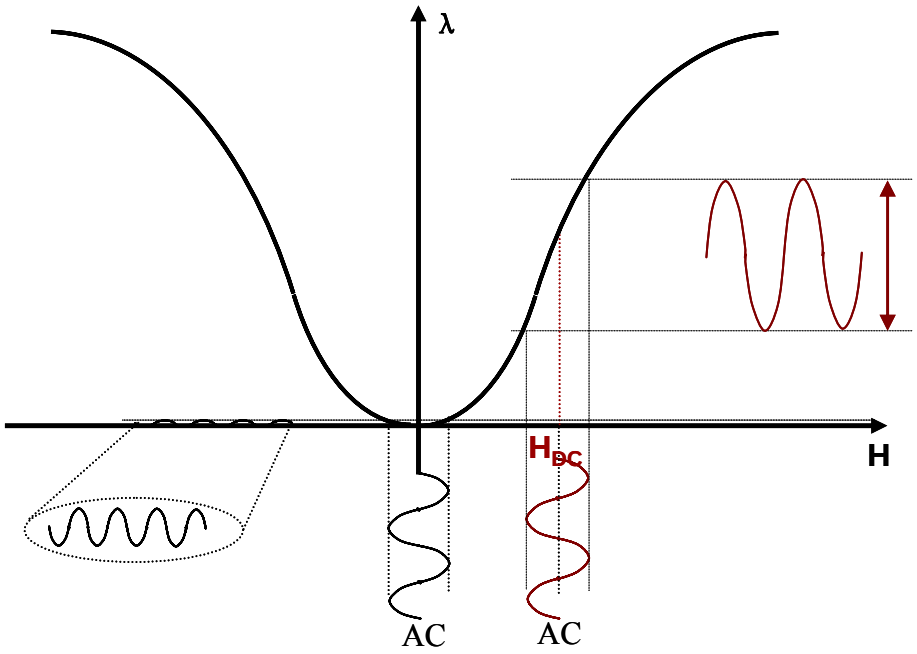

Figure 3-3. The magnetostriction response of a magnetostrictive material under the external magnetic field (H).

Wireless driving/sensing is the principal advantage of the MSMC over current MCs. Additionally, if the inactive layer is a magnetic material, the signal from the pick-up coil can be enhanced and the dc field may not be needed. This is another advantage offered by MSMC, which would be important for small-size MSMCs. That is, for MSMCs with the same size, the signal strength can be enhanced over some range, which is a desired feature for real-time detection since the distance between the sensor and the interrogation system may change over a range due to the different requirements.

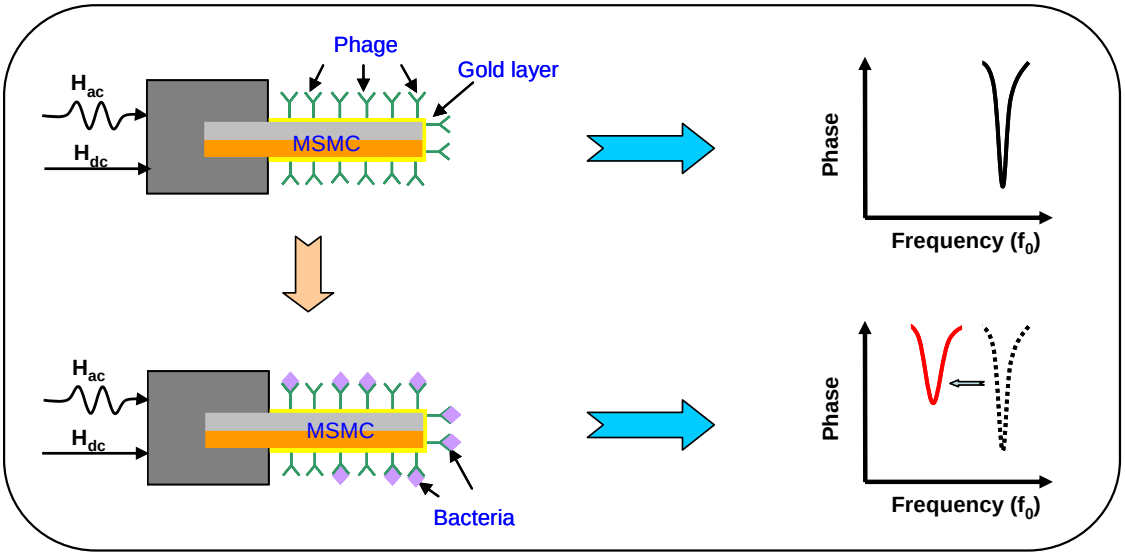

Figure 3-4. The schematic illustration of the operation principle of MSMC based biosensors for detecting bacteria. The binding of bacteria on both sides of the MSMC.

The principle of the MSMC as the biosensor platform was shown in Figure 3-4. The MSMC platform coated with the biological recognition element (e.g. phage or antibody for antigen) will lower the resonance frequency due to the bacteria/antigen binding on the sensor surface. The shift of resonance frequency caused by the mass load can be expressed as the mass sensitivity and will be discussed in Section 4.2. The binding bacteria can be obtained by analysis the frequency shift based on the mass sensitivity.

3.3 Theory

The wave equation for the bending/flexural wave motion of a rectangular cantilever beam (in the length of L, width of W, and thickness of h) without damping can be expressed as [4]:

$$M_C \frac{\partial^2 y}{\partial t^2} + E' I \frac{\partial^4 y}{\partial x^4} = 0 \tag{3-1}$$

where y is the bending deformation of the beam at the point x (x-direction is along the length of the cantilever, as shown in Figure 3-1. Under the assumption of a beam structure with $W >> h$, the effective Young's modulus is given by

$$E' = \frac{E}{1-\sigma^2} \tag{3-2}$$

where σ and E are Poisson's ratio and Young's modulus of the cantilever beam, respectively. The moment of inertia for a rectangular beam can be given

$$I = \int_0^W \int_{-h/2}^{h/2} z^2 dz dy = \frac{1}{12} W h^3 \tag{3-3}$$

$M_C = \rho W h$ is the effective mass of cantilever beam, where ρ is the effective mass density of the beam material.

For harmonic oscillations, we can substitute $y = y_0 e^{i\omega t}$ in Eq. (3-1) and obtain

$$-\omega^2 M_C y_0 + E' I \frac{\partial^4 y_0}{\partial x^4} = 0 \tag{3-4}$$

which we can write as

$$\frac{\partial^4 y_0}{\partial x^4} = \left(\frac{\lambda}{L}\right)^4 y_0 \tag{3-5}$$

where

$$(\frac{\lambda}{L})^4 = \omega^2 M_C / E'I \tag{3-6}$$

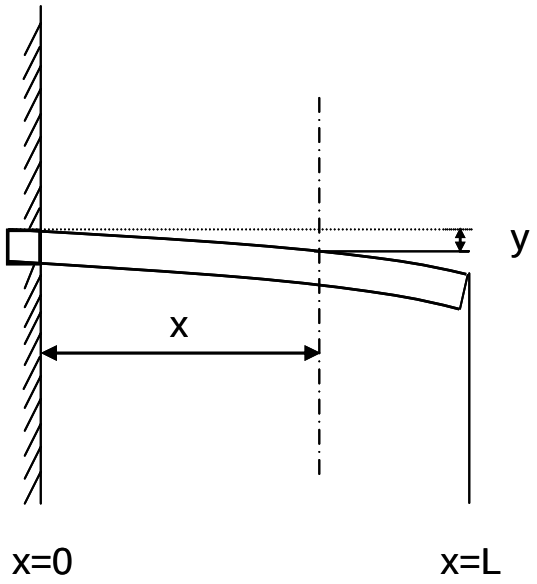

Figure 3-5. The deflection schematic of cantilever beam.

The general solution of a homogeneous fourth-order differential wave equation is the sum of four linear independent solutions

$$y_0 = A\cosh\frac{\lambda}{L}x + B\sinh\frac{\lambda}{L}x + C\cos\frac{\lambda}{L}x + D\sin\frac{\lambda}{L}x \tag{3-7}$$

where A, B, C, and D are the constants.

For a cantilever beam rigidly fixed at one end (x=0) and free at the other end (x=L) (see Figure 3-5), considering the boundary conditions for various types of attachment of the beam,

$$y_0(x=0) = 0, \quad \left.\frac{\partial y_0}{\partial x}\right|_{x=0} = 0, \text{ for } x = 0,$$

$$\left.\frac{\partial^2 y_0}{\partial x^2}\right|_{x=L} = 0, \text{ and } \left.\frac{\partial^3 y_0}{\partial x^3}\right|_{x=L} = 0, \text{ for } x = L \tag{3-8}$$

where the first two boundary conditions are due to the fact that one end of the cantilever

beam is clamped. The third one and the fourth one are due to no bending moment and shear force at the free end of the cantilever beam.

We put Eq. (3-8) into Eq. (3-7), the detailed calculation steps were listed in Appendix 1, and a characteristic relationship can be obtained [4]

$$\cos\lambda\cosh\lambda = -1 \tag{3-9}$$

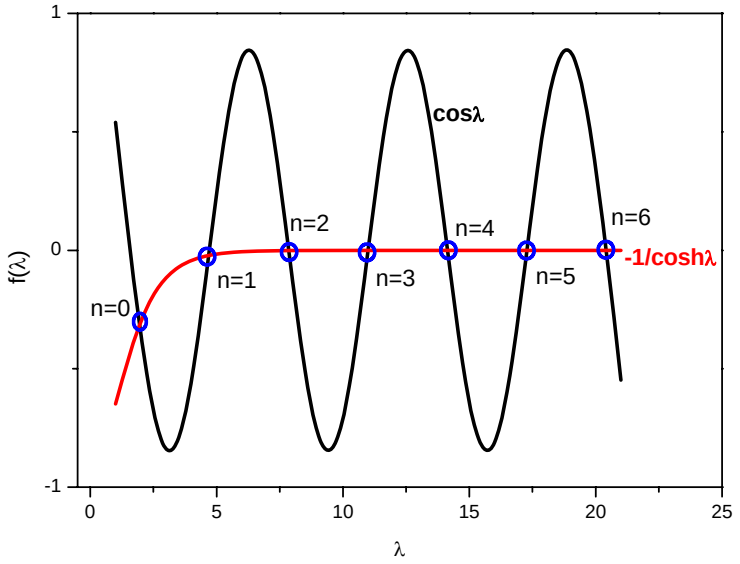

Figure 3-6. Curves of $\cos\lambda$, and $-\frac{1}{\cosh\lambda}$. The eigenvalues for a cantilever with one end free and the other end fixed can be graphically obtained from the intersections of these two curves.

The eigenvalue λ can be obtained either graphically or by approximate methods, or even using tables of functions. For example, the eigenvalue λ of different modes can be determined by graphically solved Eq. (3-9) (see Figure 3-6) and the first seven eigenvalues were given in Table 3-2. For the higher harmonic mode, the eigenvalues might be estimated by using $(n+0.5)\pi$ [6].

Table 3-2. Graphically obtained Eigenvalues for the flexural resonance modes of MSMC.

Resonance mode	λ_i	λ_i^2	f_i / f_{i-1} Theoretical
i=0	1.8751	3.5160	-
i=1	4.6941	22.035	6.267
i=2	7.8548	61.697	2.800
i=3	10.996	120.90	1.960
i=4	14.137	199.86	1.653
i=5	17.279	298.56	1.494
i=6	20.420	416.99	1.397
…	…	…	…
i=n	$(n+0.5)\pi$ [34]	$[(n+0.5)\pi]^2$	$\left(\frac{n+0.5}{n-0.5}\right)^2$

Based on the eigenvalues for the resonance harmonic modes at 0-3, we can calculate the constants A, B, C, and D for Eq. (3-7) and the results were listed in Table 3-3. Actually, A is the values of B times. For example, for the fundamental mode, $A = -C = -1.3622B$. Since B is related to the amplitude of wave Eq. (3-7), but not the shape of the oscillating motion. Thus, we just use B=1 in the plot of the harmonic motion of the cantilever beam.

Table 3-3. The constants A, B, C, and D for the first four harmonic modes.

Mode	λ	Sinh λ	Cosh λ	Sin λ	Cos λ	A	B	C	D
0	1.8751	3.1841	3.3374	0.95415	-0.29963	-1.3622	1	1.3622	-1
1	4.6941	54.646	54.658	-0.99983	-0.01829	-0.9819	1	0.9818	-1
2	7.8548	1289.0	1289.0	1.0000	-1.0008	-1.0008	1	1.0008	-1
3	10.996	29818	29818	-1.0000	-1.0000	-1.0000	1	1.0000	-1

Note: if B is 1, the data in Table 3-3 is exact value; otherwise, the constants should be B times.

The natural resonance motions of the first four harmonic modes of vibration are shown in Figure 3-7. It showed that certain regions of the cantilever (e.g. the Nodal point) do not take part in the vibration displacements and the positions of these parts are not

changing with the mode of vibration. For example, for the 0^{th} harmonic mode, the Nodal point is sitting on the clamped end of the cantilever. Therefore, the sensitivity of a cantilever to the added mass and mass responsivity is different along the cantilever at different vibration modes. The simulation by using Eq. (3-7) showed that the largest responsivity to the additional mass was achieved at its application close to the cantilever's free end for the 0^{th} mode [7], and the mass sensitivity was described and calculated in Section 4.3.

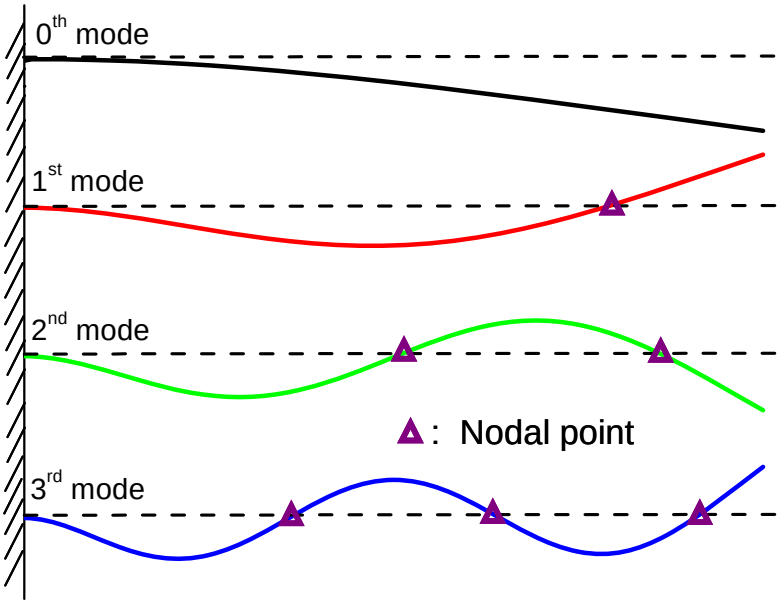

Figure 3-7. The natural vibration motion at 0^{th}-3^{rd} harmonic modes and the nodal points (violet triangles) 0-3 at the 0^{th}, 1^{st}, 2^{nd}, and 3^{rd} resonance oscillation modes of the clamped cantilever which were obtained from Eq. (3-7).

By combining Eq. (3-2), Eq. (3-3), with Eq. (3-6), the angular frequency of a rectangular cantilever can be obtained

$$\omega_n = 2\pi f_n = \lambda_n^{\ 2}\sqrt{\frac{E}{12\rho(1-\sigma^2)}}\frac{h}{L^2} \qquad \text{(n = 0, 1, 2, …)} \qquad \text{(3-10)}$$

Thus, the natural resonance frequency of the n[th]-mode without damping for a rectangular cantilever is [4, 8-9]:

$$f_n = \frac{\lambda_n^2}{2\pi\sqrt{12}}\frac{h}{L^2}\sqrt{\frac{E}{\rho(1-\sigma^2)}} \qquad \text{(n = 0, 1, 2, …)} \qquad \text{(3-11)}$$

where $\sigma = 0.5$.

Liang et al. [3] modified Eq. (3-11) by using the plane-stress or biaxial modulus as,

$$f_n = \frac{\lambda_n^2}{2\pi\sqrt{12}}\frac{h}{L^2}\sqrt{\frac{E}{\rho(1-\sigma)}} \qquad \text{(n = 0, 1, 2, …)} \qquad \text{(3-12)}$$

where $\sigma = 0.33$.

3.4 Determination of several important parameters

3.4.1 Characteristic frequency

Figure 3-8 gives a typical resonance spectrum of an MSMC obtained from the output signals (the amplitude signal and the phase signal) of the pick-up coil. The amplitude signal reflects the amplitude of the bending oscillation of the MSMC, while the phase signal represents the phase difference between the ac magnetic field and the bending oscillation. For the plot of the oscillation amplitude versus frequency, the amplitude reaches the maximum at the resonance frequency (f_r) and the minimum at the anti-resonance frequency (f_{ar}), respectively. The phase signal reaches its peak at a frequency (f_0) ($f_r < f_0 < f_{ar}$).

In the characterization of the MSMC-based sensors, the phase signal was used to determine the resonance behavior, which means f_0 is considered as the characteristic

frequency of the MSMC. Based on the results shown in Figure 3-8, the f_r, f_{ar}, and f_0 are 2585, 2602, and 2594 Hz, respectively, for an MSMC with a size of 3.0 mm x 1.0 mm x 35 μm. Thus, the characteristic frequency is 2594 Hz for the MSMC in the size of 3.0 mm x 1.0 mm x 35 μm. Clearly, the characteristic frequency determined in this way is higher than the real resonance frequency and smaller than the antiresonance frequency of the device. This method is also used in the characterization of piezoelectric-based cantilevers [10].

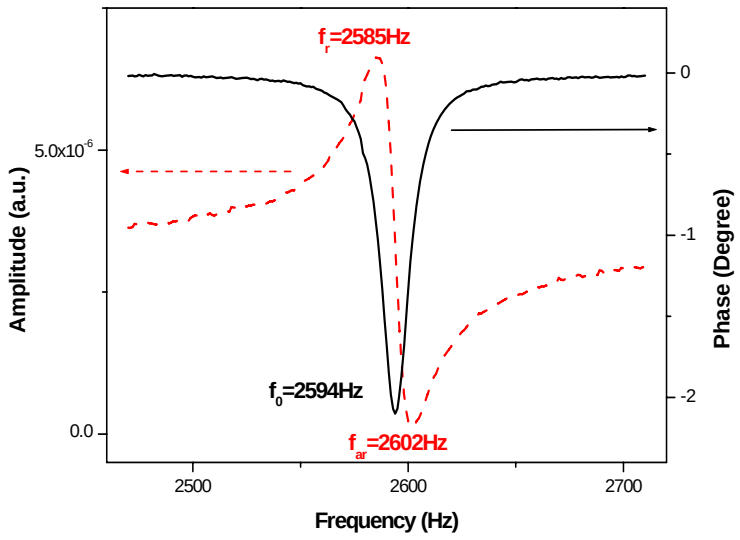

Figure 3-8. Measured resonance spectrum, amplitude and phase signals versus frequency from Lock-in amplifier for the fundamental mode of an MSMC in the size of 3.0 mm x 1.0 mm x 35 μm in air.

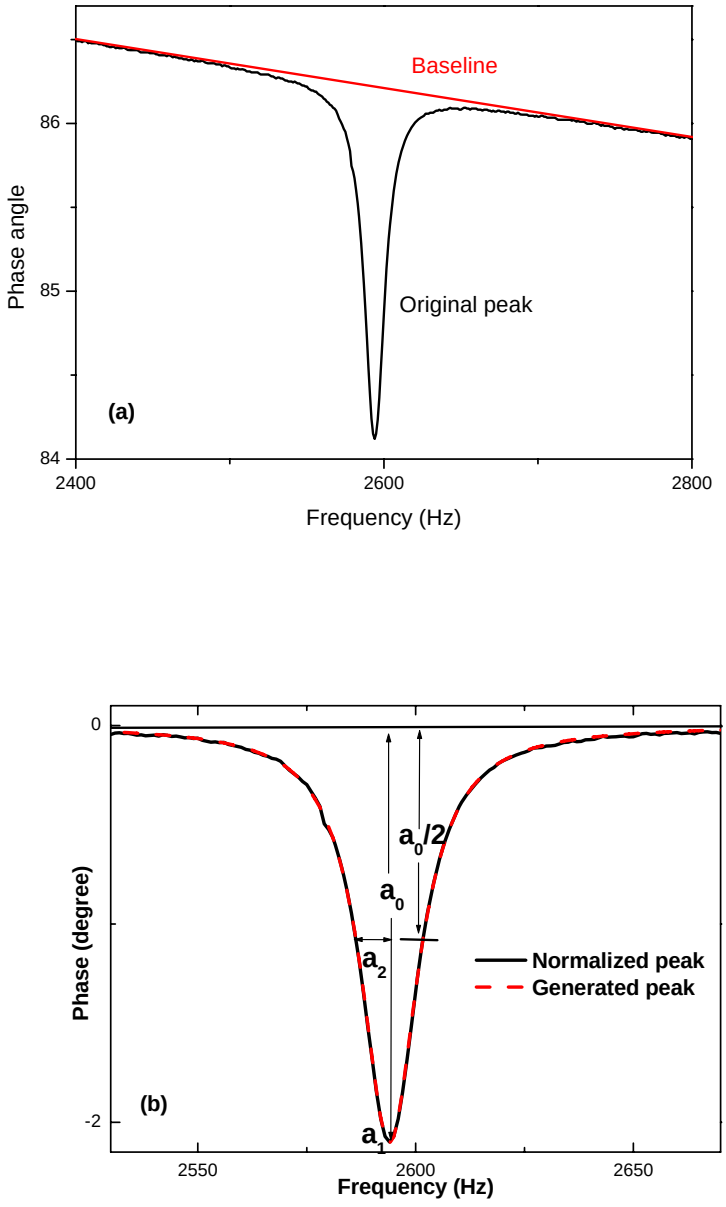

Figure 3-9. (a). The original spectrum of phase vs. frequency from the output signal. (b). The normalized spectrum (dashed black line) and generated spectrum (red solid line). The MSMC used here is in size of 3.0 mm x 1.0 mm x 35 μm for the fundamental mode. The red solid line is fitted by using the Lorentz fitting.

To precisely determine the value of characteristic frequency (f_0) from the experimental results, the phase peak of the MSMC was fitted using different functions. Before fitting, the original peak shown in Figure 3-9 (a) should subtract the background (baseline) which is from the phase delay of the system. It is found that the phase peak can be fitted well using the Lorentz function. The spectroscopy function of Lorentzian amplitude can be expressed as

$$\theta = a_0 /(1 + [(f - a_1)/a_2]^2) \qquad (3\text{-}13)$$

where θ is the phase signal at the frequency a_0, a_1, and a_2 are the resultant fitting constants. From the above equation, we can obtain the characteristic frequency $f_0 = a_1$. The curves from the experiment data and fitting data were shown in Figure 3- 9 (b). To determine the repeatability of the fitting, the same set of experimental data was fitted over different frequency ranges. For the data shown in Figure 3- 9 (b), the fitting results indicate that the error in the f_0 is smaller than 0.1 Hz.

As we discussed Section 3.3, the resonance frequency can be theoretically calculated by using Eq. (3-11). The eigenvales for the n^{th} harmonic mode can be graphically obtained and listed in Table 3-2. To confirm the theoretical analysis, the first five harmonics for the MSMC in size of 4.4 mm x 0.8 mm x 35 μm were measured in this experiment. The phase signals and the characteristic frequencies for first five harmonic peaks are shown in Figure 3-10. The resonance frequencies from Eqs. (3-11) and (3-12) (theoretical analysis) and experimental measurement from Figure 3-9 were listed in Table 3-4. It is obvious that the theoretical frequencies are very close to the experimental data. The analytical error is no more than 3.2 % from Eq. (3-11). Also, the ratio of f_i / f_{i-1}

were given in Table 3-3 and the values are very close to the ratios from the experiment. Therefore, this theory is reasonable to be used to estimate the frequency in this study.

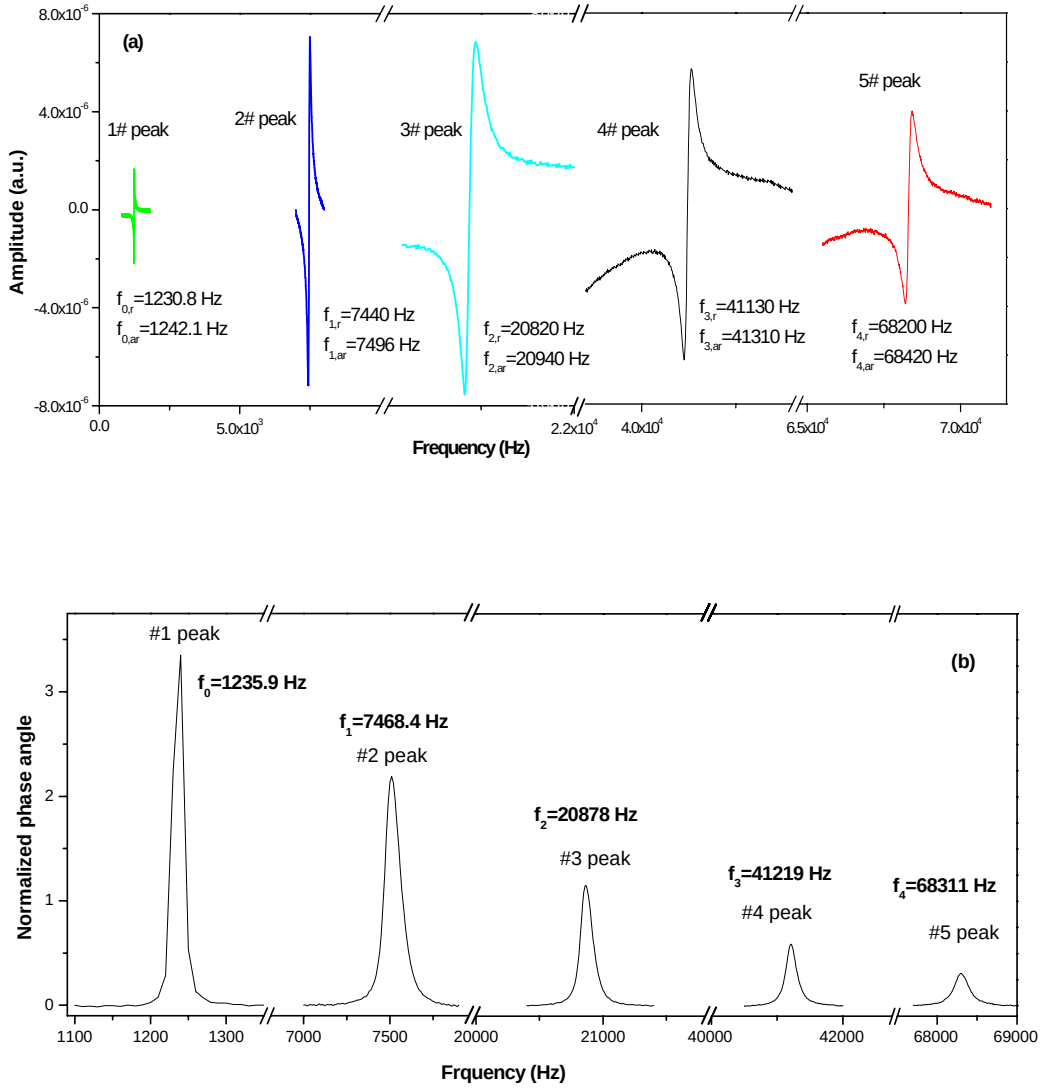

Figure 3-10. The first five harmonic peaks from (a) amplitude output and (b) phase output for the MSMC with the size of 4.4 mm x 0.8 mm x 35 μm.

Table 3-4. The resonance frequencies for the first five modes obtained from Eqs. (3-11) and (3-12) and measurement for the MSMC with the size of 4.4 mm x 0.8 mm x 35 μm.

Harmonic	0^{th} mode	1^{st} mode	2^{nd} mode	3^{rd} mode	4^{th} mode
$f_{theo,r}$ (Hz) from Eq. (3-11)	1226.0	7683.3	21513	42166	69701
$f_{theo,r}$ (Hz) From Eq. (3-12)	1297.1	8128.9	22761	44612	73743
f_r (Hz)	1230.8	7444.3	20825	41136	68216
f_{ar} (Hz)	1242.1	7492.3	20928	41306	68403
f (Hz)	1235.9	7468.4	20878	41219	68311
1- $f_r / f_{theo,r}$ From Eq. (3-11)	-0.3%	3.1%	3.2%	2.4%	2.1%
1- $f / f_{theo,r}$ From Eq. (3-12)	5.1%	8.4%	8.5%	7.8%	7.5%
1- $f / f_{theo,r}$ From Eq. (3-11)	-0.8%	2.8%	3.0%	2.2%	2.0%
1- $f / f_{theo,r}$ From Eq. (3-12)	4.7%	8.1%	8.3%	7.6%	7.4%
$\lambda^2_{n,Exp}$	-	6.043	2.796	1.974	1.657
$\lambda^2_{n,Theo}$	-	6.267	2.800	1.960	1.653
1- $\lambda^2_{n,Exp} / \lambda^2_{n,Theo}$	-	3.6%	0.2%	-0.7%	-0.2%

3.4.2 Quality factor

Usually, the improvement of sensor performance can be obtained by reducing the noise while the physical signals (e.g. mechanical signal) were converted to electrical signals/magnetic signals, or by controlling other error sources (e.g. uncompensated

thermal drift). In this process, energy dissipation in the cantilever causes the stored vibration energy to convert into heat. A higher Q value indicates a lower rate of energy dissipation relative to the oscillation frequency, so the oscillations die out more slowly. Generally Q is defined to be [11]

$$Q = \frac{2\pi(stored \quad vibration \quad energy \quad)}{dissipated \quad energy \quad per \quad period} = \frac{2\pi U_i}{U_d} \tag{3-14}$$

In this research, we provide the magnetic energy to resist the decay of oscillations of cantilever. Q value is used to characterize the sharpness of the resonance peak, and can be defined as the resonance peak/frequency over the width at half the peak height, as shown in Figure 3-8. Here, the resonance frequency might be substituted by characteristic frequency obtained from the phase signal. It also can be calculated by using Eq. (3-13) and given by

$$Q = a_1 / 2a_2 \tag{3-15}$$

The Q values of the first five modes of the MSMC were measured in this experiment. The experiment data (see Figure 3-9) were fitted by Eq. (3-13) and the Q values were calculated by Eq. (3-15). The results for the MSMC in size of 4.4 mm x 0.8 mm x 35 μm were listed in Table 3-5. Clearly, the higher harmonic mode increases Q value. Meanwhile, the signal of the harmonic peak is weaker for the higher mode. In this research, the fundamental harmonic mode would be used for fundamental study (Chapter 4) and biosensing application (Chapter 5) of MSMC.

Table 3-5. Q values for the first five modes of the MSMC in size of 4.4 mm x 0.8 mm x 35 μm.

Harmonic mode	0^{th}	1^{st}	2^{nd}	3^{rd}	4^{th}
Q value	126.4	132.6	195.5	227.3	324.3

In resonant detection systems, the frequency width of the resonant response is the fundamental instrumental limit, so Q value can be influenced by many factors (e.g. support loss, internal friction, and surrounding media). For example, the damping in the viscous fluids is the primary dissipation mechanism that limits the Q value and broadens the resonance. This factor motivates the device designs that optimize the ratio of mass to Q value of the cantilever. In the low pressure (vacuum) regime, viscous damping is eliminated but clamping loss, and internal structure (e.g. chemical coatings) can also contribute to mechanical losses and degrade Q value. The detailed influence of the viscous damping will be examined in Chapter 4.

3.4.3 Mass sensitivity

A small change in mass (mass sensitivity) is one type of device sensitivity, which can be used when detecting single small entities such as bacteria, viruses, nanoparticles, or single molecules. Sensors with a very high absolute mass sensitivity could detect single cell and enumerate analytes. Resonant MEMS and NEMS devices actuated in vacuum have demonstrated mass sensitivity in the order of attograms or less [12-15].

Usually, sensors measure changes in mass uniformly distributed over the sensor. For example, for quartz crystal microbalance with large-scale dimension, since the bacteria number in the whole surface of sensor is a huge number, the mass sensitivity is in terms

of mass per unit area, which value can be translated into a value for total mass measured. If a small mass load (Δm) is uniformly distributed on the surface of a cantilever beam, the mass sensitivity (S_m) of the cantilever can be written as [10, 16-17]:

$$S_{m,uni} = -\frac{\Delta f_n}{\Delta m} \cong \frac{f_n}{2M_C} = \frac{f_n}{2\rho Wh} \qquad (\Delta m << M) \tag{3-16}$$

where Δf_n is the shift in the resonant frequency due to the mass load (Δm).

Figure 3-11. The schematic of the point mass loaded at the free end of cantilever beam.

To examine the resonance frequency change due to a point mass loaded at the tip of the cantilever (see Figure 3-11), the effect mass of the cantilever beam should be modified as [4]

$$M_C = 0.236\rho Wh \tag{3-17}$$

Therefore, by combined Eq. (3-16) and Eq. (3-17), we can obtain

$$S_{m,tip} = -\frac{\Delta f_n}{\Delta m} \cong \frac{f_n}{2M_C} = \frac{f_n}{0.472\rho Wh} \quad (\Delta m << M) \tag{3-18}$$

Substituting Eq. (3-11) into Eqs. (3-16) and (3-18), the S_m of a rectangular cantilever is:

$$S_{m,uni} = \frac{1}{4}\frac{\lambda_n^2}{\pi\sqrt{12}}\frac{1}{WL^3}\sqrt{\frac{E}{\rho^3(1-\sigma^2)}} \qquad (\Delta m << M) \tag{3-19}$$

$$S_{m,tip} = \frac{1}{0.944}\frac{\lambda_n^2}{\pi\sqrt{12}}\frac{1}{WL^3}\sqrt{\frac{E}{\rho^3(1-\sigma^2)}} \qquad (\Delta m << M) \tag{3-20}$$

Equations (3-19) and (3-20) indicates that the S_m of a cantilever is determined by

four factors: 1) the location of the mass load, 2) resonance mode (λ_n), 3) geometry (L and W), and 4) materials properties of the cantilever beam: $\sqrt{\frac{E}{\rho^3(1-\sigma^2)}}$. The values of $\sqrt{\frac{E}{\rho^3(1-\sigma^2)}}$ for materials used in typical active MCs are given in Table 3-4, where a magnetostrictive alloy (Metglas^{TM} 2826 MB used in this study) and PZT5A (a widely used and commercially available piezoelectric ceramic) are included [1, 6, 17]. The results indicate that for cantilevers with the same dimensions, an MSMC would exhibit a S_m of about 36% higher than a piezoelectric MC. More importantly, as will be demonstrated below, the MSMC also exhibits a higher Q value. The length dependent mass sensitivity is shown in Figure 3-12. Two widths with 1.0 mm and 0.8 mm were used in this experiment for biosensing application. We also can find the mass sensitivity which the addition mass is attached at the tip of cantilever beam is higher than that which the addition mass is uniform distributed on the same cantilever beam. In Figure 3-12, two violet-color regions represent the mass sensitivities for the MSMC sensors which will be used in the biosensing application (Chapter 5).

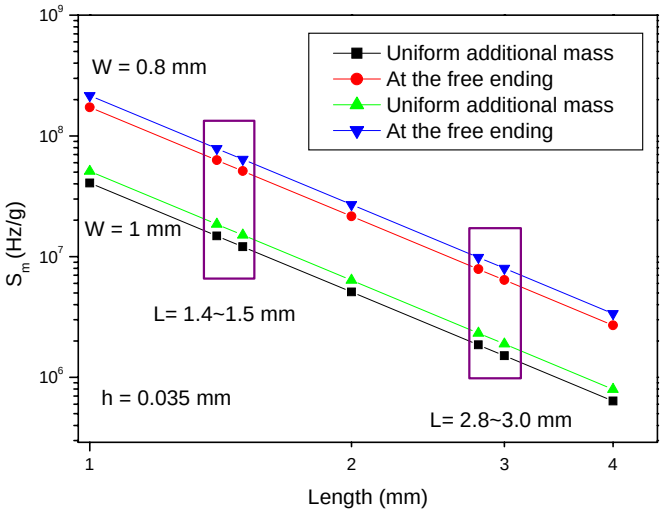

Figure 3-12. The mass sensitivity (uniform and at the free end) *vs.* length of the MSMC based sensors with the fundamental mode. Two widths with 0.8 mm and 1.0 mm were used.

3.5 Experimental flow chart

The experimental flow chart of this research is shown in Figure 3-13. It is mainly divided into three parts: fabrication of sensor's platform, fundamental study, and biosensing application.

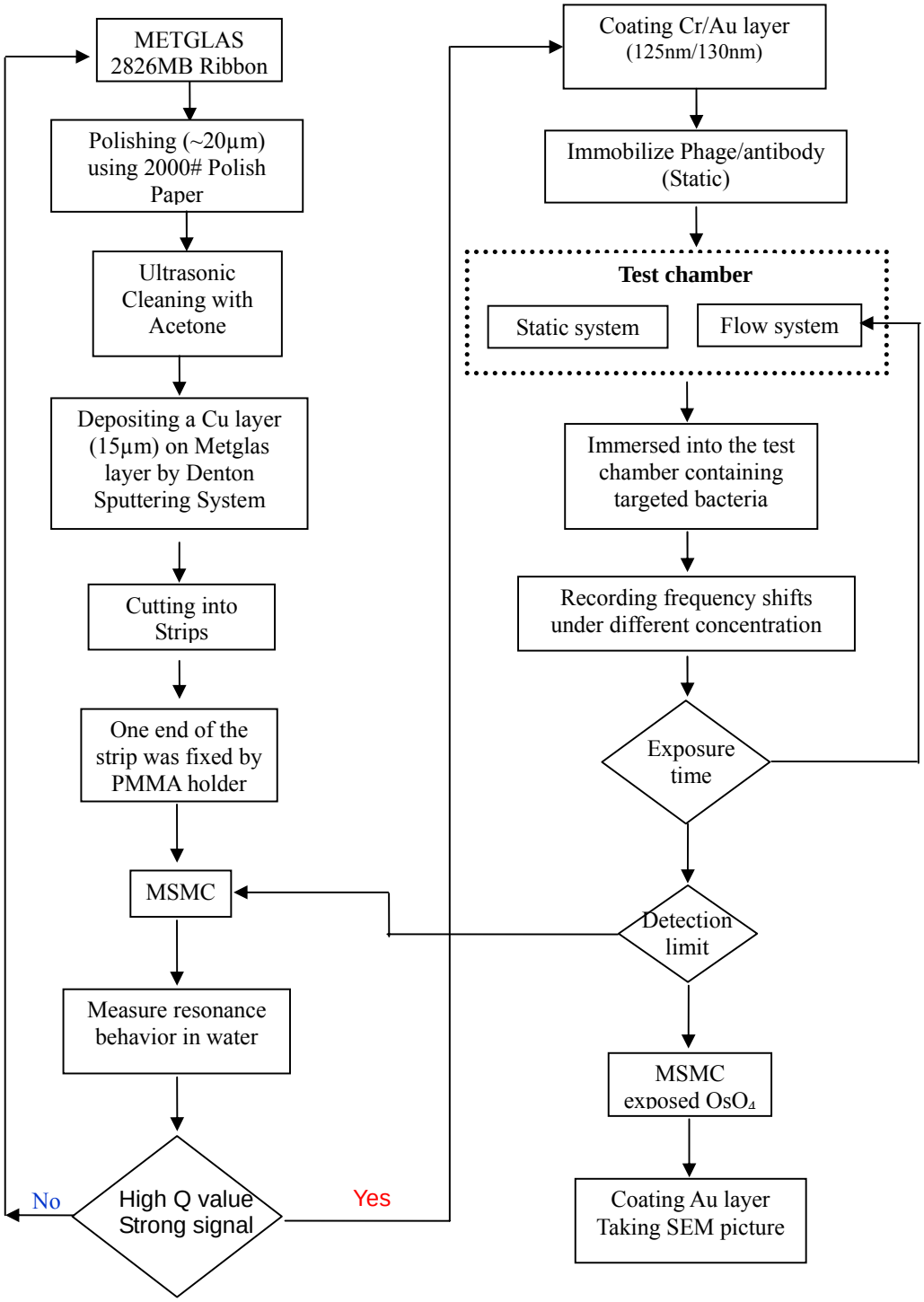

Figure 3-13. The experimental flow chart in this research.

3.6 Measurement setup

The photograph of measurement setup in this experiment is given in Figure 3-14. The setup used here to characterize the resonance behavior of the MSMC consists of a custom-designed Helmholtz coil and a pair of homemade pick-up coils. The Helmholtz coil consists of two pairs of coils: one pair can generate an ac magnetic field at frequency up to 500 kHz and the other pair can create a strong dc magnetic field which was connected to a dc power supply. The Helmholtz coil is linked to a lock-in amplifier (SRS830, Stanford Research Systems, Sunnyvale, CA) which provides a sine wave signal with constant RMS (root-mean-square). In this study, a dc magnetic field of 20 Oe was employed to offset the magnetic anisotropy of the magnetostrictive layer, while an ac magnetic field with the amplitude of 3.2 Oe was used to actuate the oscillation of the MSMC. An MSMC (see Figure 3-15 (b)) was put into a test chamber (see Figure 3-15 (a)) that was sited in the middle of the Helmholtz coil (see Figure 3-14). The pick-up coil was wound on the outside of the sample chamber to measure the magnetic signal emitted from the MSMC. To eliminate the background signal, the pick-up coil was made of two identical coils that were wound in opposite directions and connected in a series, as shown in Figure 3-15 (c). Therefore, the output signal of the pick-up coil only reflects the magnetic signal emitted from the bending vibration of the MSMC.

The signal was measured using a lock-in amplifier, which had two outputs: amplitude and phase. The amplitude represents the oscillating amplitude of the magnetostrictive cantilever, while the phase represents the phase difference between the ac driving magnetic field and the MSMC's bending vibration.

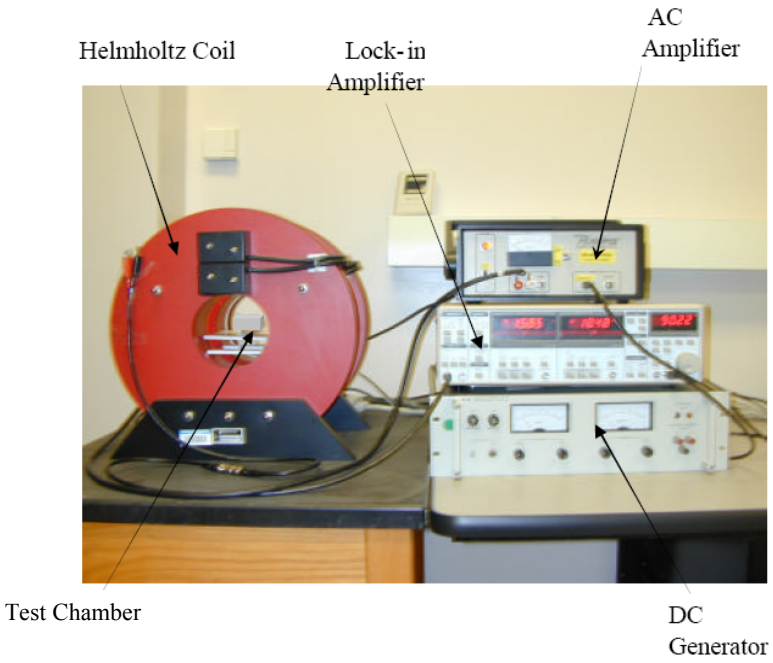

Figure 3-14. Measurement set-up in laboratory for this research.

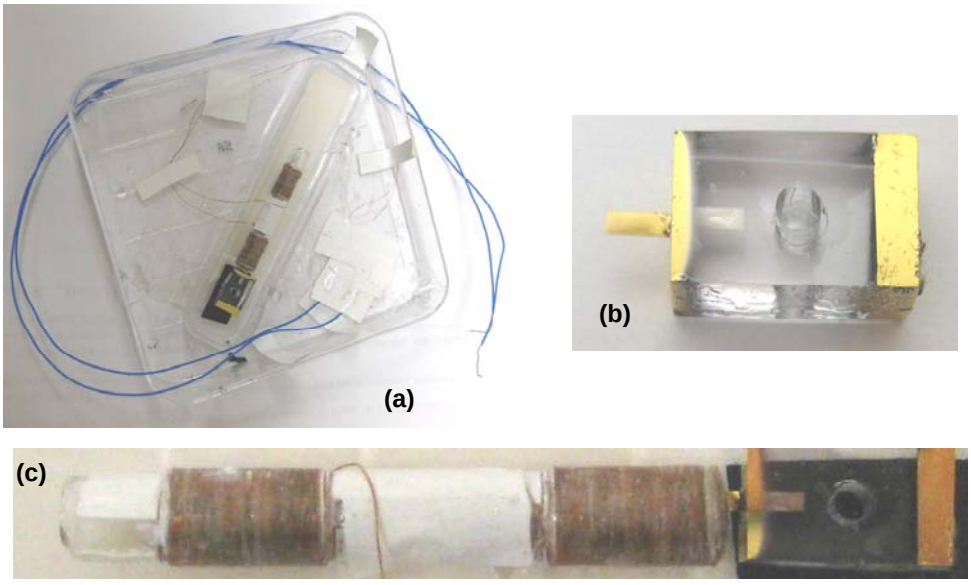

Figure 3-15. The experiment design of test chamber (a), MSMC (b), and pick-up coil (c).

The pick-up coil was used to measure the magnetic signal from the oscillation of cantilever beam. Thus, the design of the pick-up coil is very important in order to receive the magnetic signals and to further amplify the output signals. The diameter of the pick-up coil is dependent on the dimension of MSMC used in this experiment. Usually the smaller width of the MSMC used in this experiment is 1.5 mm. Thus, the diameter of the pick-up coil should be larger than 1.5 mm to contain the cantilever beam. In this experiment, the internal diameter of the tube to make pick-up coil is 2.0 mm, and the external diameter is 3 mm. The configuration of the pick-up coil was also restricted by the inductance of the pick-up coil. The inductance of the pick-up coil is proportional to the wound turns of pick-up coil, the cross section area of coil, and reversibly to the length of the coil. As we know, the stronger signal of the pick-up coil is more preferable for the experiment, which comes from the larger inductance. Thus, several layers of pick-up coil were used to get the strong signal in order to increase cross section area, and shorten the length of coil. The magnet (copper) wire used here is relative thin with the diameter of 1.37 mm.

Appedix 1. The calculation steps while Eq. (3-8) was put into Eq. (3-7).

$$0 = A\cosh 0 + B\sinh 0 + C\cos 0 + D\sin 0 \qquad \Rightarrow 0 = A + C \tag{a}$$

$$0 = A\sinh 0 + B\cosh 0 - C\sin 0 + D\cos 0 \qquad \Rightarrow 0 = B + D \tag{b}$$

$$0 = A\cosh\lambda + B\sinh\lambda - C\cos\lambda - D\sin\lambda \quad \Rightarrow 0 = A\cosh\lambda + B\sinh\lambda + A\cos\lambda + B\sin\lambda \tag{c}$$

$$0 = A\sinh\lambda + B\cosh\lambda + C\sin\lambda - D\cos\lambda \Rightarrow 0 = A\sinh\lambda + B\cosh\lambda - A\sin\lambda + B\cos\lambda \tag{d}$$

Eq. (c) + Eq. (d),

$$0 = (A+B)(\cosh\lambda + \sinh\lambda + \cos\lambda) + (B-A)\sin\lambda \quad \Rightarrow \frac{(A+B)}{(B-A)} = \frac{-\sin\lambda}{\cosh\lambda + \sinh\lambda + \cos\lambda}$$

Eq. (c) – Eq. (d),

$$0 = (A-B)(\cosh\lambda - \sinh\lambda + \cos\lambda) + (A+B)\sin\lambda \quad \Rightarrow \frac{(A+B)}{(B-A)} = \frac{\cosh\lambda - \sinh\lambda + \cos\lambda}{\sin\lambda}$$

Thus, we can obtained

$$\frac{-\sin\lambda}{\cosh\lambda + \sinh\lambda + \cos\lambda} = \frac{\cosh\lambda - \sinh\lambda + \cos\lambda}{\sin\lambda} \tag{e}$$

$$-\sin^2\lambda = (\cosh\lambda + \sinh\lambda + \cos\lambda)(\cosh\lambda - \sinh\lambda + \cos\lambda)$$
$$= (\cosh\lambda + \cos\lambda)^2 - \sinh^2\lambda$$
$$= \cosh^2\lambda + 2\cosh\lambda\cos\lambda + \cos^2\lambda - \sinh^2\lambda \Rightarrow$$

$$\Rightarrow \sin^2\lambda + \cosh^2\lambda + 2\cosh\lambda\cos\lambda + \cos^2\lambda - \sinh^2\lambda = 0$$
$$\Rightarrow 2\cosh\lambda\cos\lambda + 2 = 0$$

$$\Rightarrow \cosh\lambda\cos\lambda = -1 \tag{f}$$

References

1. http://metglas.com/downloads/2826mb.pdf
2. D.T. Read, Young's modulus of thin films by speckle interferometry, Measurement Science & Technology 9 (1998) 676-685.
3. C. Liang, S. Morshe, B.C. Prorok, Correction for longitudinal mode vibration in thin slender beams, Applied Physics Letters 90 (2007) 221912.
4. J. Merhaut, Theory of electroacoustics, New York; London: McGraw-Hill International Book Co., 1981.
5. D.A. Mendels, M. Lowe, A. Cuenat, M.G. Cain, E. Vallejo, D. Ellis, F. Mendels, Dynamic properties of AFM cantilevers and the calibration of their spring constants, Journal of Micromechanics and Microengineering 16 (2006) 1720-1733.
6. A.K. Kar, M.A. George, Improved detection of thermally induced higher resonance modes and harmonics of a microcantilever, Journal of Applied Physics 94(7) (2003) 4626-4631.
7. S. Dohn, R. Svendsen, W. Svendsen, A. Boisen, Enhanced functionality of cantilever based mass sensors using higher modes, Applied Physics Letters 86 (2005) 233501.
8. H.J. Butt, M. Jaschke, Calculation of thermal noise in atomic force microscopy, Nanotechnology 6 (1995) 1-7.
9. D. Sarid, Scanning force microscopy: with applications to electric, magnetic and atomic forces, 2nd ed. Oxford University Press, New York, 1994.

10. J.W. Yi, W.Y. Shih, W.H. Shih, Effect of length, width, and mode on the mass detection sensitivity of piezoelectric unimorph cantilevers, Journal of Applied Physics 91 (2002) 1680-1686.
11. http://en.wikipedia.org/wiki/Quality_factor
12. K.L. Ekinci, X.M.H. Huang, M.L. Roukes, Ultrasensitive nanoelectromechanical mass detection, Applied Physics Letters 84(22) (2004) 4469-4471.
13. Y.T. Yang, C. Callegari, X.L. Feng, K.L. Ekinci, M.L. Roukes, Zeptogram-scale nanomechanical mass sensing, Nano Letters 6(4) (2006) 583-586.
14. B. Ilic, H.G. Craighead, S. Krylo, W. Senaratne, C. Ober, P. Neuzil, Attogram detection using nanoelectromechanical oscillators, Journal Applied Physics 95(7) (2004) 3694-3703.
15. B. Ilic, Y. Yang, K. Aubin, R. Reichenbach, S. Krylov, H.G. Craighead, Enunmeration of DNA molecules bound to a nanomechanical oscillator, Nano Letters 5(5) (2005) 925-929.
16. C. Ziegler, Cantilever-based biosensors, Analytical and Bioanalytical Chemistry 379 (2004) 946-959.
17. S. Q. Li, L. Orona, Z. M. Li, Z.-Y. Cheng, Biosensor based on magnetostrictive microcantilever, Applied Physics Letters 88 (2006) 073507.
18. D. E. Gray, American Institute of Physics Handbook, 3rd ed., chapter 3, McGraw hill, New York, 1973.

CHAPTER 4

FUNDAMENTAL STUDY of MSMC

4.1 Introduction

As we discussed in Chapter 3, all AW devices including MCs suffer the damping effect in a viscous medium, such as air or liquid. The damping effect reflects the influence of different factors on the sensor device. The vibration damping may be caused by internal friction (e.g. the beam materials), support loss (e.g. the cantilever holder), and the flow force from the surrounding media such as air and viscous liquids as shown in Figure 4-1.

The internal friction and support loss, which are dominant damping factors in ordinary size machines, have been extensively studied by using structural damping theory, slip damping theory and wave propagation theory [1-4]. The internal damping is inherent from the cantilever devices. Therefore, the internal damping study is not covered in this research.

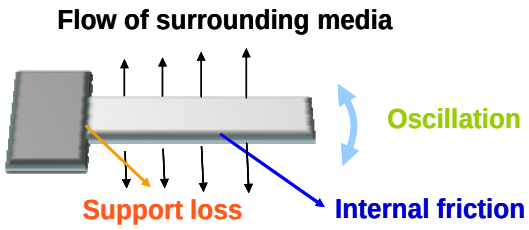

Figure 4-1. The damping mechanism of Q value of a cantilever.

The damping effect of a medium on an AW device depends on the medium (density and viscosity) and the AW device (structure, dimension, and vibration mode) [5-7]. The damping effect is experimentally observed by a shift in the resonance frequency to a lower frequency and a reduction in the Q value. That is, the influence of the damping effect on the resonance behavior has some similarity with the mass influence on the resonance behavior. The damping plays an important role in various cantilever's applications. For examples, cantilevers have been widely explored in biosensors, and chemical sensors. The sensitivity and resolution of the cantilever devices strongly depend on its Q value which is related to the damping. Therefore, it is important to predict the Q value for the cantilever design. The apparent Q value of a cantilever can be expressed as [53]

$$\frac{1}{Q} = \sum_i \frac{1}{Q_i} = \frac{1}{Q_{\text{int}}} + \frac{1}{Q_{\text{sup}}} + \frac{1}{Q_{ext}} \tag{4-1}$$

where Q_{int} and Q_{sup} represent the dissipation effects due to the internal friction of the cantilever and the support loss, whereas Q_{ext} include the external effects (e.g. viscous media) that act on the cantilever.

4.2 Theoretical model

The Q value of a vibrating cantilever in a viscous fluid has been studied theoretically using several models. The simplest method is based on the harmonic oscillating sphere theory. In this theory, an MSMC in liquid behaves as the oscillation of a damped string of spheres [8-11]. To consider the effect of the surrounding viscous media on the MSMC beam, there are several assumptions and approximations implemented in this theoretical model:

(1) The cross section of the beam is uniform over its entire length;

(2) The length of the beam *L* greatly exceeds its nominal width *W (L>>W)*;

(3) The beam is an isotropic linearly elastic solid and internal frictional effects are negligible;

(4) The vibration amplitude of the beam is far smaller than any length scale in the beam geometry;

(5) The drag force of the beam is the sum of drag force from the individual sphere.

This model has been widely applied to many areas: the development of micro power generator; study of air viscous damping effects by a Farby-Perot micro-opto-mechanical device; absolute pressure measurement; mass sensing resonators; measurement of liquid's viscosity and density; and design of atomic force microscopy probes [12].

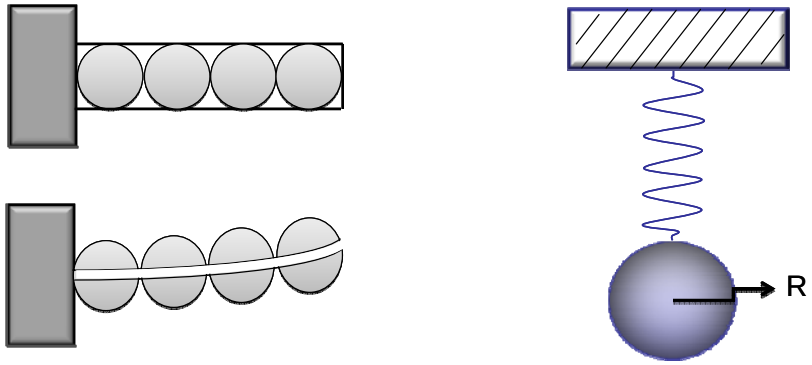

Figure 4-2. The schematic of a damped string of oscillating spheres. R is the effect radius of an oscillating sphere.

When an oscillator is immersed into a liquid and driven by an external harmonic force $fe^{i\omega t}$, the motion of an initially flat, thin, homogeneous cantilever can be described by using the one - dimensional Euler-Bernoulli differential equation, which can be written as [8]

$$(M_C + M_I)\frac{\partial^2 y}{\partial t^2} + b\frac{\partial y}{\partial t} + E'I\frac{\partial^4 y}{\partial x^4} = fe^{i\omega t} \qquad (4\text{-}2)$$

In this equation, the term ($M_I \frac{\partial^2 y}{\partial t^2}$) represents the inertial force in potential flow past the cantilever, and $b\frac{\partial y}{\partial t}$ is the dissipative force due to the viscous drag. Where y, x, and f represent beam deflection, longitudinal position, and force amplitude; b is the damping coefficient due to the viscous liquid and intrinsic structure of the cantilever. The intrinsic damping coefficient may come in part from the epoxy/glue between the active layer and inactive layer (e.g. PZT and stainless steel for piezoelectric MC) and other internal dissipation mechanisms. Here, we just consider the influence of viscous liquid on the cantilever and ignore the damping from the internal structure.

Under the assumption of a beam structure with $W >> h$, the apparent Young's modulus is given by $E' = \frac{E}{1-\sigma^2}$, where σ and E are Poisson's ratio and Young's modulus of the beam material, respectively. $I = \int_0^W \int_{-h/2}^{h/2} z^2 dz dy = \frac{1}{12}Wh^3$, is the moment of inertia for a rectangular beam. $M_C = \rho Wh$ and M_I represent the effective mass of cantilever beam and the induced mass respectively, where ρ is the specific mass density of the beam material. The induced mass M_I can either exist due to absorbing molecules on the surface or it describes the mass of molecules of the surrounding media that are accelerated by the vibration of the beam. This leads to a dependency of the resonance frequency on the resonance behavior in general from the surrounding media.

Solving Eq. (4-2) under the condition of resonance yields the eigenvalues for the damped angular resonance frequencies

$$\omega_{dn} = \left[\frac{\lambda_n^4 E' I}{(M_C + M_I)} - \frac{1}{4}\left(\frac{b}{(M_C + M_I)} \right)^2 \right]^{1/2} \tag{4-3}$$

$$\omega_{dn} \cong \left(\frac{\lambda_n^4 E' I}{(M_C + M_I)} \right)^{1/2} \cong \omega_n \left(1 - \frac{1}{2} \frac{M_I}{M_C} \right) \tag{4-4}$$

where ω_n is the nth order undamped angular resonance frequency, given by

$$\omega_n = 2\pi f_n = 2\pi \frac{\lambda_n^2 h}{L^2} \sqrt{\frac{E}{12\rho(1-\sigma^2)}} \tag{3-10}$$

For an oscillating sphere of an effective radius R in a liquid of density ρ_L and viscosity η both M_I and b have analytic expressions [8]

$$M_I = \frac{2\pi R^3}{3} \rho \left(1 + \frac{9}{2} \frac{\delta}{R} \right) \tag{4-5}$$

$$b = \frac{6\pi\eta R^2}{\delta} \left(1 + \frac{\delta}{R} \right) = 6\pi\eta R \left(1 + \frac{R}{\delta} \right) \tag{4-6}$$

Where $\delta_L = \sqrt{2\eta / \rho\omega}_{dn} = \sqrt{\eta / \pi\rho f_{dn}}$ (η is the viscosity of the surrounding liquid media, and f_{dn} is the resonance frequency in the medium) is the decay length in the liquid, which means the thickness of liquid molecules sticking on the cantilever.

For the relative frequency shift of the first-order resonance frequency we derive, combining Eqs. (3-10), (4-4), and (4-5)

$$\Delta f = -\frac{\pi R^3 \rho_L}{3\rho L W h} (1 + \frac{9}{2} \frac{\delta_L}{R}) f_0 \tag{4-7}$$

Where f_0 is the first-order resonance frequency of the cantilever without damping, as given by

$$S = \frac{\Delta f_n}{\Delta m} = \frac{\Delta f_n}{M_I} \cong \frac{f_n}{2M_C} (M_I << M_C) \tag{3-18}$$

For relative low viscosity or high frequency ($\delta_L << R$), Eq. (4-7) can be simplified to Eq. (4-8).

$$\Delta f \approx -\frac{\pi R^3 \rho_L}{3\rho LWh} f_0 \tag{4-8}$$

The Q value can be expressed as [13]:

$$Q = \frac{(M_C + M_I)\omega_{dn}}{b/L} \tag{4-9}$$

Here ω_{dn} is the damped angular resonance frequency.

Since $M_C >> M_I$, we ignore the contribution of the induced mass to the Q value, Eq. (4-4) can be simplified to $\omega_{dn} \approx \omega_n$. Based on this, we can combine Eqs. (4-6) and (4-9), and finally obtain the Q value of a vibrating beam in the viscous region, approximated by an oscillating sphere with radius R

$$Q = \frac{\lambda_n^2 Wh^2 \sqrt{\rho E/12(1-\sigma^2)}}{6\pi\eta RL(1+R/\delta_L)} \tag{4-10}$$

This result indicates an increasing Q value with decreasing length or increasing resonance frequency.

For relatively low viscosity or high frequency ($\delta_L/R<<1$), the effect of the second term on the right-hand of Eq. (4-10) is negligible so that Eq. (4-11) is obtained,

$$Q \approx \frac{\lambda_n^2 Wh^2 \sqrt{\rho E/12(1-\sigma^2)}}{6\pi\eta RL}\frac{\delta_L}{R} \propto \frac{\delta_L}{\eta} \propto \sqrt{1/\rho\eta f_{dn}} \tag{4-11}$$

Q value is an important parameter in the resonance characteristics of a cantilever. A higher Q value indicates a smaller minimum detectable frequency change and therefore a better resolution (sensitivity) of the sensor system.

4.3 Materials and methods

4.3.1 Measurement set-up

4.3.1.1 In vacuum

The resonant behavior of MSMCs in air at different pressures was investigated at room temperature. In this experiment, the pressure of the test chamber was obtained by a Varian SD-300 mechanical pump and monitored using a Varian multi-Gauge. As shown in Figure 4-3, a three-way control valve, which connected the mechanical pump, thermal couple sensor, and the test chamber containing the MSMC, was employed to maintain a given pressure. After the pressure reached the designated pressure and was maintained about 10 minutes, then the resonance behavior of the MSMC was measured.

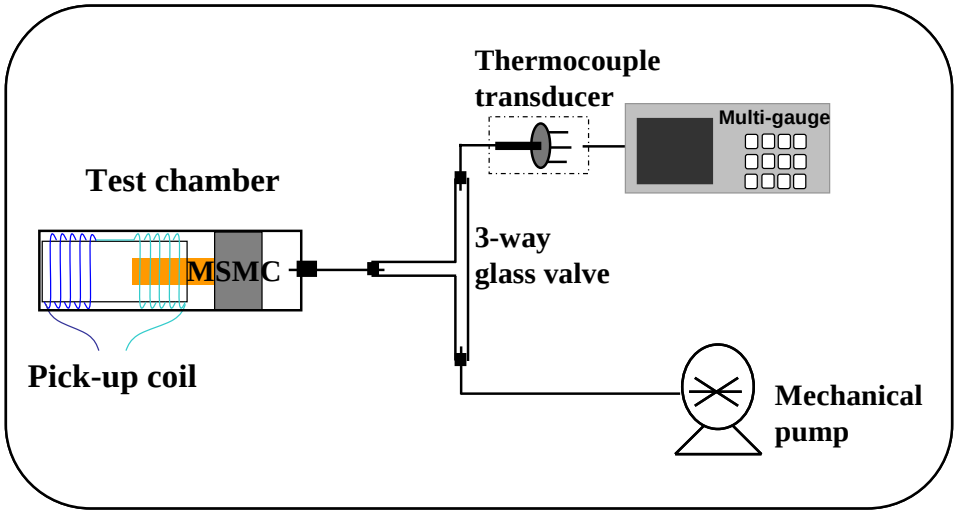

Figure 4-3. The scheme of measurement set-up in vacuum.

4.3.1.2 In liquids

As shown in Figure 4-4, the experimental setup consisted of a Helmholtz coil, lock-in amplifier, a computer-based output system, and a test chamber maintained at about 20^{o}C. A cleaned MSMC sensor was put into the test chamber containing the test liquid. The lock-in amplifier was connected to the pick-up coil interfaced to a data

acquisition PC for obtaining amplitude and phase angle measurements.

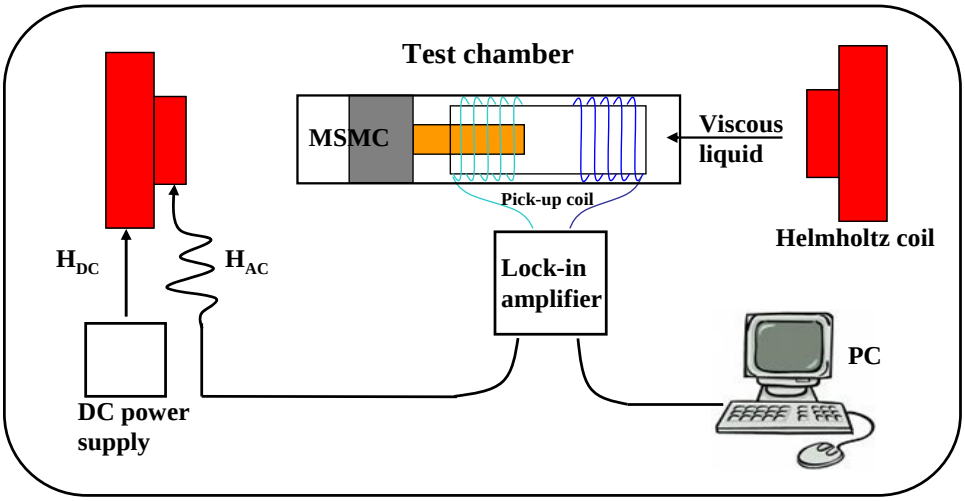

Figure 4-4. The schematic of measurement set-up in liquids.

4.3.2 Design of MSMC sensor dimensions

Table 4-1. MSMCs were used to measure the resonance behavior in vacuum and in liquids.

Sample	Length mm	Width mm	Thickness μm	Theoretical frequency (0^{th} harmonic) Hz
1	4	1	35	1293
2	3	1	35	2298
3	2	1	35	5171
4	1	1	35	10342
5	3	0.3	35	2298
6	3	0.6	35	2298
7	2	1.5	35	5171
8	4	0.75	35	1293

To characterize the effect of MSMC geometry on the resonant behavior, MSMC having different length with same width, different width with same length and the same area (length x width) were designed in this research. The size dimensions and the theoretical resonant frequencies from Eq. (3-11) of these samples were listed in Table 4-1.

4.3.3 Selection of liquid reagents

4.3.3.1 Glycerol/water mixture system

The glycerol/water mixture system was frequently employed to determine the density or viscosity of liquids by using cantilevers [14-16]. The reason why we choose glycerol/water mixture is that glycerol and water can dissolve each other completely to obtain uniform solution.

Table 4-2. The viscosity and density of glycerol/water mixture system was measured by Viscometer and Tensiometer at 20 ^{o}C.

Sample	Ratio of water : glycerol vol%	Density x Viscosity (cp • g/cm^3)	Density (g/cm^3) (at 20 ^{o}C)	Viscosity (cP) (at 20^{o}C)
1	100:0	1.011	0.9982	1.012
2	95:5	1.225	1.014	1.208
3	90:10	1.718	1.030	1.669
4	85:15	2.029	1.046	1.940
5	80:20	2.690	1.067	2.520
6	75:25	2.963	1.074	2.760
7	70:30	3.890	1.094	3.556
8	60:40	5.513	1.113	4.950
9	50:50	10.90	1.147	9.502

The test samples were deionized water and various concentration of glycerol solutions prepared in deionized water as shown in Table 4-2. The percentages of glycerol in water/glycerol mixture system used here are 5 vol%, 10 vol%, 15 vol%, 20 vol%, 25 vol%, 30 vol%, 40 vol%, and 50 vol% respectively. The viscosities and densities of various glycerol concentration solutions were also listed in Table 4-2. The density of each test sample was measured by using Sigma 702 Tensiometer, while the product of viscosity and density was measured by using Viscoliner 1710 Series Viscometer. Thus, we can obtain the viscosity for each test sample solution. Figure 4-5 gives the densities of various glycerol/water solutions from the measurement and calculation which based on

the assumption of no volume change before and after mixture of water and glycerol. In Figure 4-5, there is very small deviation of the experiment data from the calculation data, which means not obvious volume change before and after mixing. We can simply use the densities from the calculation (assuming no volume change).

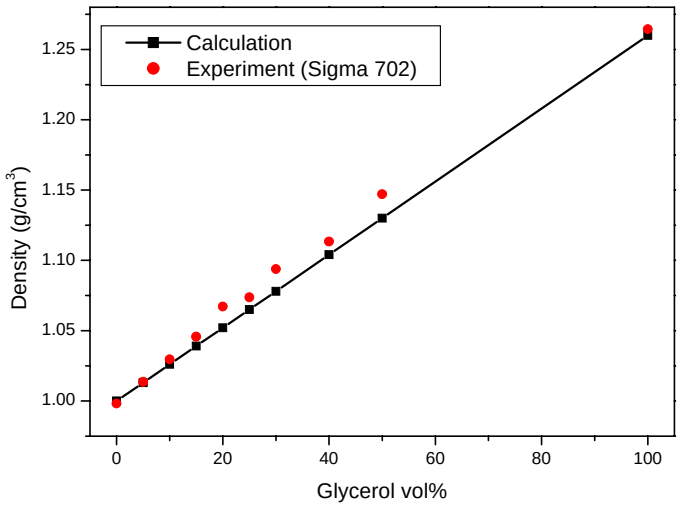

Figure 4-5. The density vs. the percentage of glycerol in glycerol/water mixture system. The black squares represent the value from the calculation which based on no volume change after mixture. The red dots represent the experiment data which measured by Tensiometer.

4.3.3.2 Several organic solvents

To determine the influence of the surrounding liquid media on the resonance behavior of an MSMC, the device was characterized in six different solvents including water, ethanol, methanol, 2-propanol, hexane and ethylene glycol. The densities and viscosities of these liquid media at room temperature (20 ^{o}C) were listed in Table 4-3. In all these experiments, the MSMCs were completely immersed in liquid.

Table 4-3. Density and viscosity of liquids at 20°C from the literature [17].

	Density (g/cm^3) (at 20 °C)	Viscosity (cP) (at 20°C)
Water	1.000	1.0
Ethanol	0.7893	1.22
Methanol	0.7914	0.59
2-propanol	0.7855	2.27
Hexane	0.6548	0.31
Ethylene glycol	1.1088	21.0

4.4 Results and discussions

4.4.1 Resonance behavior in vacuum

The damping in air is profound due to the complicated dynamics between the coupling of structure and airflow; it is still a challenge to establish the analytical model to predict the Q value of MSMC. Some simplified analytical approaches have been reported to estimate Q value instead. For example, Newell [18] has applied Stoke's law to yield the Q value for the first harmonic peak, as given in

$$Q_{Newell} = \frac{1}{24}\frac{Wh^2\sqrt{\rho E}}{\eta L^2} \tag{4-12}$$

Furthermore, Hosaka and Itao have also employed the string of oscillating spheres model and the equation is presented as follows [19]

$$Q_{Hosakal} \cong 0.22\frac{Wh^2\sqrt{\rho E}}{\eta L^2} \tag{4-13}$$

which is the similar as Q_{Newell}. Therefore, for cantilever in air, Q value changes with the geometry of the cantilever, harmonic mode and the viscosity is given by

$$Q \propto \frac{\lambda_n^2 Wh^2}{\eta L^2} \tag{4-14}$$

While it is the same as the behavior of cantilever in the viscous liquid media, as shown in Eq. (4-11). Eq. (4-14) shows that the Q value is linearly dependent on the reciprocal of

the viscosity. It is also indicated that the Q value is strongly dependent on the geometry of the cantilever. That is, the Q value increases with decreasing length, while it increases with increasing thickness and width. Therefore, if an MSMC with smaller length is used, the Q value would be higher than what is reported here. For a damped cantilever, the oscillation reaches a maximum at a frequency, apparent resonance frequency (f_r), lower than the real resonance frequency (f_n) as [20]

$$f_r = f_n\sqrt{1-\left(4Q^2\right)^{-1}} < f_n \qquad (4\text{-}15)$$

To determine the damping effect of air on the MSMC experimentally, the resonance behavior of MSMCs was characterized in air at different pressures.

A set of experimental results about the pressure dependence of the resonance behavior is shown in Figure 4-6(a), in which an MSMC in the size of 3.0 mm x 1.0 mm x 35 μm was used. The corresponding characteristic frequency and Q value of the MSMC at each pressure are plotted in Figure 4-6 (b), in which the normalized characteristic frequency and the normalized Q value are used. The normalized characteristic frequency is the characteristic frequency of the MSMC at a given pressure divided by the characteristic frequency (f_0) of the MSMC at one atmosphere pressure, while the normalized Q value is the Q value of the MSMC at the pressure divided by the Q value of the MSMC at one atmosphere pressure.

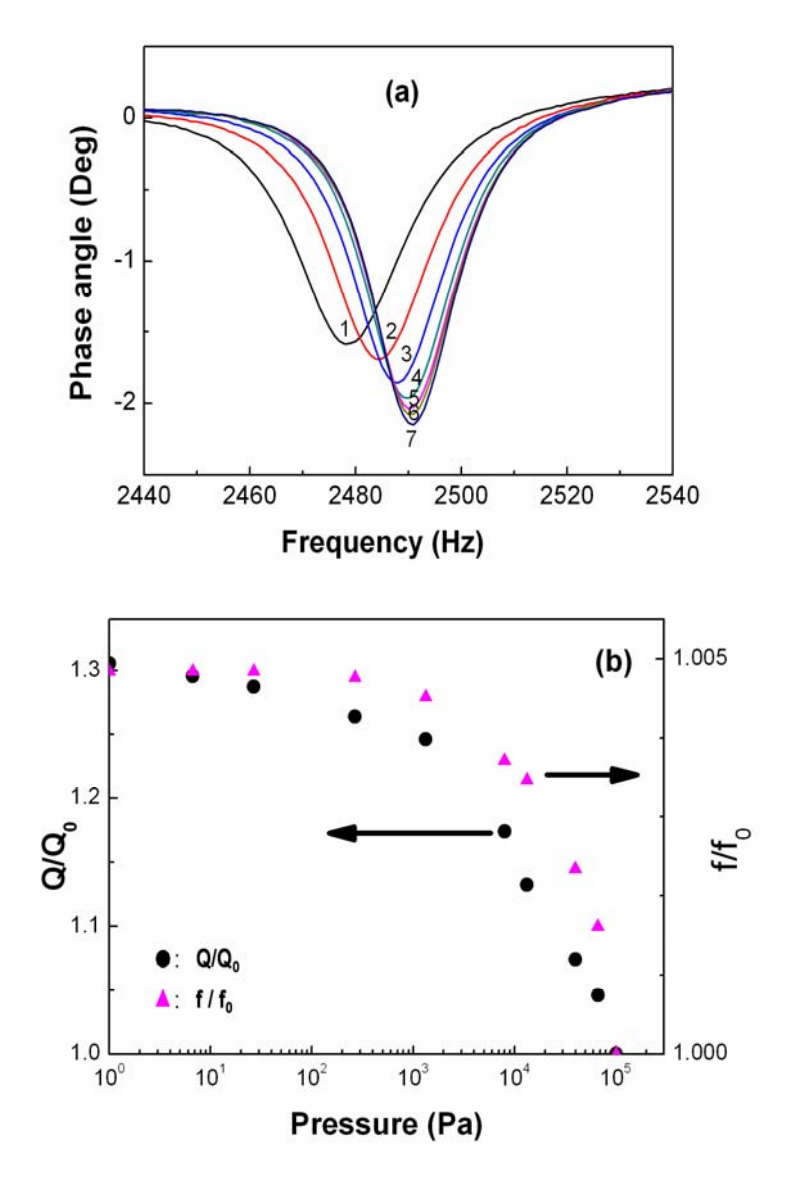

Figure 4-6. (a) The resonance behaviors of an MSMC in size of 3.0mm x 1.0mm x 35μm at room temperature in air at different pressures: 1). 1.0 x 10^5 Pa; 2). 8.0 x 10^4 Pa; 3). 4.0 x 10^4 Pa; 4). 1.0 x 10^3 Pa; 5). 1.0 x 10^2 Pa; 6). 1.0 x 10^1 Pa; 7). 1.0 x 10^0 Pa. (b) The normalized Q value (Q/Q_0) (Solid Circle) and normalized resonant frequency (f/f_0) (Solid Triangle) as a function of air pressure. The Q_0 and f_0 represent the Q value and characteristic frequency of the MSMC at one atmosphere pressure.

As shown in Figure 4-6 (a), the characteristic frequency increases as the pressure decreases. The characteristic frequency of the MSMC is 2478 Hz at one atmosphere pressure (1.0 x 10^5 Pa) and 2491 Hz at 1 Pa. As expected from Eqs. (4-14) and (4-15), both the resonance frequency and the Q value of the MSMC change with pressure. For the pressure above 10^3 Pa, the characteristic frequency and the Q value are strongly dependent on the pressure. When the pressure is lower than 100 Pa, the characteristic frequency is almost independent on the pressure, but the Q value continuously increases with lowering pressure. This is easy to understand based on Eqs. (4-14) and (4-15). Based on Eq. (4-14), the Q value is directly related to the viscosity, which is related to the pressure. However, when the pressure is very low at which the MSMC exhibits a high Q value, Eq. (4-15) indicates that the frequency is very weakly dependent on the Q value. For MSMCs at low pressures, the Q value is mainly determined by the anchor effect due to the fact that the PMMA used as a holder has a much smaller Young's modulus than the cantilever beam [21]. This conclusion might be verified by another theoretical model as described below [22].

Under atmospheric pressure, air damping is the predominant mechanism for energy dissipation [23]. However, Air damping becomes less effective while the pressure goes down, and then it is easier to identify the effects of other energy dissipation mechanisms. Q value dependence on pressure can be calculated using Eqs. (4-10), or (4-12) and (4-13), in which can not give satisfied solution to air damping in full pressure range because it based on viscous approximation [22]. Therefore, there are some new assumptions given. Blom et al. provided a superposition of damping mechanisms which based on the pressure range from vacuum to atmospheric pressure can be divided into

three regions: the intrinsic, the molecular, and the viscous region [22, 24-25]. In the viscous region, the air damping acts as a viscous fluid and the drag force must be calculated using fluid mechanics. Thus, Q value can be obtained from Eq. (4-10). When pressure reduced into the molecular region, the damping is caused by independent collisions of noninteracting air molecules with the moving surface of the vibrating beam. In this region the drag force can be determined by means of the kinetic theory of gases [24]. And Q value can be given

$$Q = \frac{\lambda_n^{\,2}}{k_m}\left(\frac{h}{L}\right)^2\left(\frac{\rho E}{12(1-\sigma^2)}\right)^{1/2}\frac{1}{p} \qquad (4\text{-}16)$$

where $k_m = (32M/9\pi RT)^{1/2}$. For air molecular, M equals 28.964 g/mol, so at room temperature (300K), $k_m = 3.6*10^{-3}\,s/m$.

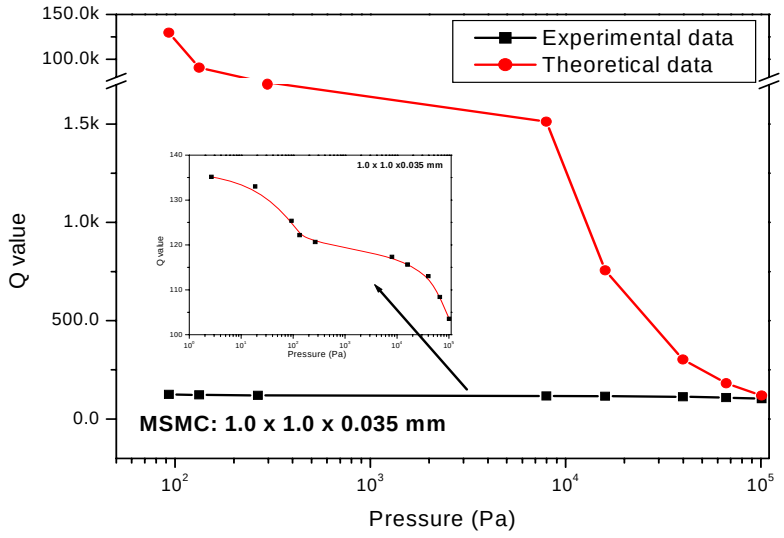

Figure 4-7. Measured and theoretical calculated Q values of the MSMC under various pressures. The theoretical prediction of the dependence of Q value on pressure when the air damping in the molecular region by using Eq. (4-16).

In the intrinsic region air pressure is so low that air damping is negligible compared to the intrinsic damping of vibrating beam itself. In this region, both characteristic frequency and Q value are independent of air pressure and beam geometry and Q value reaches a maximum value.

Based on the Eq. (4-16), the theoretical Q values of the MSMC in size of 1.0 x 1.0 x 0.035 mm were calculated under various pressures. The curves of experimental values and of theoretical values were drawn in Figure 4-7. Apparently, the calculated Q values are larger than the experimental data. Blom et al. reported this model is suitable for silicon cantilever. For MSMC, It indicated that unforeseen energy dissipation exists and this mechanism is comparable to other mechanism in the molecular region [22]. Based on Eq. (4-1), we might find that one of the reasons is the support loss, as we mentioned above. The other one might be inter-friction between each layer. Sekaric et al. studied the effects of thin metal films on energy dissipation in nano-scale silicon nitride mechanical resonators, and they found that the absence of Au/Cr deposition on the beam results in a three to four times higher Q value [26]. Thus, for MSMC, air damping is minor factor for Q value, compare to the other damping effects.

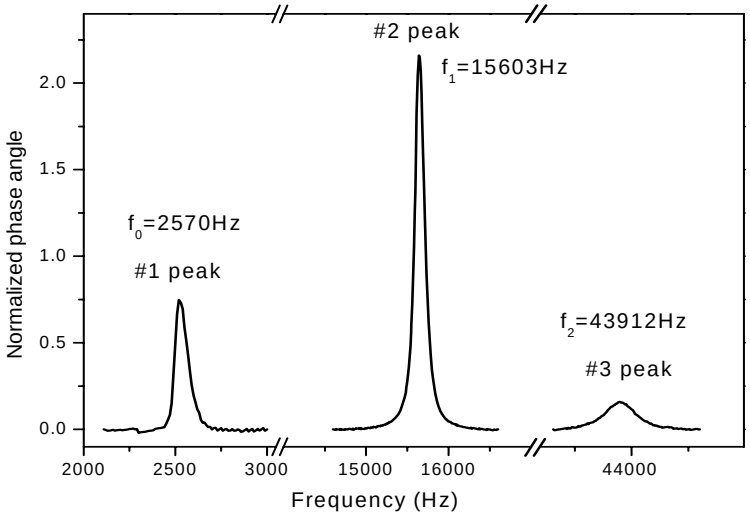

Figure 4-8. The first three harmonic peaks and their characteristic frequencies for the MSMC with the size of 3.0 mm x 1.0 mm x 35 μm.

Furthermore, based on Eq. (4-15), we can find the relationship between Q values and λ_n^2, which means the higher the resonance mode, the higher the Q value. To confirm this, a MSMC with the size of 3.0 mm x 1.0 mm x 0.035 μm was used and the first three resonance frequencies were shown in Figure 4-8. The resonance behaviors for the first three harmonic peaks were measured under various air pressures and the results were given in Figure 4-9.

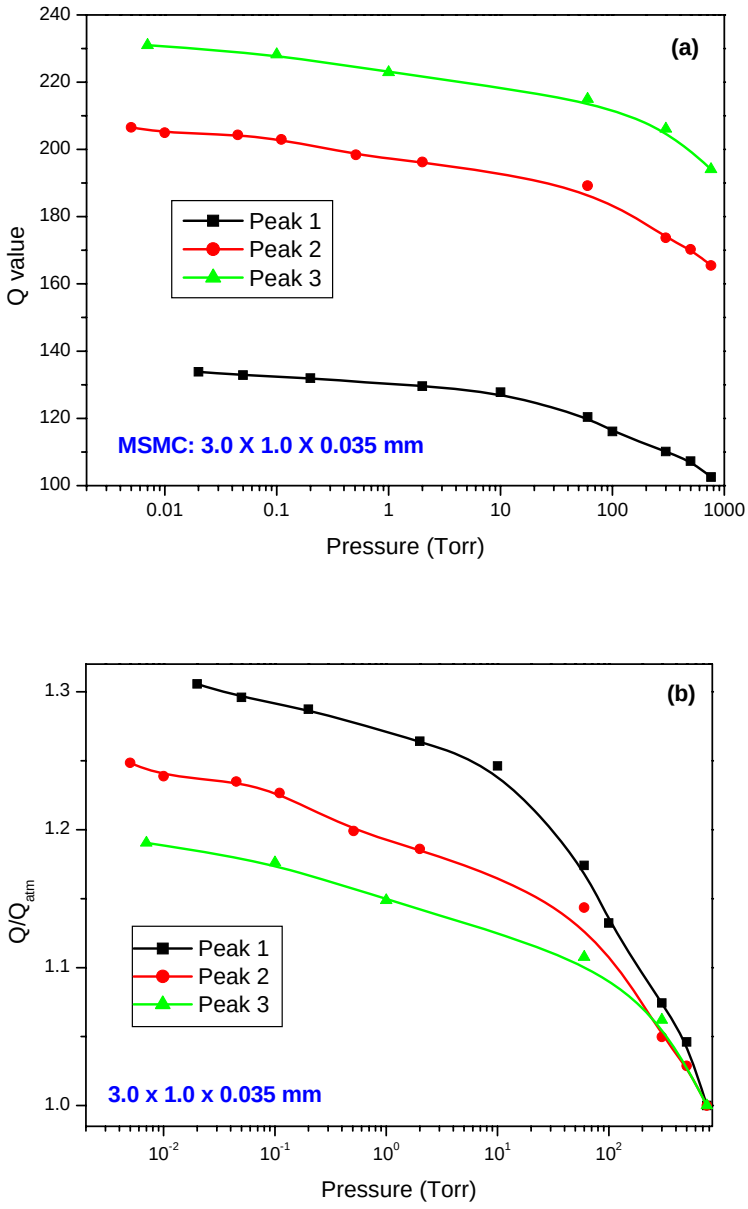

Figure 4-9. The Q value *vs.* pressure (a) and the Q/Q_{atm} *vs.* pressure (b) of the MSMC with the size of 3.0 x 1.0 x 0.035 mm for the first three harmonic peaks.

From Chapter 3, we know the dimensionless eigenvalues of the first three resonance mode are 1.875, 4.694, and 7.855 respectively. Clearly, as shown in Figure 4-9,

the Q value increases as the resonance mode increases under the same air pressure. As we know, the ratio of λ_1^2 over λ_0^2, and λ_2^2 over λ_1^2 are 6.27 and 2.80 respectively. Thus, the difference between the curves of Q value *vs.* pressure for the first mode resonance modes is bigger than that for the following two resonance modes. Additionally, when the mode number and the resonance frequency increased, the change of the Q value became smaller, which means the airflow damping decreased. It is good agreement with the experimental results as shown in Figure 4-9(b). Therefore, the MSMC operating higher resonance mode can improve the sensor's performance, and the total damping in higher modes converged towards internal and support damping.

4.4.2 Resonance behavior in liquids

4.4.2.1 Glycerol/water mixture system

An MSMC with the size of 2.9 x 1.0 x 0.035 mm was used in this experiment. The characteristic frequency and Q value are 2500 Hz and 150 in air respectively. The MSMC was immersed into the glycerol/water mixture system and the resonance behaviors were measured under various glycerol concentrations. The phase spectra obtained from glycerol/water mixture system were shown in Figure 4-10 (a). Since the raw curves have strong background noises, so we use PeakFit software to simulate the curve, and the fitting spectra were shown in Figure 4-10 (b). Clearly, as the viscosity of the liquid increases with the glycerol content, the height of the resonance peak progressively decreases and the peak is broaden, which further decrease Q value of the MSMC.

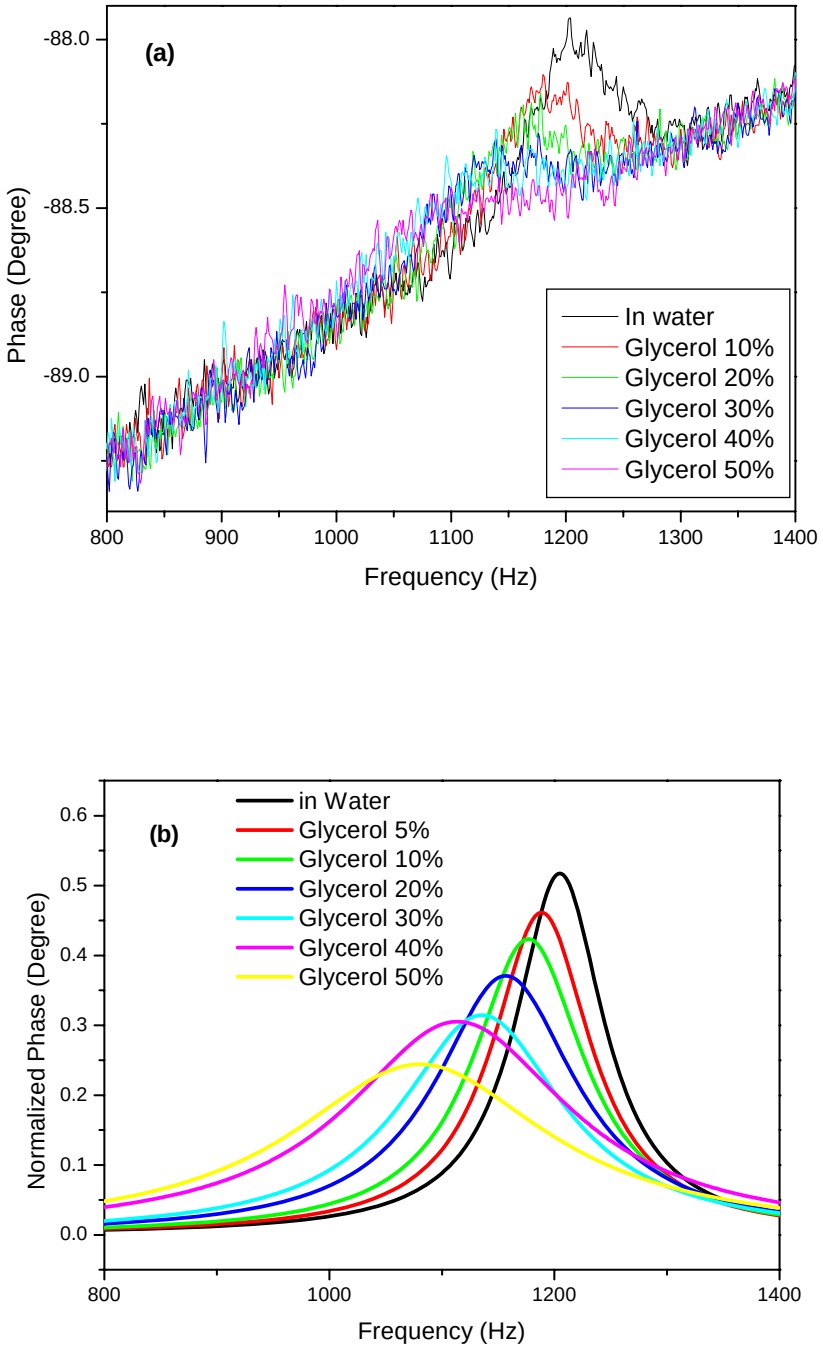

Figure 4-10. The phase spectrum *vs.* the percentage of glycerol in the glycerol/water mixture system. (a) the raw data; (b) the fitting data by using PeakFit software.

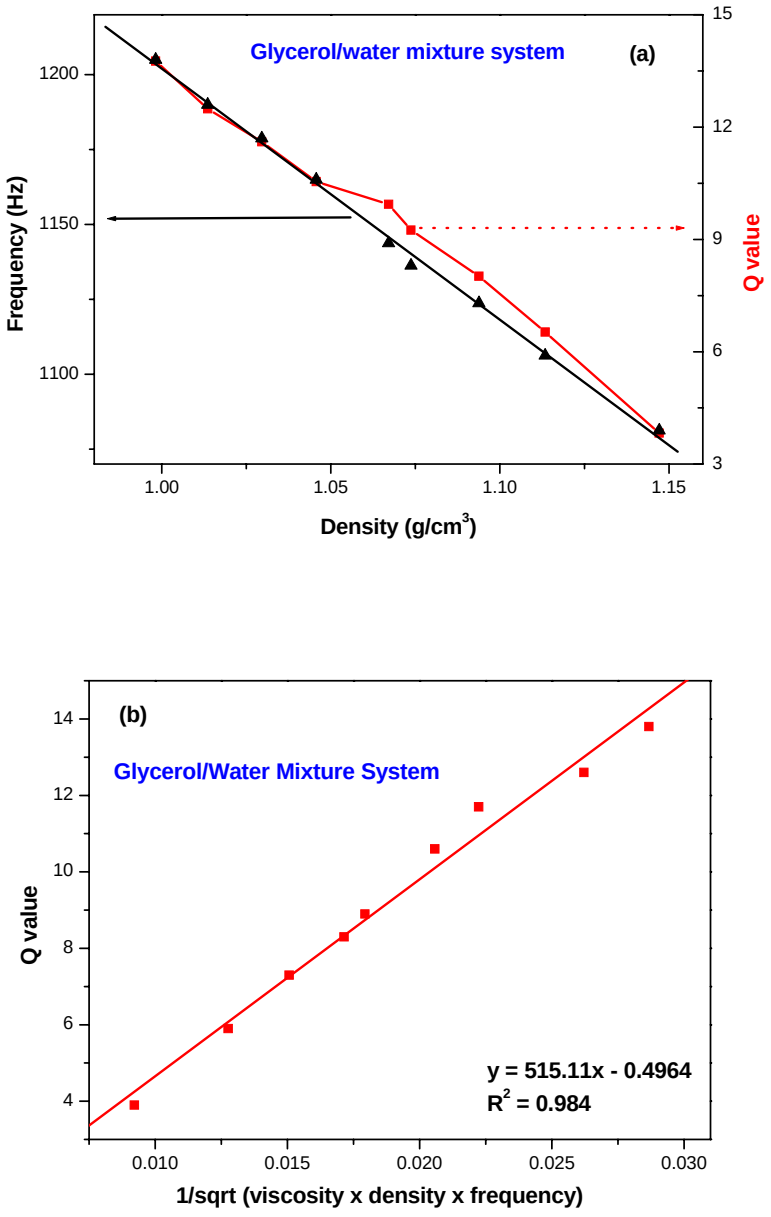

Figure 4-11. The density and viscosity dependence of characteristic frequency and Q value in the glycerol/water mixture system: (a) f_{d0} and Q *vs.* ρ and (b). Q *vs.* $1/\sqrt{\eta\rho f_{dn}}$. The solid line is the linear fitting results of the original experimental data.

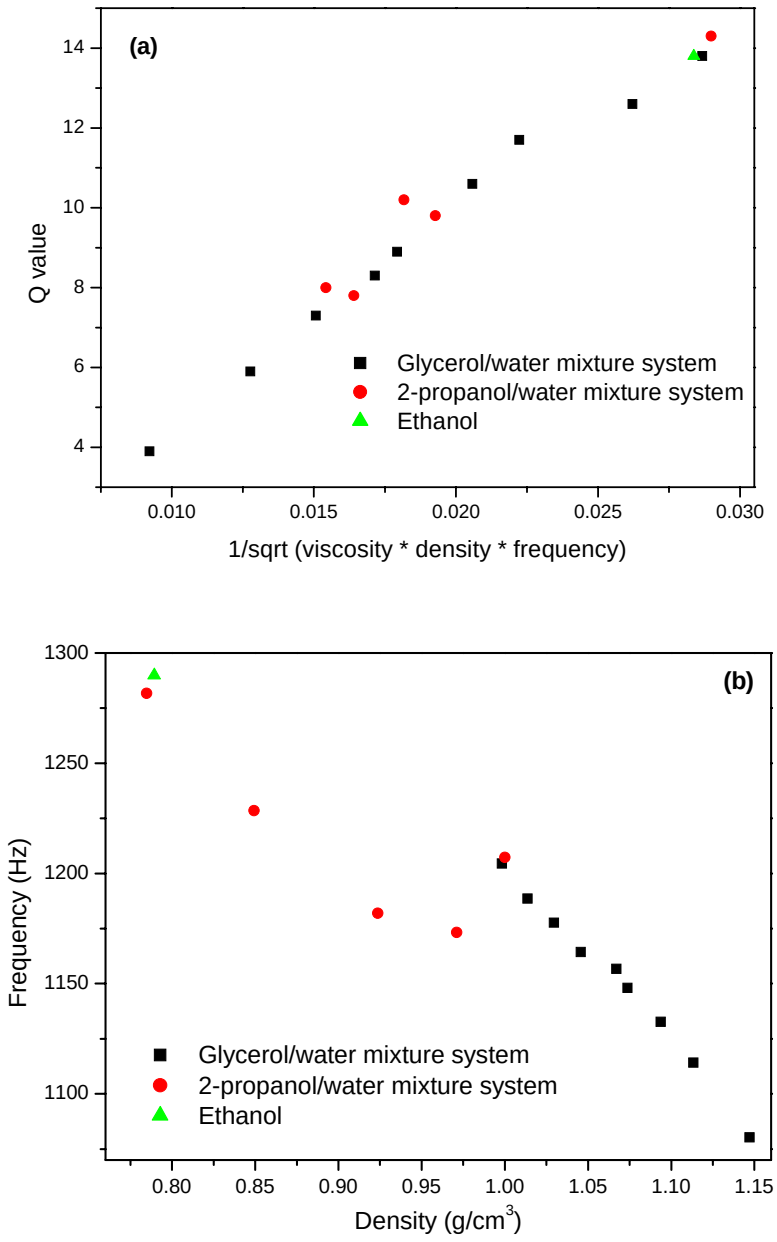

Figure 4-12. The dependence of Q value on the viscosity of the liquid media (a) Q *vs.* $1/\sqrt{\eta\rho f_{dn}}$ for the different mixture systems. The dependence of resonance frequency on the density of the liquid media (b) f_{dn} *vs.* ρ for several liquid media.

To determine the influence of viscosity and density on the resonance behavior, the spectra of characteristic frequency and Q value vs. density and viscosity of glycerol/water mixture system were plotted and shown in Figure 4-11 by combining Figure 4-10 and Table 4-2. Figure 4-11 (a) and (b) showed the density dependent and viscosity dependent characteristic frequency and Q value respectively. In Figure 4-11 (a), we can find the good linear relationship between characteristic frequency and density, and the different case for Q value. To examine the influence of liquid media on Q value, according to Eq. (4-11), the curve between Q value and viscosity was plotted in Figure 4-11 (b). The result indicated Q value was determined by the density and viscosity of the liquids, and the frequency of MSMC in the liquids. To examine the material properties of liquids on the resonance behavior of MSMC, two different solvents include methanol and 2-proponal were also used in this experiment. And the Q value *vs.* $1/\sqrt{\eta\rho f_{dn}}$, and frequency *vs.* ρ for these several systems were given in Figure 4-12 (a) and (b). Figure 4-12 (a) reveals the good linear relationship between Q value *vs.* $1/\sqrt{\eta\rho f_{dn}}$ was exhibited even in the different liquids. But for the density dependent frequency, the frequencies of MSMC in methanol and 2-proponal were deviated from the linear curve of MSMC in glycerol/water mixture system.

4.4.2.2 Several organic solvents

According to Eq. (4-7), the resonance frequency depends on the density of the liquid. As we discussed above, the influence from the viscosity drag must be considered, and the influence from the inertial part of the viscosity drag is negligible. Characteristic frequencies f_0 , were measured for several liquids, and are plotted as a function of density in Figure 4-10. The result shows good linear relationship between characteristic

frequency and density. The characteristic frequency decreased monotonically with an increase in density. It is accordance with Eq. (4-8). The measurement error of the characteristic frequency was about 80 Hz caused mainly be the relatively low Q value. The measured frequency responds only to the density, independent of the viscosity.

Eq. (4-8) indicates that the change in the frequency is linearly dependent on the density of the liquid. Eq. (4-11) shows that the Q value is inverse proportional to the square root of the product of the density and the viscosity of the liquid, and the resonance frequency in the liquid.

Table 4-4. The characteristic frequencies and Q values of MSMCs were used in the liquids measurement.

Sample	Length mm	Width mm	Thickness μm	Frequency Hz	Q value
1	4.0	1.0	35	1271.0	171.8
2	3.0	1.0	35	2297.9	104.9
3	2.0	1.0	35	5346.9	104.0
4	3.0	0.5	35	2096.3	101.8
2	3.0	1.0	35	2297.9	104.9
5	3.0	1.5	35	2290.5	148.7
6	4.0	0.75	35	1323.5	135.1
2	3.0	1.0	35	2297.9	104.9
7	2.0	1.5	35	5600.0	121.0

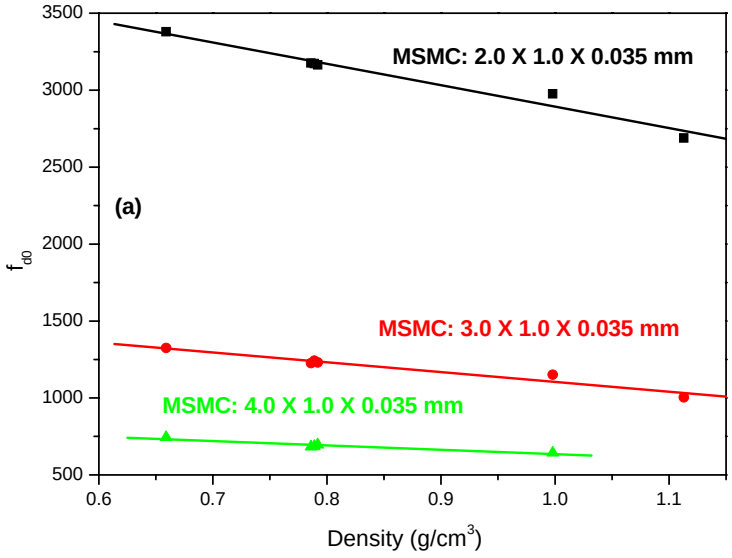
3500
3000
2500
2000
1500
1000
500
0.6
0.7
0.8
0.9
1.0
1.1
(a)
MSMC: 2.0 X 1.0 X 0.035 mm
MSMC: 3.0 X 1.0 X 0.035 mm
MSMC: 4.0 X 1.0 X 0.035 mm
f_d0
Density (g/cm3)

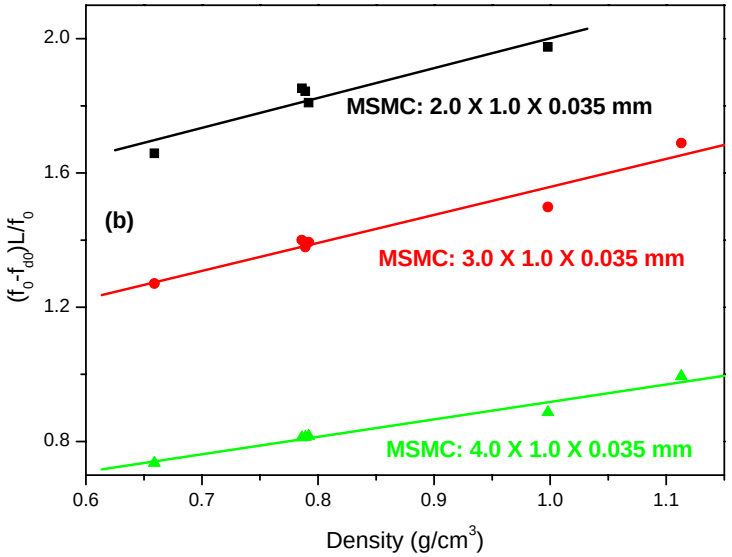
2.0
1.6
1.2
0.8
0.6
0.7
0.8
0.9
1.0
1.1
(b)
MSMC: 2.0 X 1.0 X 0.035 mm
MSMC: 3.0 X 1.0 X 0.035 mm
MSMC: 4.0 X 1.0 X 0.035 mm
(f0-fd0)L/f0
Density (g/cm3)

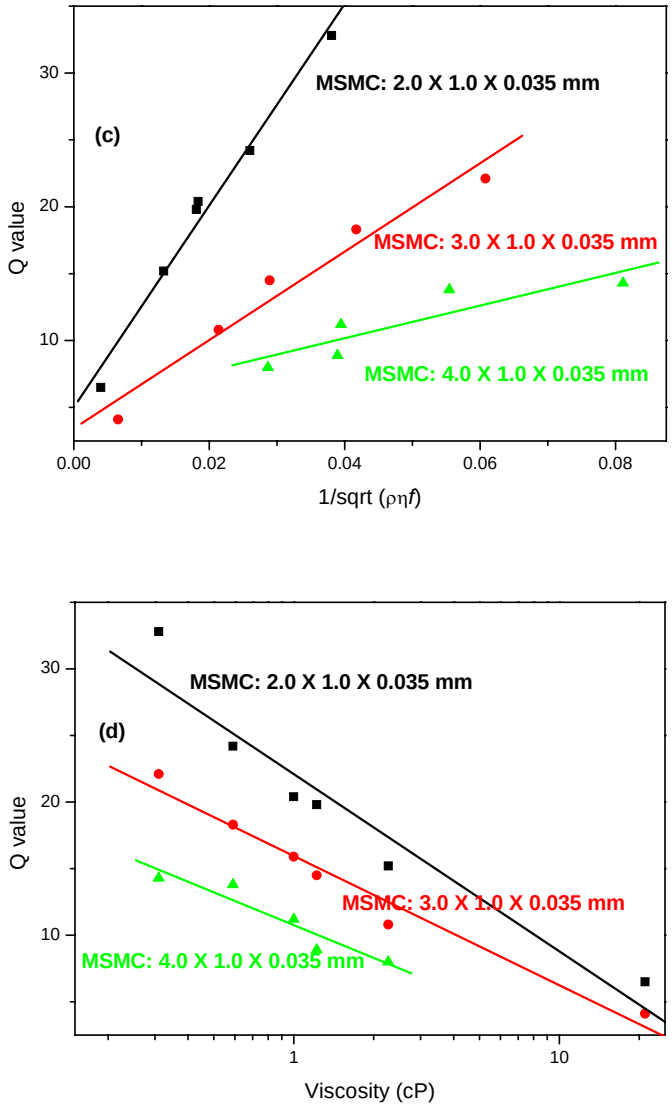

Figure 4-13. The dependence of the f_{d0} and Q value of three MSMCs with the same width (1.0 mm) and different length (4.0, 3.0, and 2.0 mm): (a) the f_{d0} vs. the density of the liquid media, (b) $(\Delta f / f) \bullet L$ vs. the density of the liquid media, (c) the Q value *vs.* $\sqrt{1/\eta\rho_L f}$, and (d) the Q value vs. the viscosity of the liquid media.

Figure 4-13 shows the characteristic frequencies and Q values of three MSMCs in different liquid media, where the density and viscosity of the media are used as the

independent variables. The three MSMCs have the same width (1.0 mm) but different lengths of 2, 3, and 4 mm, respectively. When operated in air, the three MSMCs, in the length of 2, 3, and 4 mm, exhibit the characteristic frequencies (f_0) of 5346.9, 2297.9, and 1271.0 Hz, and the Q values of 104.0, 104.9, and 171.8, respectively, as shown in Table 4-4. The results shown in Figure 4-13 (a) indicate that, when the whole MSMC was immersed in the liquid, the characteristic frequency of the MSMC is linearly dependent on the density of the liquid media, which is consistent with Eq. (4-8). Figure 4-13 (b) shows $(\Delta f / f) \bullet L$ versus the density of the liquids. The linear relationships shown in Figure 4-13(b) indicate that, for a given cantilever, the R value is constant regardless of the density and the viscosity of the liquids. This confirms the validity of the model used to evaluate the resonance behavior of the cantilever in viscous media. The data shown in Figure 4-13 (c) reveals that the Q value depended on the product of density, viscosity and frequency. As shown in Eq. (4-11), the Q value of an MSMC in liquid is proportional to $\sqrt{1/\eta\rho_L f}$. Also as indicated in by Eq. (4-10), the Q value of the MSMC increases with decreasing length. Considering the characteristic frequency linearly decreasing with the density of the liquid, the dependence of the Q value on viscosity can be further simplified as the Q value is approximately linearly dependent on the logarithm of the viscosity, as shown in Figure 4-13 (d).

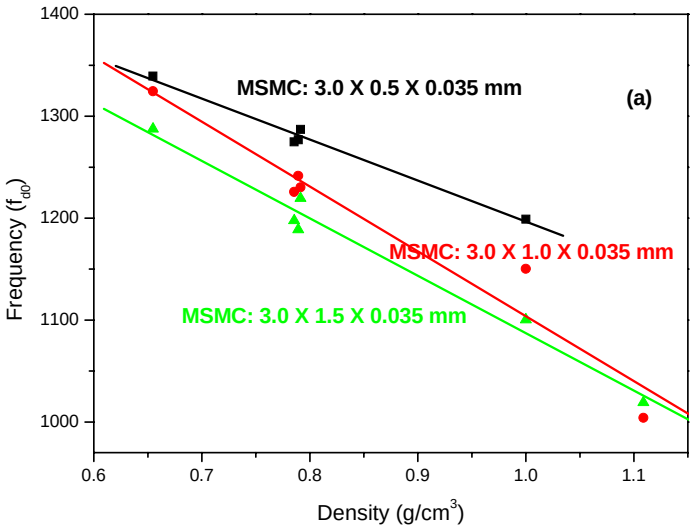
1400
1300
1200
1100
1000
0.6
0.7
0.8
0.9
1.0
1.1
Frequency (f_{d0})
Density (g/cm^3)
MSMC: 3.0 X 0.5 X 0.035 mm
(a)
MSMC: 3.0 X 1.0 X 0.035 mm
MSMC: 3.0 X 1.5 X 0.035 mm

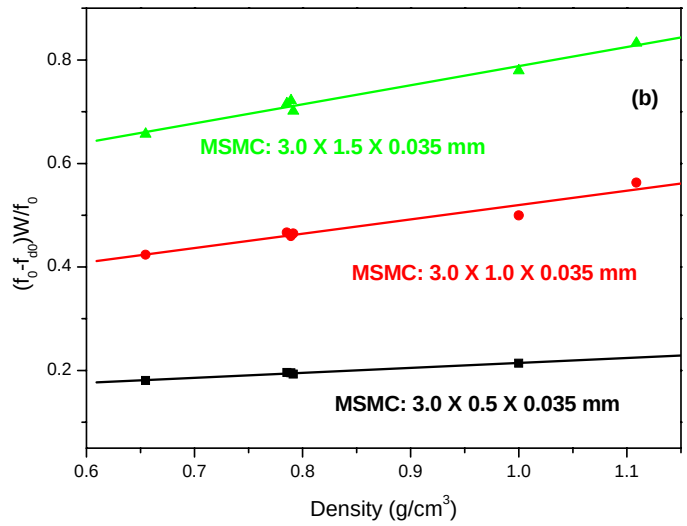
0.8
0.6
0.4
0.2
0.6
0.7
0.8
0.9
1.0
1.1
$(f_0-f_{d0})W/f_0$
Density (g/cm^3)
(b)
MSMC: 3.0 X 1.5 X 0.035 mm
MSMC: 3.0 X 1.0 X 0.035 mm
MSMC: 3.0 X 0.5 X 0.035 mm

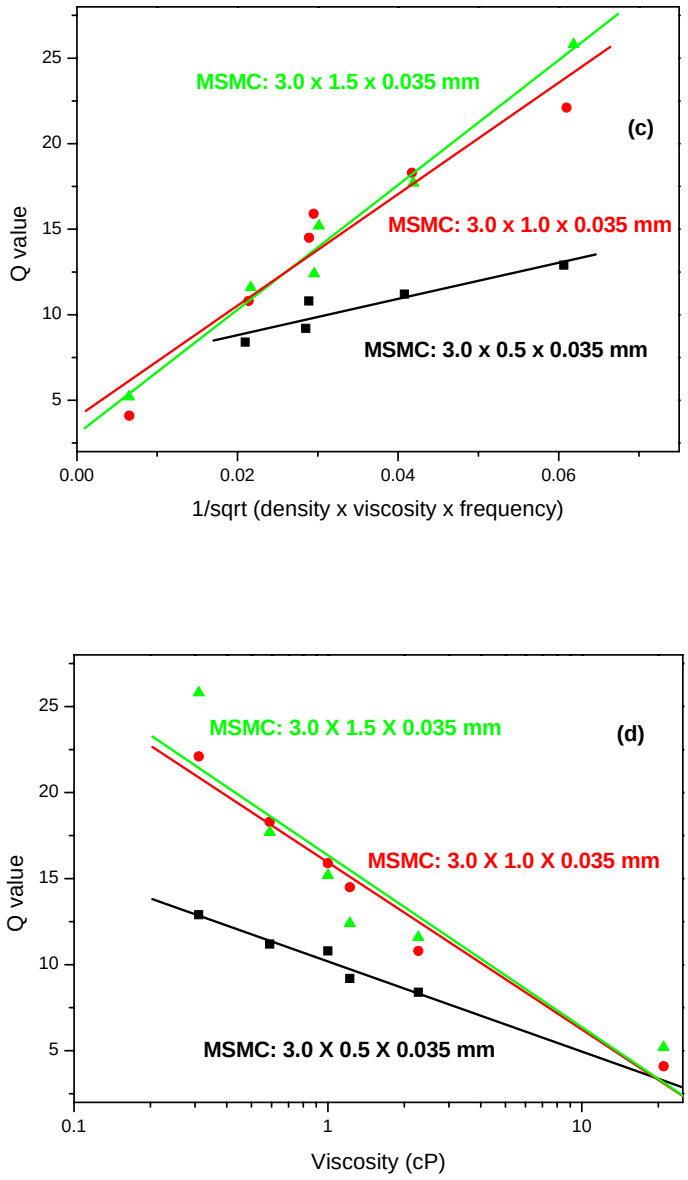

Figure 4-14. The dependence of the f_{d0} and Q value of three MSMCs with the same length (3.0 mm) and different width (1.5, 1.0 and 0.5 mm): (a) the f_{d0} vs. the density of the liquid media, (b) $(\Delta f / f) \bullet W$ vs. the density of the liquid media, (c) the Q value *vs.* $\sqrt{1/\eta\rho_L f}$, and (d) the Q value vs. the viscosity of the liquid media.

Figure 4-14 shows the other size effect (width change) on the characteristic frequencies and Q values of three MSMCs in different liquid media, where the density and viscosity of the media are used as the independent variables. The three MSMCs have the same length (3.0 mm) but different widths of 0.5, 1.0, and 1.5 mm, respectively. When operated in air, the three MSMCs, in the width of 0.5, 1.0, and 1.5 mm, exhibit the characteristic frequencies of 2096.3, 2297.9, and 2290.5 Hz, and the Q values of 101.8, 104.9, and 171.8, respectively, as shown in Table 4-4. While the width of the MSMC increases, the characteristic frequency decreases and Q value increases for the MSMC in the same liquid media, as shown in Figure 4-14 (a) and (d). The results also showed the size effect is not obvious while the width of the MSMC is above 1.0 mm. It indicated that there is an optimal ratio of length over width of MSMC. Below the optimal ratio, the Q value can be no more improved. Here the ratio is about 2. Furthermore, it should be mentioned that, since the plastic (PMMA) holder has a strong anchor effect (support loss) on the MSMC [21], the Q values reported here are actually the results of two different damping effects - anchor effect and media effect. Therefore, if a stiff material is used to build the holder, the Q value of the MSMC would be higher.

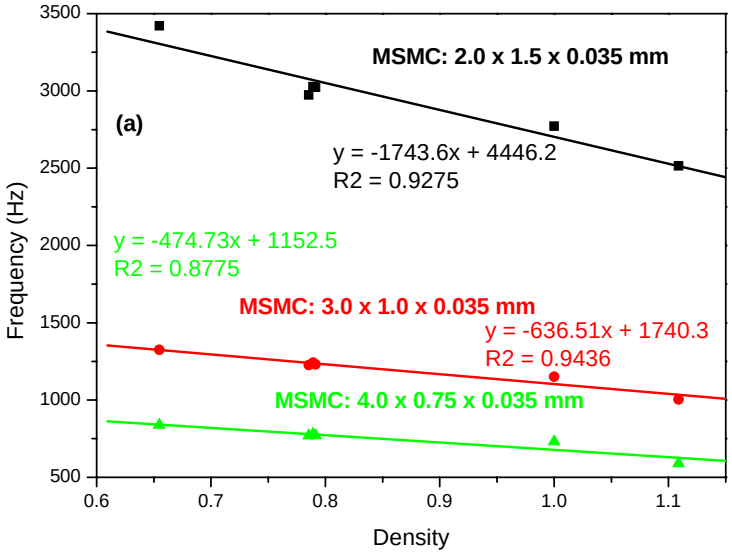

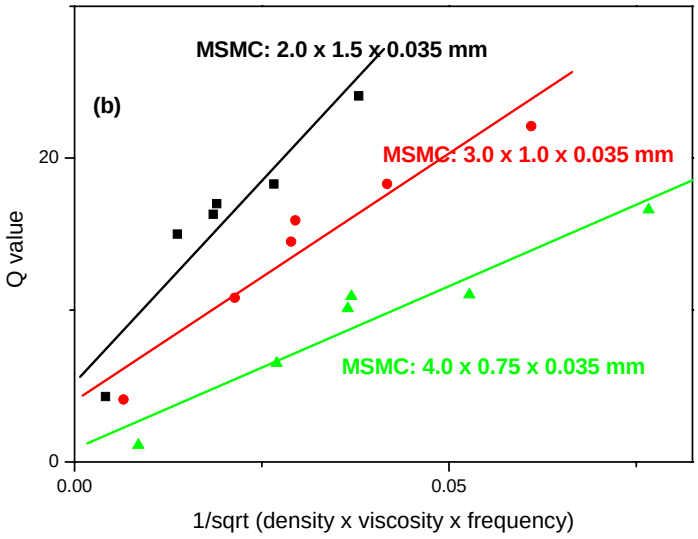

Figure 4-15. The dependence of the f_{d0} and Q value of three MSMCs with the same cross-section area (2.0 mm x 1.5 mm, 3.0 mm x 1.0 mm and 4.0 mm x 0.75 mm): (a) the f_{d0} vs. the density of the liquid media, (b) the Q value *vs.* $\sqrt{1/\eta\rho_L f}$. The thickness for all the MSMCs is 35 μm.

To obtain empirically the effect radius R of this model, the slopes of the linear fitting curves (Q *vs.* $\sqrt{1/\eta\rho_L f}$) were given in the second column on Table 4-5.

Table 4-5. The effective radius obtained from the experiment (Eq. (4-18)) and the cross-section approximation (Eq. (4-19)).

Size of MSMC L x W x h (mm)	Slope (κ) Figure ⟺	Slope (κ) Calculate	R (mm)	R_{appr} (mm)	$1-\frac{R_{appr}}{R}$
2.0 x 1.0 x 0.035	753.2	$560.1/R^2$	0.862	0.798	7.4%
3.0 x 1.0 x 0.035	330.3	$373.4/R^2$	1.063	0.977	8%
4.0 x 1.0 x 0.035	121.9	$280.1/R^2$	1.516	1.129	25%
3.0 x 0.5 x 0.035	115.9	$186.6/R^2$	1.269	0.691	45%
3.0 x 1.0 x 0.035	330.3	$373.4/R^2$	1.063	0.977	8%
3.0 x 1.5 x 0.035	365.8	$560.1/R^2$	1.237	1.197	3.2%
2.0 x 1.5 x 0.035	531.82	$840.1/R^2$	1.256	0.977	22%
3.0 x 1.0 x 0.035	330.3	$373.3/R^2$	1.063	0.977	8%
4.0 x 0.75 x 0.035	214.52	$210/R^2$	0.989	0.977	1.2%

We also can calculate the theoretical slopes of the MSMCs with different dimension from Eq. (4-11) as follows,

$$\kappa = \frac{\lambda_n^2 W h^2 \sqrt{\rho E/12\pi(1-\sigma^2)}}{6\pi R^2 L} \qquad (4\text{-}17)$$

where λ_0 =1.875, for the first harmonic mode.

And the results were listed in the third column on Table 4-5. By combining the results in the second and third column, we can obtain the effective radius of oscillating sphere for various lengths of MSMCs and it can be given

$$R = \sqrt{\frac{\lambda_n^2 W h^2 \sqrt{\rho E/12\pi(1-\sigma^2)}}{6\pi L \kappa}} \qquad (4\text{-}18)$$

The effective radius R for various lengths of MSMCs were calculated and listed in the

fourth column on Table 4-5. These results were compared with a relationship derived from the equivalent cross-section approximation [27]

$$R_{appr} = \sqrt{\frac{WL}{\pi}} \tag{4-19}$$

in which the cross-section area of the equivalent sphere is identical to that of the cantilever surface area (WL).

Based on Eq. (4-19), for the same cross-section area of the different MSMCs, the effect radius R should be very close to each other. However, as shown in Figure 4-15, the slopes for the MSMCs with different dimensions are not similar. One of the reasons might be the cross-section area is not exactly the same since we cut the cantilever beams by hand.

For the cantilevers with the length-to-width ratio are 2 or 3, the equivalent cross-section approximation provided completely good agreement with our measured results. The vibrating sphere model with an equivalent cross-section approximation can be considered a good tool for cantilevers of such dimensions. On the other hand, the agreement for cantilevers with the ratio of length to width is of 4:1 was not completely satisfactory. There was explicit difference of 25% between the calculated and measured values. The difference may have been caused by the support loss effect of cantilevers.

4.5 Conclusions

The resonance behaviors of MSMCs in air and reduced air (vacuum) were investigated. Several theoretical analyses indicated that the Q value is size, mode and viscosity dependent as shown in Eq. (4-14). And this result was confirmed by experiments. The curves drawn by using experiment data exhibited a good linear

relationship between Q value and viscosity of surrounding air while the same MSMC with the same dimensions was used. The experiment data and the theoretical analysis both show that higher operating harmonic mode, higher Q value. Additionally, the damping of Q value at higher operating mode is not mainly from the surrounding media, but from the intrinsic damping and support loss.

On the basis of a damped string of oscillating spheres model of the MSMC, the viscosity dependent MSMCs in the surrounding media including air and liquids have been theoretically investigated. The experimental data were fitted by using the equations derived from the model and exhibited good linear relationship. The experimental results and the theoretical analysis both show that the frequency is density dependent and Q value is viscosity dependent.

We also obtained the effect radius R of an oscillating sphere in this model. The effect radius R exhibited a good agreement with the one estimated by using the cross-section area approximation when the length-to-width ratio is about 2~3.

References

1. B.J. Lazan, 1968, Damping of materials and members in structural mechanics, Pergamon Press, New York.
2. C.M. Harris, C.E. Crede, eds., 1976. Shock and vibration Handbook, 2nd ed., McGraw-Hill, pp. 36.1-36.28.
3. E.A. Avallone, ed., 1987, Standard handbook for mechanical engineers, McGraw-Hill, New York, pp. 5-69.
4. Y. Jimbo, K. Itao, Energy loss of a cantilever vibrator, Journal of Japanese Horological Institute 47 (1968) 1-15.

5. J.W. Yi, W.Y. Shih, W.-H. Shih, Effect of length, width, and mode on the mass detection sensitivity of piezoelectric unimorph cantilevers, Journal of Applied Physics 91 (3) (2002) 1680-1686.
6. J.E. Sader, Frequency response of cantilever beams immersed in viscous fluids with applications to the atomic force microscope, Journal of Applied Physics 84(1) 1998 64-76.
7. G.Y. Chen, R.J. Warmack, T. Thundat, D.P. Allison, A. Huang, Resonance response of scanning force microscopy cantilevers, Rev. Sci. Instrum. 65(8) 1994 2532-2537.
8. L.D. Landau, E.M. Lifshitz, 1987. Fluid Mechanics 2nd Ed (Burlington: Elsevier Butterworth-Heinemann) pp 83-90. Oxford, England; New York: Pergamon Press.
9. S. Inaba, K. Akaishi, T. Mori, K. Hane, Analysis of the resonance characteristics of a cantilever vibrated photothermally in a liquid, Journal of Applied Physics 73 (6) (1993) 2654-2658.
10. S. Rast, C. Wattinger, U. Gysin, E. Meyer, Dynamics of damped cantilevers, Review of Scientific Instruments 71(7) (2000) 2772-2775.
11. K. Rijal, R. Mutharasan, Piezoelectric-excited millimeter-sized cantilever sensors detect density differences of a few micrograms/mL in liquid medium, Sensors and Actuators B: Chemical 124 (2007) 237-244.
12. J.H. Lee, S.T. Lee, C.M. Yao, W.L. Fan, Comments on the size effect on the microcantilever quality factor in free air space, Journal of Micromechanics and Microengineering 17 (2007) 139-146.
13. C. Ziegler, Cantilever-based biosensors, Analytical and Bioanalytical Chemistry 379 (7-8) (2004) 946-959.

14. N. Mcloughlin, S.L. Lee, G. Hahner, Simultaneous determination of density and viscosity of liquids based on resonance curves of uncalibrated microcantilevers, Applied Physics Letters 89 (18) (2006) 184106.1-184106.3.
15. W.Y. Shih, X.P. Li, H.M. Gu, W.H. Shih, I.A. Aksay, Simultaneous liquid viscosity and density determination with piezoelectric unimorph cantilevers, Journal of Applied Physics 89 (2001) 1497-1505.
16. T.L. Wilson, G.A. Campbell, R. Mutharasan, Viscosity and density values from excitation level response of piezoelectric-excited cantilever sensors, Sensors and Actuators A: Physical 138 (2007) 44-51.
17. C. Marsden, 1963. Solvents guide, Interscience Publishers, New York.
18. W.E. Newell, Miniaturization of tuning forks, Science 161(1968) 1320-1326.
19. H. Hosaka, K. Itao, Theoretical and experimental study on airflow damping of vibrating microcantilevers, Transactions of the ASME 121 (1999) 64-69.
20. W. Benenson, J.W. Harris, H. Stocker, H. Lutz, 2002. Handbook of Physics, New York, Springer-Verlag, 274.
21. S. Li, L. Orona, Z. Li, Z.-Y. Cheng, Biosensor based on magnetostrictive microcantilever, Applied Physics Letters 88 (7) (2006) 073507.
22. F.R. Blom, S. Bouwstra, M. Elwenspoek, J.H.J. Fluitman, Dependence of the quality factor of micromachined silicon beam resonators on pressure and geometry, J. Vac. Technol. B. 10 (1992) 19-26.
23. J. Lu, T. Ikehara, Y. Zhang, T. Mihara, R. Maeda, Mechanical quality factor of micro cantilevers for mass sensing applications, SPIE Microelectronics, MEMS, and Nanotechnology 2007, Austria, Dec 2007.

24. H.W. Drawin, Vakuum-Technik, 11 (1962) 45, in German.

25. W.E. Newell, Miniaturization of tuning forks, Science 161 (3848) (1968) 1320-1326.

26. L. Sekaric, D.W. Carr, S. Evoy, J.W. Parpia, H.G. Craighead, Nanomechanical resonant structures in silicon nitride: fabrication, operation and dissipation issues, Sensors and Actuators A: Physical 101 (2002) 215-219.

27. T. Terasawa, Y. Kawamura, K. Sato, S. Tanaka, Bulletin of the Japan Society of Precision Engineering 22 (1988) 49-54.

CHAPTER 5

PHAGE IMMOBILIZED MAGNETOSTRICTIVE BIOSENSORS

5.1 Introduction

As we discussed in Chapter 2, microcantilevers have been extensively studied and exhibited high performance as the biosensor platforms due to its higher sensitivity, compact size, ease to integrate with analysis circuits [1-3]. MCs as biosensor platforms can be operated based on two different principles: static and dynamic mode [4]. Static mode is based on the displacement of a cantilever under mass load, while MCs based on the dynamic mode are AW devices, which are based on the resonance frequency shift caused by the mass load on the device surface. MCs based on the dynamic mode have many advantages over those based on the static mode, such that both surfaces of the device can be used for sensing and no preferable orientation of cantilever beam (in static mode, the cantilever beam has to be horizontal). Dynamic MCs investigated so far can be classified into two types [4-5]: passive and active. The passive MCs, e.g. silicon-based MCs [6], require a mechanical system to actuate the device oscillation and an optical system to measure the vibration of the device. On the other side,

the active MCs, e.g. piezoelectric MCs [7], can be actuated by simply applying an electric field, and the vibration of active MCs can be easily monitored (e.g. impedance for piezoelectric MCs). However, silicon-based MCs have been much more widely investigated than active MCs because of the availability of microfabrication techniques for silicon-based materials and devices. Additionally, silicon-based MCs exhibit a larger Q value and a higher S_m than piezoelectric-based MCs [8]. However, it is still a big challenge for current MC-based biosensors operating in liquids. For example, the Q value of these cantilevers in liquid is barely more than 10 [4-5].

By using magnetostrictive materials, a new type of active cantilever, magnetostrictive cantilever, was introduced recently as a biosensor platform. Magnetostrictive milli/micro cantilevers (MSMCs) can be easily actuated and sensed. More importantly, they exhibit a high Q value, ~500 in air and ~30 in water, respectively [8]. Actually, magnetostrictive materials have been widely used in the development of actuators and sensors due to their low cost and robustness [9-15].

Two types of bacteria, *Bacillus anthracis* spores and *Salmonella typhimurium*, were used to demonstrate the performance of MSMC biosensors in this experiment. *Bacillus anthracis*, a spore-forming pathogenic bacterium, is a causative agent of anthrax. The *B. anthracis* spore is a dormant stage in the life cycle of the anthrax organism and stays for a long period in the natural environment [16]. *B. anthracis* spores are particularly dangerous because they persist in the environment, and relatively small numbers can cause death [17]. It is a big challenge to discriminate *B. anthracis* spores and vegetative cells from closely related bacteria. *B. anthracis* spores have been used as biological weapons since it is deadly, contagious and dispersed by spores and the

possibility of their further use requires surveillance systems that can accurately and reliably detect their presence in the environment. If the strain is a virulent one and a person inhales a few thousand spores, the spores may establish themselves in that person's lungs, producing an infection that is often fatal. Prevention of diseases caused by *B. anthracis* spores depends on quickly detection and control of the pathogenic spores in the environment. The other type of bacteria used in this experiment is a foodborne pathogen, *Salmonella typhimurium*. *S. typhimurium*, a nonspore-forming bacterium of the family enterobacteriaceae, is a leading cause bacterial food-borne disease such as human gastroenteritis, diarrhea, abdominal pain and typhoid fever. Salmonellosis is a very serious health issue and a major cause of many food poisoning cases [18]. The major vehicles of foodborne salmonellosis throughout the world are pork, dried or frozen eggs, dairy products, shellfish from contaminated water, etc [19]. So diseases caused by *S. typhimurium* constitute a world-wide increasing public health problem, which also required rapid detection of *S. typhimurium* contamination in food.

As we know, all biosensors require a biomolecular recognition element for biological/chemical analysis. Currently, antibodies, including monoclonal and polyclonal antibodies as the bio-recognition probes, are widely used in biological analysis. The advantages and disadvantages of antibody used in bio-analysis are well known. Polyclonal antibody has not selectivity and high cost due to affinity purification; monoclonal antibody exhibits narrow specificity but it is easy to fragile and low stability especially in unfavorable environment [20]. Recently, filamentous bacteriophages as a substitute to antibodies have been developed. Filamentous bacteriophages are thread-shaped bacterial viruses. It outer coat is a tube formed by thousands equal copies

of the major coat protein pVIII. Libraries of random peptides fused to pVIII domains were used for selection of phages probes specific for test antigens and biological threat agents. As an interface in-field test, phages may be superior to antibodies, since they are inexpensive, highly specific and strong binders even in high temperatures and unfavorable environment [21-23].

In this chapter, a biosensor by combining MSMC with affinity-selected phage was developed to detect *B. anthracis* spores or *S. typhimurium* in water. The resonance behaviors of MSMCs in air and in water were characterized. The phages were immobilized onto the sensor surface through physical adsorption. The performance of the biosensor in real-time detection of *B. anthracis* spores or *S. typhimurium* in water was demonstrated. The phage immobilization and bacteria binding measurement on the MSMC sensor surface were examined by using SEM.

5.2 Materials and methods

5.2.1 Fabrication of MSMC

In configuring MSMCs, a commercially available magnetostrictive alloy, Metglas^{TM} 2826MB ribbon (Honeywell, Morristown, NJ), was used as the active layer, and copper was used as the inactive layer in this study. Firstly, the Metglas^{TM} 2826MB ribbon was polished to about 20 μm of the thickness by using 2000# polish paper and then cleaned with acetone in a Cole Parmer 8891 ultrasonic cleaner for ten minutes. The copper layer (~15 μm in thickness) was sputtered onto the polished Metglas thin film. Before that, a chromium thin film of 100 nm in thickness was sputtered onto the polished Metglas to enhance the bonding between the Metglas layer and the copper layer. The Metglas/copper bi-layer ribbon was cut into rectangular-shaped strips, and each strip was

anchored by using a PMMA plastic holder to form an MSMC. Finally, to promote phage immobilization, a gold layer with a thickness of 130 nm was coated onto the MSMC. Prior to the gold deposition, a thin layer of chromium with a thickness of 125 nm was sputtered onto the MSMC as the adhesion layer and corrosion-resistance layer. The Denton Sputtering System was employed in all the sputtering steps.

5.2.2 Measurement set-up

The resonance behavior of the MSMC was characterized using a set-up that consists of a custom-designed Helmholtz coil and a home-made pick-up coil. The Helmholtz coil, serving as a driving coil, consists of two pairs of coils used to generate a uniform ac magnetic field and a dc magnetic field, respectively. The MSMC was put into a test chamber that was placed in the middle of the Helmholtz coil. In this study, a dc magnetic field of 20 Oe was employed to offset the magnetic anisotropy of the magnetostrictive layer, while an ac magnetic field with the amplitude of 3.2 Oe was used to actuate the oscillation of the MSMC. The pick-up coil was wound on the outside of the sample chamber to measure the magnetic signal emitted from the MSMC. To eliminate the background signal, the pick-up coil was made of two identical coils that were wound in opposite directions and connected in a series. Therefore, the output signal of the pick-up coil only reflects the magnetic signal emitted from the MSMC. The signal was measured using a lock-in amplifier (SRS830, Stanford Research Systems, Sunnyvale, CA), which had two outputs: amplitude and phase. In this study, the phase signal was used to determine the resonance behavior, which means f_0 was considered as the characteristic frequency of the MSMC and the Q value of the MSMC was defined as $f_0 / \Delta f_{HW}$, where Δf_{HW} is the width of the phase peak at half its height (see Figure 5-1 (b)).

This method is also used in the characterization of other active cantilevers, such as piezoelectric-based cantilever sensors [7].

5.2.2.1 Static system

In static system, the test chamber was contained a MSMC biosensor, pick-up coil, and bacteria solution (shown in Figure 5-1 (a)). The test chamber was sited on the middle of the Helmholtz coil.

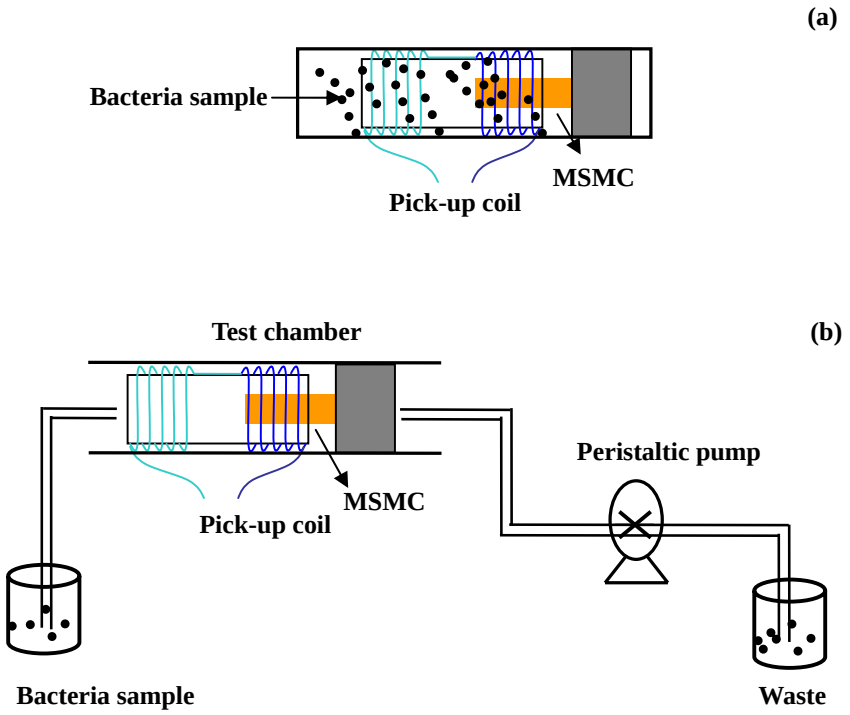

Figure 5-1. Scheme of the set-up of (a) the static system and (b) dynamic system based on MSMC biosensor.

5.2.2.2 Dynamic system

Compared to the static system, a peristaltic pump (Cole-Parmer, EW-78017-10) was used to control and adjust the flow rate of bacteria sample in the dynamic system. The schematic diagram of the flow system is shown in Figure 5-1 (b). Two reservoirs

were used in this system setup. One is contained bacteria sample with various concentrations. The other one is used to collect bacteria waste after measurement. The MSMC based biosensor and pick-up coil were put into the test chamber. The reason for the connection of peristaltic pump close to waste reservoir is elimination of the bubbles due to the squeeze of 3-stop color coded Tygon tubing (Cole-Parmer). The diameter is the Tygon tubing used in this experiment is 1.02 mm.

5.2.3 Phage and its immobilization

The filamentous bacteriophages were selected for bacteria by using phage landscape library. “Landscape” phage means that the peptides specified by the foreign DNA coding sequence show a unique conformation based on the constriction of the viral surface. A mixture of filamentous phages with different foreign DNA sequences pVIII were composed a phage-display library [24]. Thus, according to different bacteria, a specified phage can be selected from the phage-display library through the affinity-selection procedures. Furthermore, the filamentous phage exhibits high affinity to bind the targeted bacteria due to the high surface density (300-400 m^2/g) and thousands of active binding sites per phage. The filamentous phage used in this experiment was demonstrated and identified by Dr. Petrenko and his group at Auburn University and exhibited the capability of forming a huge number of antigen-binding sites on its surface [23, 25].

5.2.3.1 Phage JRB7

The fresh gold-coated surface of the MSMC was used to bind the biological probe. In this experiment, phage JRB7 displaying peptide EPRLSPHS as the bioprobe for the *B. anthracis* spores was provided by the Department of Biology at Auburn University,

which was selected from the f8/8 landscape phage library [23]. MSMCs were immersed into the phage JRB7 solution with a concentration of 2.26 x 10^{12} virions/ml for 80 minutes with rotating. The volume of phage JRB7 solution for each MSMC was 1 ml. Then, the sensors were rinsed with deionized (DI) water three times to remove the impurities and were dried in air. These phage-immobilized MSMCs were ready for biological detection.

5.2.3.2 Phage E2

In the experiments, another filamentous phage, E2, was employed as the bio-recognition element to capture the target *S. typhimurium* cells. Phage E2 displaying foreign peptide VTPPTQHQ used here is a selective probe for detecting *S. typhimurium*. The phage was immobilized onto the surface of MSMC by direct physical absorption. That is, MSMC with freshly sputtered gold layer was immersed in 1.0 ml of phage E2 culture with the concentration of 1.06 x 10^{12} virions/ml for 80 minutes with rotating. Then MSMC was rinsed three times using DI water. The MSMC thus made is a biosensor and ready for detection of *S. typhimurium*.

5.2.4 Bacteria

5.2.4.1 *Bacillus anthracis* spores

In this project, the nonpathogenic Sterne strain of *B. anthracis* spores provide by the Department of Biology at Auburn University will be employed. However, the Sterne strain has the same antigenic markers on its exterior as the pathogenic strain so the binding efficiency of phage to spores of Sterne strain should be identical to that of pathogenic strain.

5.2.4.2 *Salmonella typhimurium*

In this research, the functional performance of the biosensors was evaluated with bacterial suspensions. *S. typhimurium* (ATCC 13311) obtained from the American Type Culture Collection (Manassas, VA) was confirmed for identity and propagated by Department of Biology at Auburn University. The test solutions were prepared by diluting the concentrated bacteria suspension (5 x 10^8 cfu/ml) into DI water and stored in the refrigerator at 4 °C. Then bring it to room temperature before test.

5.2.5 Bacteria binding measurement

The spores of *B. anthracis* (nonpathogenic Sterne strain) and *S. typhimurium* were employed in this study. Prior to real-time detection, the phage-coated MSMC sensor was immersed into DI water for 30 minutes to eliminate the background signal while surrounding media of the sensor was shifted from air to liquid. Then the phage-immobilized MSMC sensor was placed into the test chamber, which was filled with 9 ml of *B. anthracis* spores or *S. typhimurium* solution. The characteristic frequency as a function of time was measured continuously using the computer-based real-time monitoring program. The concentration of *B. anthracis* spores or *S. typhimurium* used in this experiment was increased from 5 x 10^4 to 5 x 10^8 cfu/ml. For each concentration, the sensor was measured two hours and the data was recorded in five-minute intervals.

In dynamic system, the procedure of detecting *B. anthracis* spores is the same that in the static system. The only difference is that the flow rate with 0.3 ml/min is used to supply bacteria solution. For each spore concentration, the sensor was measured for 30 minutes so the total volume for each concentration is 9 ml.

5.2.6 SEM images

To confirm the immobilization of phages and the capture of *B. anthracis* spores or

S. typhimurium on the sensor surface, a JEOL-7000F scanning electron microscopy (SEM) operated at 20keV was employed to observe the phages and cells. The samples for SEM observation were prepared as follows: For the phage observation, the MSMC sensors after the phage immobilization were rinsed with DI water three times and dried in air at room temperature for several minutes. Then, the samples were exposed to osmium tetroxide (OsO_4) for one hour. For the spore observation, the MSMC sensor after the binding measurement was also rinsed with DI water three times and dried in air at room temperature. Then, the samples were exposed to OsO_4 for one hour. Finally the sensor surface was coated with a very thin gold layer (about 50 nm) using a PELCO SC-6 Sputter Coater. Both rinsing steps were used to clean the debris and to get a clean surface of the sensor for microscopic analysis.

5.2.7 Specificity

The specificity of the phage-coated MSMC biosensors was conducted against several genetically similar *Bacillus* spores species including spores of *B. anthracis*, *B. cereus* and *B. megaterium* [7]. A group of phage-coated MSMC sensors were stabilized in DI water for 30 minutes, then the sensors were exposed to a concentrated solution of *B. anthracis* spores, *B. cereus* spores, and *B. megaterium* spores respectively under the identical condition. The concentration of spore solution was 10^8 cfu/ml. The corresponding frequency shifts were recorded in two hours and the captured spore density on the sensor surface was obtained by SEM analysis.

5.3 Results and discussion

5.3.1 Sensor platform

The resonant behaviors of MSMCs used in the experiments were characterized in

air and in water. To demonstrate the size effect on the mass sensitivity and the limit of detection (LOD) of MSMC biosensors, two typical sizes of MSMC sensors were used and their typical resonance behaviors were given in Figure 5-2, where the sizes of the MSMC were 2.8 mm x 1.0 mm x 35 μm and 1.4 mm x 0.8 mm x 35 μm. As we discussed in Chapter 4, the characteristic frequency (f_0) of MSMCs in water was lower than that in air due to the damping effect. For example, in Figure 5-2 (a), the characteristic frequency decreased from about 2300 Hz to 1200 Hz. Regarding the Q value, it changes from about 195 in air to 22 in water for the MSMC biosensor in size of 2.8 mm x 1.0 mm x 35 μm, as shown in Figure 5-2 (a). For an MSMC with a size of 1.4 mm x 0.8 mm x 35 μm, the Q value is about 25 in water, as shown in Figure 5-2 (b). That is, the MSMCs in water exhibit a Q value of more than 20. This Q value is significantly higher than that observed from other cantilevers [5].

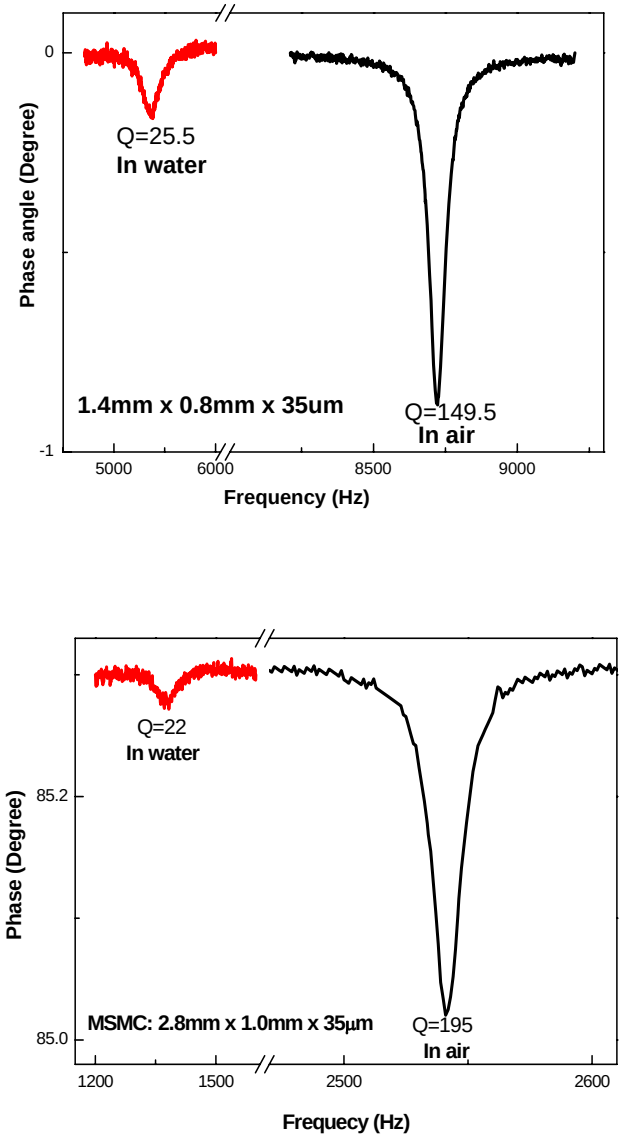

Figure 5-2. The typical resonant behavior of the MSMCs in size of 2.8 mm x 1.0 mm x 35 μm and in size of 1.4 mm x 0.8 mm x 35 μm in air and in water, respectively.

5.3.2 Phase immobilization

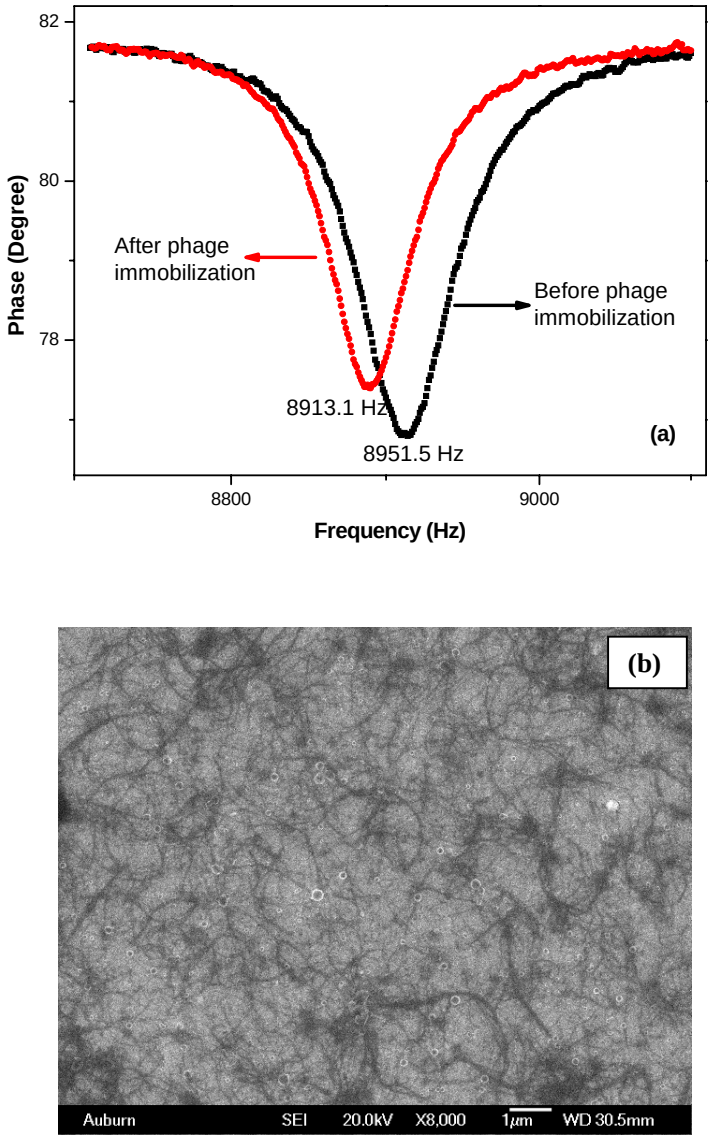

Figure 5-3. (a) The resonance peak of the MSMC in air before and after phage immobilization. (b) A typical SEM image of the phages binding on the surface of an MSMC sensor. The black fiber-like materials are phage bundles.

In the experiments, to examine the phage immobilization, the characteristic frequencies of MSMCs in air were measured before and after phage immobilization. The

sensors were cleaned with DI water and then completely dried in air at room temperature after phage immobilization. A typical set of the results is shown in Figure 5-3 (a), where the size of the MSMC was 1.4 mm x 0.8 mm x 35 μm. The result indicated that the characteristic frequency was shifted from 8951 Hz down to 8913 Hz. That is, the phage on the surface of the MSMC causes a shift (Δf) of 38 Hz in the characteristic frequency. Considering that the effective density of the MSMC is 8.33 g cm^{-3} [8], based on Eq. (3-19), this frequency shift would correspond to a uniform mass load of ~1.4 μg. The filamentous phage is a rod-shaped virus, which has a length of about 800-900 nm and a diameter of ~6.5 nm [22]. To simplify the calculation, assume the density and the length of the phage are 1 g/cm^3 and 850 nm, respectively. That is, a phage is about 2.82 x 10^{-11} μg. Considering that 1 ml phage solution with the concentration of 2.26 x 10^{12} virions/ml (~63.7 μg) was used to immobilize phage on an MSMC sensor, the attached phage on the sensor surface is about ~2.2 % of the total phage used in the immobilization. For the MSMC in size of 1.4 mm x 0.8 mm x 35 μm, the total surface area is ~2.4 mm^2. If all phages are lying on the sensor surface, considering each phage covers an area of ~5.5 x10^{-3} μm^2, i.e., 1.4 μg phage would occupy an area of ~270 mm^2, which is much bigger than the sensor surface (~2.4 mm^2). This means that phage bundles on the sensor surface. SEM was also used to observe the sensor surface after phage immobilization. A typical SEM image is shown in Figure 5-3 (b). Clearly, phage bundles are observed on the MSMC sensor surface.

The above result was obtained from phage JRB7. Phage E2 also exhibited the similar binding as phage JRB7 on the sensor surface.

5.3.3 Static system

5.3.3.1 *Bacillus anthracis* spores

Dose response

A typical set of results for an MSMC-based sensor detecting *B. anthracis* spores in water was shown in Figure 5-4, where the size of the MSMC was 1.4 mm x 0.8 mm x 35 μm. Clearly, under each concentration, the characteristic frequency of the MSMC sensor eventually reaches its saturation frequency. It seems that about ~80-minute is needed for the characteristic frequency of an MSMC to reach its saturation, which may reflect the dynamics of phage-spore interaction.

Based on the experimental results of the characteristic frequency vs. time in Figure 5-5, the dose response curve (the shift in the saturation frequency vs. the bacteria concentration) was determined as shown in Figure 5-5 (a). For comparison, the results from the MSMCs in a size of 2.8 mm x 1.0 mm x 35 μm are also presented in Figure 5-5 (a). Each point in Figure 5-5 is the average value of three sensors with the same size. The solid lines (dose response curves) are simulated by using a sigmoid fit. It is clearly shown that the smaller the MSMC, the larger the shift in frequency (i.e. higher mass sensitivity). This is consistent with the theoretical sensitivity described by Eqs. (3-19) and (3-20). Additionally, a better detection limit is obtained for a smaller MSMC sensor. For example, from the data shown in Figure 5-5 (a), an obvious response is observed for the smaller MSMC sensor (1.4 mm x 0.8 mm x 35 μm) in the culture of 5 x 10^4 cfu/ml, but no significant response is found for the bigger one (2.8 mm x 1.0 mm x 35 μm).

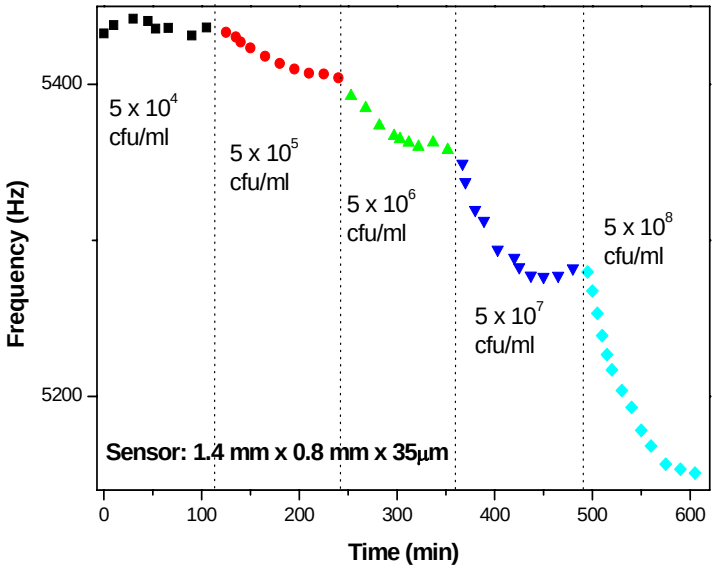

Figure 5-4. A typical curve of the characteristic frequency *vs.* time of an MSMC biosensor that was exposed to *B. anthracis* spore solutions with various concentrations. The concentration was increased from 5 x 10^4 cfu/ml to 5 x 10^8 cfu/ml. The dimensions of the MSMCs are 1.4 mm x 0.8 mm x 35 μm.

To confirm the frequency shift is caused by the phage-bacteria interaction, a reference sensor without phage immobilization was employed and characterized in the same manner. The results obtained from the biosensor and the reference sensor were given in Figure 5-5 (b), where the biosensor and the reference sensor had the same size of 2.8 mm x 1.0 mm x 35 μm. It is clearly shown that the reference sensor exhibited a much smaller frequency shift than the MSMC sensor under the same bacterial concentration.

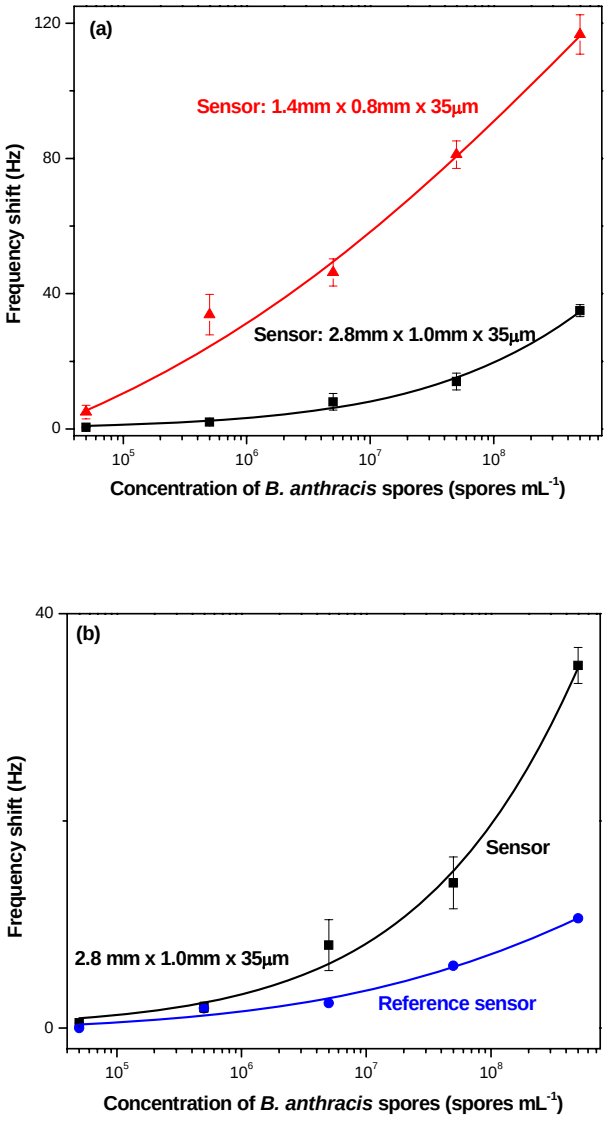

Figure 5-5. Dose response curve of MSMC biosensors for detecting *B. anthracis* spores in water. Each point is the average value of the three sensors. The response curves were plotted by using the sigmoid fit. (a) Two typical sizes of MSMC sensors: 2.8 mm x 1.0 mm x 35 µm ($\chi^2 = 0.01$, $R^2 = 0.99$) and 1.4 mm x 0.8 mm x 35 µm ($\chi^2 = 3.18$, $R^2 = 0.99$). (b) The comparison of the MSMC sensor and the reference sensor ($\chi^2 = 0.84$, $R^2 = 0.99$) with the same size of 2.8 mm x 1.0 mm x 35 µm.

SEM images

Figure 5-6 shows the typical SEM images of the MSMC biosensor after exposure to a *B. anthracis* spores culture with a concentration of 5.0 x 10^8 cfu/ml. It can be clearly seen that the number of spores binding on the sensor surface, as shown in Figure 5-6 (a) and Figure 5-6 (b), is significantly more than that on the reference sensor (shown in Figure 5-7 (c), which is consistent with the results shown in Figure 5-5 (b). The bacteria attached on the reference sensor are from a non-specific binding of *B. anthracis* spores. Clearly, the amount of non-specific binding is very small. Furthermore, the captured *B. anthracis* spores have a higher density in the area close to the tip of the MSMC sensor. According to Eqs. (3-19) and (3-20), a mass load at the tip of the sensor would result in a higher larger frequency shift than the same mass uniformly distributed over the sensor surface. That is, more binding at the tip of the MSMC biosensor is more favorable for detection.

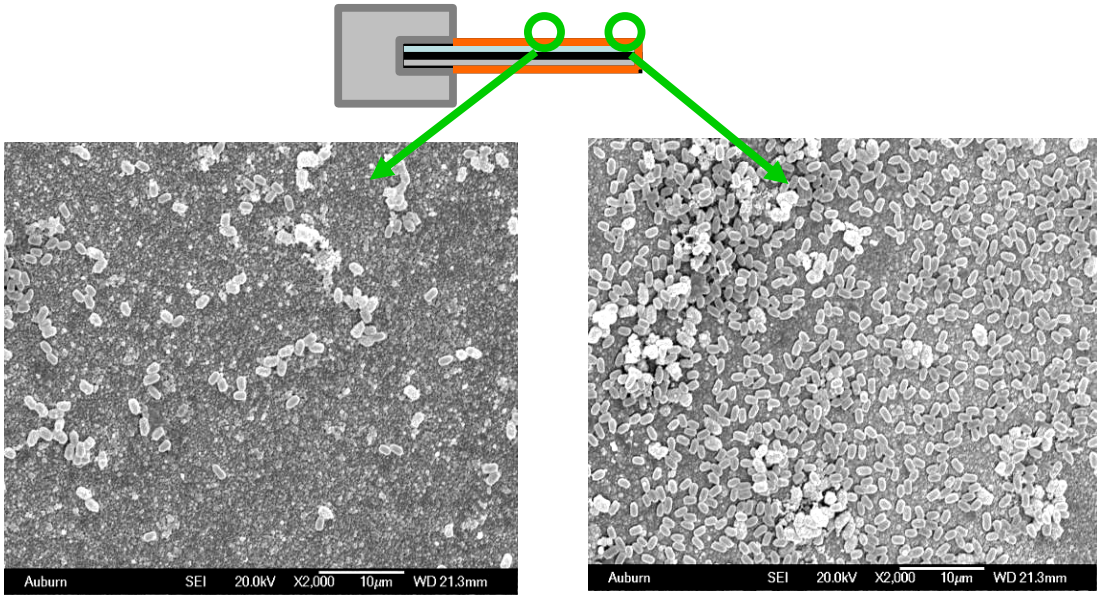

(a) At the middle of the cantilever (b) At the tip of the cantilever

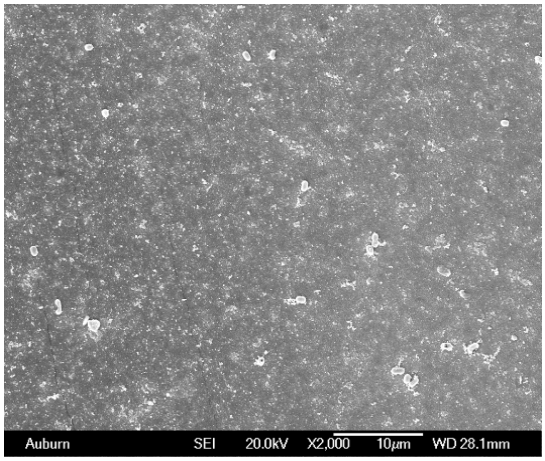

(c) Reference sensor

Figure 5-6. Typical SEM images of the surface of the MSMC biosensors exposed to the *B. anthracis* spore suspension with the concentration of 5 x 10^8 cfu/ml for 2 hours: (a) at the middle of the cantilever beam; (b) at the tip of the cantilever beam; and (c) the whole beam of the reference sensor (devoid of phage immobilization).

Specificity

The specificity of phage-immobilized MSMC biosensor was examined in the different spores of *Bacillus* species. The frequency change was monitored and the corresponding captured spore density on the sensor surface was obtained by using SEM and the results were shown in Figure 5-7. It indicated that the specificity of the MSMC sensors to *B. anthracis* spores is better than to *B. cereus* spores (eighteen fold) and *B. megaterium* spores (thirty fold).

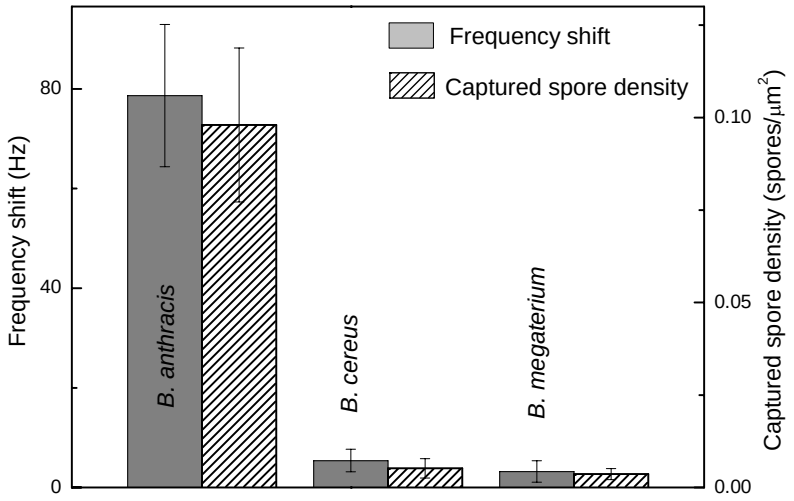

Figure 5-7. The specificity of MSMC sensor to several *Bacillus* species. The size of MSMC sensor was 1.4 mm x 0.8 mm x 35 μm. Identical phage-coated MSMC sensors were exposed to different *Bacillus* species under the identical condition.

5.3.3.2 *Salmonella typhimurium*

The shift in a characteristic frequency was given in Figure 5-8(a) and 8(b) due to the bacteria attachment in different concentrations of 5 x 10^5 cfu/ml and 5 x 10^7 cfu/ml. The size of MSMC used here is 2.8 x 1.0 x 0.035 mm. The frequency shift of the MSMC

sensor was recorded in two hours. The bacteria attachments on the MSMC biosensor weaken the phase signal and lower the characteristic frequency. It is obvious that the higher bacteria concentration led to the larger characteristic frequency. The change in the characteristic frequency is very small while the MSMC sensor was exposed into the bacteria with the concentration of 5 x 10^5 cfu/ml. While the bacteria concentration increased to 5 x 10^7 cfu/ml, an obvious shift, 20Hz, was found in Figure 5-8(b). To confirm the characteristic frequency shift is from the attachment of *S. typhimurium*, the MSMC sensor surface was examined by using SEM. The SEM images for the sensor surface exposed into the bacteria concentration of 5 x 10^5 cfu/ml and 5 x 10^7 cfu/ml were shown in Figure 5-8(c) and 8(d), respectively. Compared to Figure 5-8(c), there are more bacteria on the MSMC sensor surface due to the higher bacteria concentration, as shown in Figure 5-8 (d). Additionally, the distribution of *S. typhimurium* on the MSMC sensor surface is similar as the results of *B. anthracis* spores. More bacteria were bound at the tip of cantilever beam.

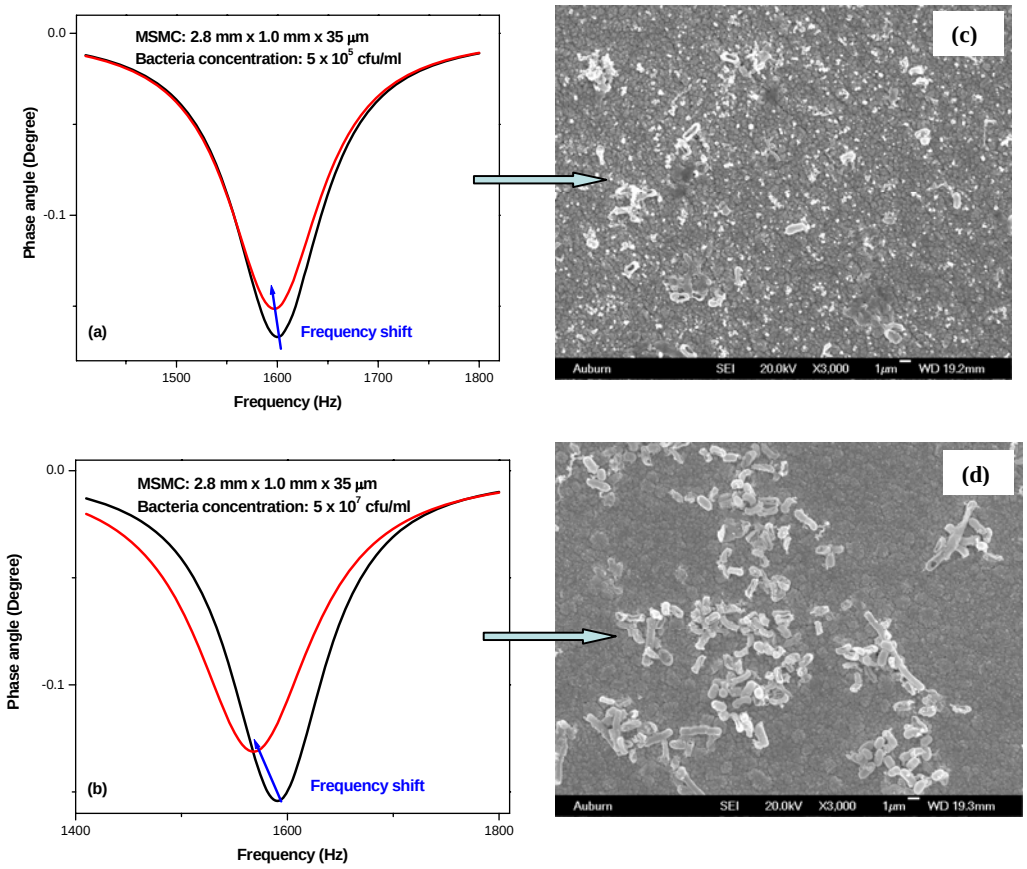

Figure 5-8. The shift in a characteristic frequency due to the various concentrations of *S. typhimurium* with (a) 5 x 10^5 cfu/ml and (b) 5 x 10^7 cfu/ml. The corresponding SEM images of *S. typhimurium* with the concentrations of (c) 5 x 10^5 cfu/ml and (d) 5 x 10^7 cfu/ml. The size of MSMC used here was 2.8 x 1.0 x 0.035 mm. The duration was two hours.

Figure 5-9 shows the typical response frequency shifts as a function of the bacteria concentrations of *S. typhimurium* suspension, which were measured by the phage-coated MSMC biosensors with two sizes. Each point in Figure 5-9 is the average value of three sensors. The response curve (solid line) was plotted by using Sigmoid fit.

Similar as the detection of *B. anthracis* spores, the result indicated that the smaller the MSMCs, the higher the mass sensitivity. Also, the limit of detection (LOD) can be improved due to the size reduction. The LODs were 10^4 cfu/ml and 10^5 cfu/ml for the MSMC biosensors with the size of 2.8 mm x 1.0 mm x 35 μm and 1.4 mm x 0.8 mm x 35 μm respectively.

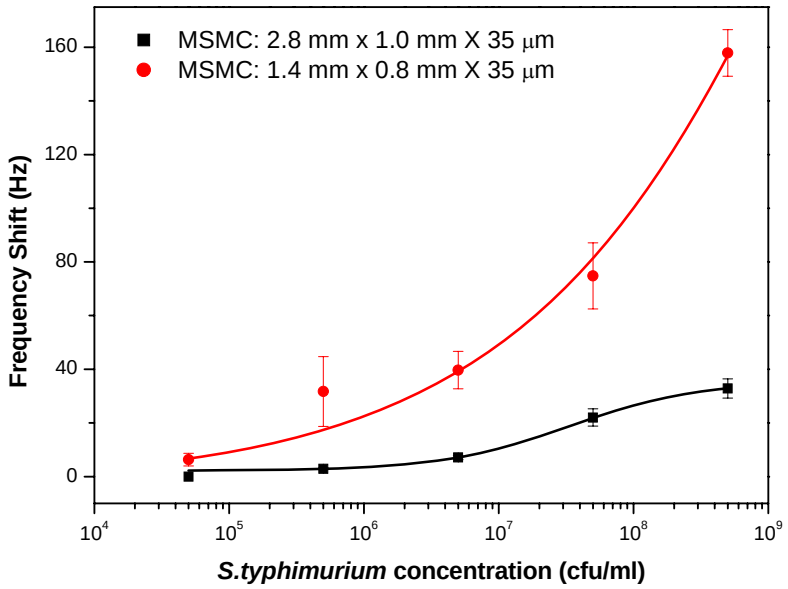

Figure 5-9. Dose response curve of MSMC biosensors for detecting *S. typhimurium* in water. Each point is the average value of the three sensors. The response curves were plotted by using the sigmoid fit. Two typical sizes of MSMC sensors: 2.8 mm x 1.0 mm x 35 μm ($\chi^2 = 0.42$, $R^2 = 0.99$) and 1.4 mm x 0.8 mm x 35 μm ($\chi^2 = 1.54$, $R^2 = 0.99$).

5.3.4 Dynamic system

5.3.4.1 Stability of dynamic system under various flow rates

The resonance behaviors of MSMC sensors were measured under the increasing flow rates from 0.1, 1.0 to 5.0 ml/min. The MSMC sensor used here is in size of 2.8 x 1.0

x 0.035 mm. Firstly the MSMC sensor was immersed into DI water for 30 minutes to stabilize it. Then the flow rate was adjusted to 0.1, 1.0, and 5.0 ml/min consequently and each flow rate was maintained about 60 min. The changes in the characteristic frequency under the three flow rates were recorded and listed in Figure 5-10. The frequency changes under the flow rate with 0.1 ml/min and 1.0 ml/min are smaller than 3 Hz, while the change in characteristic frequency is about 5 Hz under 5.0 ml/min in the flow rate, and the trend still goes lower frequency. The reason might be that the MSMC sensor suffered a larger shear stress from the higher flow rate. Thus, in the following experiments, the flow rate was limited to 1 ml/min.

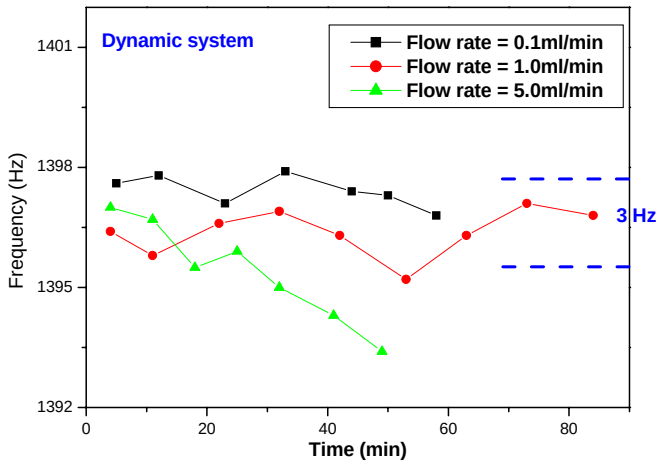

Figure 5-10. Flow rate dependence of characteristic frequency of MSMC based biosensor at 0.1 ml/min, 1.0 ml/min, and 5.0 ml/min. 3Hz of frequency shift means the experiment error from the measurement system.

5.3.4.2 The sensor response under various flow conditions

The spore binding to phage-coated MSMC biosensor surface under various flow rates were measured by the shift in the characteristic frequency. The phage-immobilized

MSMC biosensors were exposed to *B. anthracis* spores suspension of 5 x 10^7 cfu/ml concentration for one hour under various flow rate (0, 0.3, and 1.0 ml/min). The flow rate affected sensor response is shown in Figure 5-11. It can be clearly found that the time to reach the saturation frequency decreased significantly as the flow rate increased from 0 to 1.0 ml/min. The results indicated that MSMC sensor has faster response (i.e. sharper slope), that is, the spore binding was more rapid, under the higher flow rate. The control response curve shown in Figure 5-11 is the response of the MSMC sensor (devoid of phage) to the same bacteria suspension in static condition. Compared to the control sensor, we can confirm the characteristic frequency shift is caused by the spore binding on phage-coated MSMC biosensor. It is believed that at the higher flow rate, the binding of spores to the MSMC sensor surface was enhanced.

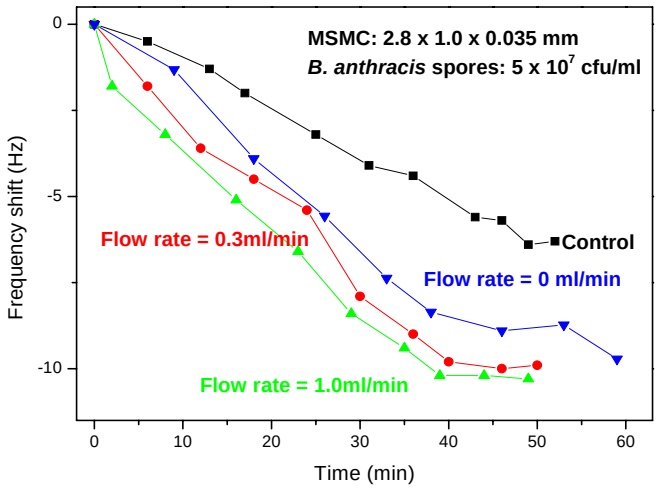

Figure 5-11. The effects of flow rate on sensor response. The binding of *B. anthracis* spores, 5 x 10^7 cfu/ml, to MSMC sensor at flow rate of (b) 0 ml/min, (c) 0.3 ml/min, and (d) 1.0 ml/min. The control (a) shown is the response of an MSMC sensor without phage immobilization.

Considering response time together with the amount of bacteria sample, the following real-time detection experiments were carried out under the flow rate of 0.3 ml/min for 30 minutes.

Furthermore, the spore attachment to MSMC biosensor surface is measured by the frequency change. Flow rate affected the total sensor response as shown above. As shown in Figure 5-11, MSMC sensor has faster response while the response curves with sharper slope. Thus, the spore binding was more rapid at the higher flow rate. The control response shown in Figure 5-11 is the response of the MSMC sensor without phage immobilization to the same bacteria sample with the concentration of 5×10^7 cfu/ml. Based on the results given in Figure 5-11, we conclude that 0.3 ml/min flow rate reduces detection time while decreasing the amount of bacteria sample and not affecting the steady state response significantly. Hence, subsequent real time detection experiments were conducted at 0.3 ml/min.

5.3.4.3 Real detection of MSMC

A series of experiments were conducted where the spore concentrations in water were systematically increases from 5×10^3 cfu/ml to 5×10^8 cfu/ml. The size of MSMC biosensors is 2.8 x 1.0 x 0.035 mm. A typical dose response (frequency shift vs. spore concentration) is shown in Figure 5-12 (a). The results indicated that the sensor took about 40 minutes (see Figure 5-11) to reach a saturated frequency in dynamic system, which is shorter than the response time (~80 min) via static system as shown in Figure 5-4. To verify that the *B. anthracis* spores detected in suspension was indeed specifically bound to the sensor surface rather than directly nonspecific adsorb onto the surface of MSMC sensor, a control experiment by exposure of MSMC (devoid of phage) into the

same suspension of *B. anthracis* spores was performed and the result was given in Figure 5-12 (a). For the control sensor, the characteristic frequency shifts might be caused by the nonspecific binding of *B. anthracis* spores and impurities in the sample suspensions. Compare to the control sensor, the phage immobilized MSMC biosensor displayed a much larger shift in the characteristic frequency, and it can be seen that the spores capture by the MSMC biosensor is due to the immobilized phage.

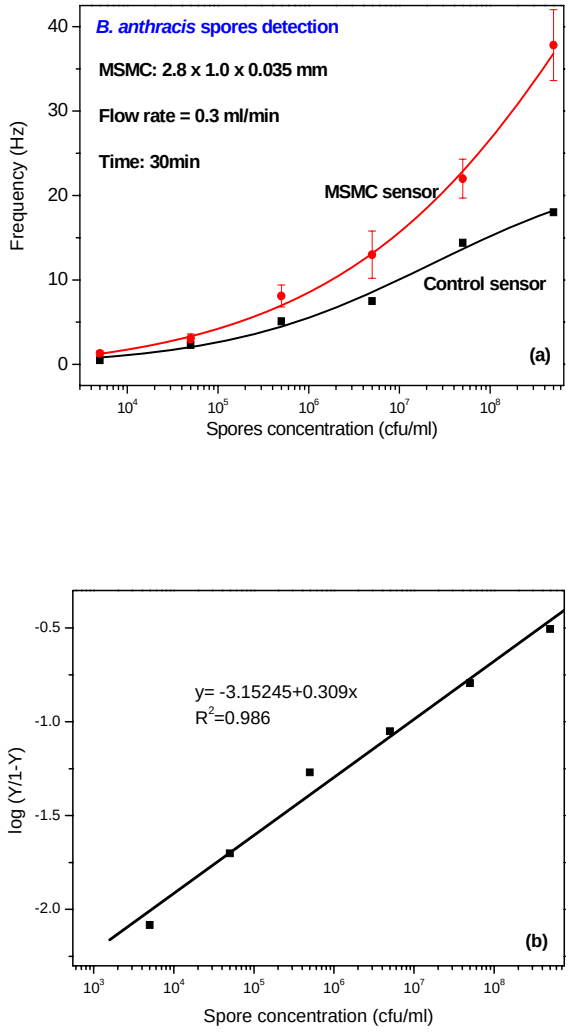

Figure 5-12. (a) The typical dose responses of MSMC sensors (χ^2 = 1.02, R^2 = 0.99) and reference sensor via dynamic system with the flow rate of 0.3 ml/min for 30 min. Each point is the average value of the three sensors. The response curves were plotted by using the sigmoid fit. The size of MSMC is 2.8 x 1.0 x 0.035 mm. (b) Hill plots of binding isotherms for the MSMC sensors. The ratio of occupied and free phages is shown as a function of *B. anthracis* spores concentrations measured by a phage-coated MSMC sensor. The straight line is the linear least squares fit to the sensor data (R=0.99, slope = 0.309).

5.3.4.4 Binding equations and Hill plot

The propose of this section is to present a quantitative description of binding by using known binding equations and to describe the interaction of analytes and phage and resulting complexes in terms of binding parameters. The applicability of the binding equations to the analyte-phage system is not trivial and special considerations are required. The reaction between analyte and phage can be schematically presented as

$$nA + P \underset{K_d}{\overset{K_a}{\rightleftharpoons}} PA_n \qquad (5\text{-}1)$$

where n is the number of molecules of the analyte bound to a single binding site on the phage. We accept that one, two or more binding sites on the phage can be involved in the binding of one molecule of the analyte depending on mono-, bi- or multivalency of binding. Then, n might be equal to 1, 0.5 or 1/*k*, where *k* is the valency of binding. K_a is the association binding constant, and $K_d = 1/K_a$ is the apparent dissociation binding constant of the analyte-phage complex.

The association binding constant (K_a) for this reaction can be defined using the mass action law [26-27]

$$K_a = [PA_n] / ([P] * [A]^n) \qquad (5\text{-}2)$$

If we neglect the number of phages bound to nonspecific molecules, then the total number of the phage binding sites (C_P) is composed of the free binding sites and the sites bound to the analyte molecules:

$$C_P = [P] + [PA_n] \qquad (5\text{-}3)$$

Combining Eqs. (5-2) with (5-3), we can determine the fraction of the phage binding sites occupied by the analyte

$$Y = [PA_n]/C_P = K_a[A]^n/(1 + K_a[A]^n) \quad (5\text{-}4)$$

The ratio of occupied and free phage binding sites can be defined as

$$Y/(1-Y) = K_a[A]^n \quad (5\text{-}5)$$

Taking the logarithm of both sides, we get

$$\log(Y/(1-Y)) = \log K_a + n\log[A] \quad (5\text{-}6)$$

A plot of the left-hand side of Eq. (5-6) versus $\log[A]$ is known as a Hill plot. It gives an estimate of n from the slope, K_a from the ordinate intercept.

Since the MSMC is a mass sensor, the concentration of phage-analyte complex is directly proportional to the change of mass on the sensor, we can obtain for MSMC

$$Y = \Delta m / \Delta m_{\max} = \Delta f / \Delta f_{\max} \quad (5\text{-}7)$$

Thus, Figure 5-12 (a) can be replotted by using Eqs. (5-6) and (5-7) and the Hill plot is shown in Figure 5-12 (b). The slope (n) of the linear fit to the sensor data is 0.309, which indicated that three binding sites are needed to anchor one spore to the MSMC sensor [27]. But it does not mean that one spore need two phage molecules since a phage might provide one, two or more binding sites [28]. K_d, $(1/K_a)$, the apparent dissociation binding constant of the phage - spore complex, is 1420 cfu/ml, which is obtained from Figure 5-12 (b). The smaller K_d represents the stronger phage-spore interaction, and higher sensitivity of the MSMC sensors.

5.4 Conclusions

In this paper, an MSMC sensor with a high Q value for real-time detecting of *B. anthracis* spores or *S. typhimurium* in water is developed. The MSMC based biosensors

exhibited the similar performance in detecting *B. anthracis* spores or *S. typhimurium* in water. The phage was immobilized onto the sensor surface through physical adsorption. And the immobilization of phage on the sensor surface was confirmed by frequency shifts and SEM images. A detection limit of 10^4 cfu/ml, and 10^5 cfu/ml are obtained for the MSMC sensor with the dimension of 1.4 mm x 0.8 mm x 35 μm and 2.8 mm x 1.0 mm x 35 μm, respectively. The SEM observation of MSMC sensor confirmed that the frequency shifts of the sensor are caused by the bacteria binding. In dynamic system, the flow rate in this research was limited 1.0 ml/min. For the bacteria concentration of 5 x 10^7 cfu/ml, the saturation frequencies of MSMC biosensor in size of 2.8 x 1.0 x 0.035 mm are similar under various different flow rates, but the response time is different. Higher flow rate, faster characteristic frequency shift.

References

1. B. Ilic, H.G. Craighead, Attogram detection using nanoelectromechanical oscillators, Journal of Applied Physics 95(7) (2004) 3694-3703.
2. G.A. Campbell, R. Mutharasan, Piezoelectric-excited millimeter-sized cantilever (PEMC) sensors detect *Bacillus anthracis* at 300 spores/mL, Biosensors and Bioelectronics 21(9) (2006) 1684-1692.
3. T.P. Burg, M. Godin, S.M. Knudsen, W. Shen, G. Carlson, J.S. Foster, K. Babcock, S.R. Manalis, Weighing of biomolecules, single cells and single nanoparticles in fluid, Nature 446 (7139) (2007) 1066-1069.
4. C. Ziegler, Cantilever-based biosensors, Analytical and Bioanalytical Chemistry 379 (7-8) (2004) 946-959.
5. N.V. Lavrik, M.J. Sepaniak, P.G. Datskos, Cantilever transducers as a platform for

chemical and biological sensors, Review of Scientific Instruments 75 (7) (2004) 2229-2253.

6. B. Ilic, D. Czaplewski, H.G. Craighead, P. Neuzil, C. Campagnolo, C. Batt, Mechanical resonant immunospecific biological detector, Applied Physics Letters 77 (2000) 450-452.
7. J. Brigati, D.D. Williams, I.B. Sorokulova, V. Nanduri, I-H. Chen, C.L. Turnbough Jr., V.A. Petrenko, Diagnostic probes for *Bacillus anthracis* spores selected from a landscape phage library, Clinical Chemistry 50 (11) (2004) 1899-1906.
8. S. Li, L. Orona, Z. Li, Z.-Y. Cheng, Biosensors based on magnetostrictive microcantilever, Applied Physics Letters 88 (7) (2006) 073507.
9. C.A. Grimes, D. Kouzoudis, K.G. Ong, R. Crump, Thin-film magnetoelastic microsensors for remote query biomedical monitoring, Biomedical Microdevices 2 (1) (1999) 51-60.
10. Q. Cai, C. Grimes, A remote query magnetoelastic pH sensor, Sensors and Actuators B: Chemical 71 (1) (2000) 112-117.
11. L. Puckett, G. Barrett, D. Kouzoudis, C. Grimes, L. Bachas, Monitoring blood coagulation with magnetoelastic sensors, Biosensors and Bioelectronics 18 (5-6) (2003) 675-681.
12. C. Ruan, K. Zeng, O.K. Varghese, C.A. Grimes, Magnetoelastic immunosensors: amplified mass immunosorbent assay for detection of *Escherichia coli* O157:H7, Analytical Chemistry 75 (23) (2003) 6494-6498.
13. K. Zeng, C.A. Grimes, Wireless magnetoelastic physical, chemical, and biological sensors, IEEE Transactions on Magnetics 43 (6) (2007) 2358-2363.

14. R. Guntupalli, J. Hu, R.S. Lakshmanan, T.S. Huang, J.M. Barbaree, B.A. Chin, A magnetoelastic resonance biosensor immobilized with polyclonal antibody for the detection of *Salmonella typhimurium,* Biosensors and Bioelectronics 22(7) (2007) 1474-1479.
15. M.L. Johnson, J. Wan, S. Huang, Z.-Y. Cheng, V.A. Petrenko, D.-J. Kim, I.-H. Chen, J.M. Barbaree, J.W. Hong, B.A. Chin, A wireless biosensor using microfabricated phage-interfaced magnetoelastic particles, Sensors & Actuators A: Physical 144 (1) (2008) 38-47.
16. M. Mock, A. Fouet, Anthrax, Annu. Rev. Microbiol. 55 (2001) 647-671.
17. T.V. Inglesby, D.A. Henderson, J.G. Bartlett, M.S. Ascher, E. Eitzen, A.M. Friedlander, J. Hauer, J. McDade, M.T. Osterholm, T. O'Toole, G. Parker, T.M. Perl, P.K. Russell, K. Tonat, Anthrax as a biological weapon medical and public health management, JAMA271 (18) (1999) 1735–1963.
18. G.H. Reed, Dairy Food Environ. San. 13 (12) (1993) 706.
19. L.A. Shimeld, A.T. Rodgers, Essentials of diagnostic microbiology. Delmar Publishers, New York, 1999.
20. P.B. Luppa, L.J. Sokoll, D.W. Chan, Immunosensors-principles and applications to clinical chemistry (Review). Clinica. Chimica. Acta. 314 (2001) 1-26.
21. V.A. Petrenko, V.J. Vodyanoy, Phage display for detection of biological threat agents. Journal of Microbiological Methods 53 (2) (2003) 243-252.
22. V.A. Petrenko, Landscape phage as a molecular recognition interface for detection devices, Microelectronics Journal 39 (2) (2008) 202-207.
23. J. Brigati, D.D. Williams, I.B. Sorokulova, V. Nanduri, I-H. Chen, C.L. Turnbough

Jr[2]., V.A. Petrenko, Diagnostic probes for *Bacillus anthracis* spores selected from a landscape phage library, Clinical Chemistry 50 (11) (2004) 1899-1906.

24. G.P. Smith, V.A. Petrenko, Phage display, Chemical Reviews 97(2) (1997) 391-410.
25. I.B. Sorokulova, E.V. Olsen, I-H. Chen, B. Fiebor, J.M. Barbaree, V.J. Vodyanoy, B.A. Chin, V.A. Petrenko, Landscape phage probes for *Salmonella typhimurium*, Journal of Microbiological Methods 63 (1) (2005) 55-72.
26. K.A. Connors, Binding constants. The measurements of molecular complex stability. Wiley, New York, 1987.
27. P.W. Kunchel, G.B. Ralston, Theory and problems of biochemistry. McGraw-Hill, New York, 1988.
28. V.A. Petrenko, V.J. Vodyanoy, Phage display for detection of biological threat agents, Journal of Microbiological Methods 53 (2003) 253-262.

CHAPTER 6

ANTIBODY MODIFICATION

6.1 Introduction

Antibodies are host proteins which were found in plasma and extracellular fluids. They serve as the first response and comprise one of the principle effectors of the adaptive immune system. By through ultimately neutralization and elimination, the antibodies can be response to molecules and organisms. Based on the binding ability of antibodies to antigens with a high degree of affinity and specificity, antibodies were widely used in a variety of diagnostic, medical analysis and become an important therapeutic tool in the clinical application to treat disease. Additionally, many biosensors used for point-of-care diagnostics and biodefense systems also rely upon the specific recognition and binding of antibodies to antigens. The antibodies are typically immobilized on a fixed solid-state surface. Thus, it is necessary to give some detail review of antibodies including the antibody structure, polyclonal antibodies and monoclonal antibodies, and methodology of antibody immobilization on the solid state sensors.

6.1.1 Antibody structure

An antibody is an immune system-related protein that binds to the target antigen with high specificity. Each antibody consists of four polypeptides-two heavy chains and two light chains joined to form a "Y" shaped molecule, as shown in Figure 6-1 [1]. Different antibodies have different amino acid sequences in the tips of "Y", which were called antigen binding sites. These variable binding sites were composed of 110-130 amino acids and given the antibody its specificity for binding antigen [2]. In Figure 6-l, the association of heavy chains and light chains through a series disulfide bridges form the fragment antigen binding region (Fab). Fabs contain the variable regions of antibodies to response to antigen, compared to the constant fragment crystallizable (Fc) region. Fabs can be used to against a variety of antigens ranging from large proteins (e.g. EGP-2) to small molecules [3]. The constant Fc region determined the mechanism used to destroy antigen. Based on the constant Fc region structure and immune function, the antibodies are mainly divided into five types, IgM, IgG, IgA, IgD, and IgE.

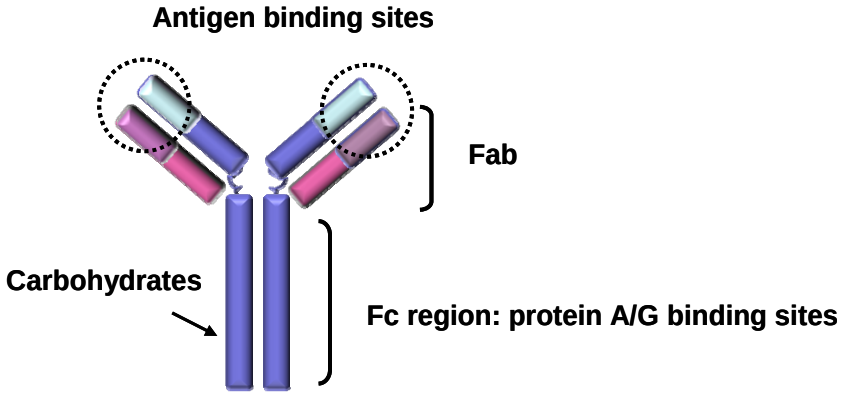

Figure 6-1. The schematic of antibody crystal structure: Fc (fragment crystallizable) and Fab (fragment antigen binding) regions, carbohydrates, and antigen binding sites.

6.1.2 Polyclonal antibody vs. monoclonal antibody

Generally, antibody has two main types: polyclonal, and monoclonal.

Polyclonal antibodies (PAbs) bind to multiple epitopes of a targeted antigen. The sequences of produce of polyclonal antibody as follows: immunizing a mammal (e.g. goat or rabbit) with an antigen, then bleeding the animal periodically and extractin the antibodies directly form the serum [4]. Monoclonal antibodies (MAbs) are derived from a single clone of antibody-producing B cells. Different with the produce of PAbs, after immunizing the mammal, the animal's spleen (location of B cell production) was extracted and the B cells were fused to immortal myeloma cells; the fused B cells and myeloma cells, also called hybridomas, are screened via ELISA, and the selected hybridoma line is injected into a second mammal. The myeloma component of the hybridoma induces localized tumor growth in the animal, and an antibody-rich fluid, called ascites, can be extracted from the tumor; the antibodies are then isolated themselves through column chromatography [5].

The use of PAbs or MAbs depends on several factors, and the most important one is its intended use and availability of the antibody from commercial supplies/researchers. Compared to MAbs, PAbs can be produced more quickly at low cost and less technical skills. The homogeneity and consistency, principle advantages of MAbs, can be used to evaluate the small changes in molecular conformation of protein, and the protein-protein interactions. Furthermore, the antibody on a molecule level might be determined through the structural analysis (e.g. XRD or gene sequencing). However, the application of MAbs was also limited by the monospecificity. For example, a MAb might be lost the function due to small changes in the structure of an epitope (e.g., as a result of genetic polymorphism, glycosylation, and denaturation). Thus, MAbs should be generated for the antigens which eventually need to bind. Furthermore, the MAbs can be produced as a constant and renewable resource once the desired hybridoma generated. Compared to MAbs, the small change

of single or small numbers of epitopes is not obvious since PAbs are heterogeneous and can recognize a host of antigenic epitopes. Another advantage of PAbs is the stability over a broad pH and salt concentration. However, the different animals were used to immobilize to generate PAbs for the same antigen, which might cause the change in the avidity (the overall binding intensity between antibody and antigen with multiple epitopes) and limit the quantity of PAbs.

The specificity of an antibody can be defined as the ability to recognize a specific epitope in many other epitopes' presence. There is less cross-reactivity for the antibody with high specificity. PAbs usually have higher specificity than MAbs since they are produced by a large number of B cell clones, each generated antibody has a specific epitope, and polyclonal serum is a mixture of antibodies with unique specificities. However, MAbs have higher purity level of specific than PAbs. For example, MAbs generated as ascites or in specialized cell culture vessels are 10-fold higher in concentration and of much higher purity than PAbs.

Many disadvantages of MAbs can be overcome by pooling several MAbs of desired specificities. This pooled MAbs are available in limitless quantity. However, it is a big challenge to identify MAbs of desired specificity even with high cost, and time consuming.

6.1.3 The oriented attachments of Antibody on solid surface

Due to the high specificity and easy binding of antibodies to antigens, the immobilized antibodies on various solid-phase surfaces (e.g. silicon, gold) have been widely used in many fields such as purification of materials, diagnostic immunoassays, biodefense systems, and biosensors. However, there are several limitations for antibody immobilization. For example, while the antibody is immobilized on a solid-state surface, its binding activity is frequently less than that of soluble one. One

of the main reasons for this reduction of binding activity is due to steric hindrance of the molecules in the solid-phase. Another possible reason is attributed to the random orientation of the antibody molecules on the solid-phase surface, as shown in Figure 6-2 (a). Therefore, surface chemistry and antibody immobilization strategies to develop a highly oriented manner have been extensively investigated. The optimized/ideal orientation of antibody attachment on the solid-phase surface was given in Figure 6-2 (b).

(a) Random orientation

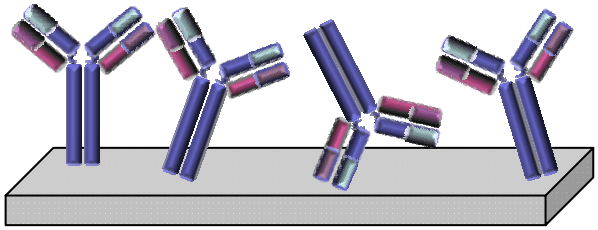

(b) Optimized orientation

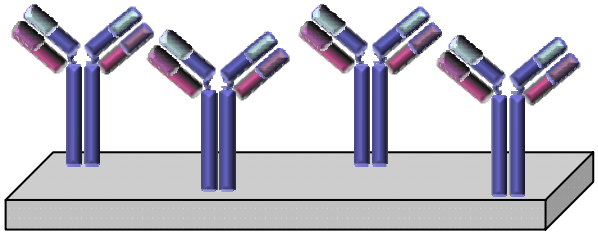

(c) Protein binding

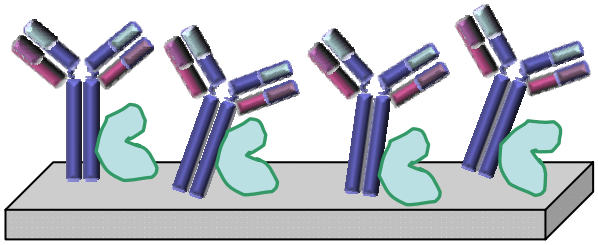

Figure 6-2. Schematic of the antibody immobilization on the gold-coated surface of the sensors with (a) random orientation, (b) ideal orientation, and (c) protein A binding-mediated orientation.

In order to prevent antibody from washing off and to retain the antibody activity, it is required an immobilization scheme which provided the highest irreversible surface loading. To overcome this problem, Langmuir-Blodgett (LB) film technique was employed for antibody immobilization [11, 30]. In this method, a monolayer of antibody with phospholipids was formed at the air/water interface and then transferred to the solid surface [12], as shown in Figure 6-3 (a) and (b). However, this method suffered from instability of the antibody monolayer on the solid-state surface of biosensors due to the poor adhesion between them. Moreover, it is difficult to control the orientation of antibody since hydrophobic and hydrophilic parts of antibody are not separated precisely as in the lipid molecules. A comparative study of several antibody immobilization techniques including physical adsorption, covalent binding, and protein A binding were carried out [8-10]. As we know, the simplest antibody immobilization technique is directly physical adsorption [6]. This method has no antibody modification, high-level antibody loading, and low cost. However, during and after antibody immobilization, the denaturation or conformational changes of antibody might reduce the sensitivity of biosensors [7]. Additionally, due to the reversible nature of physical attachment, the adsorbed surfaces in solution are more susceptible to instability since the desorption may occur.

(a)

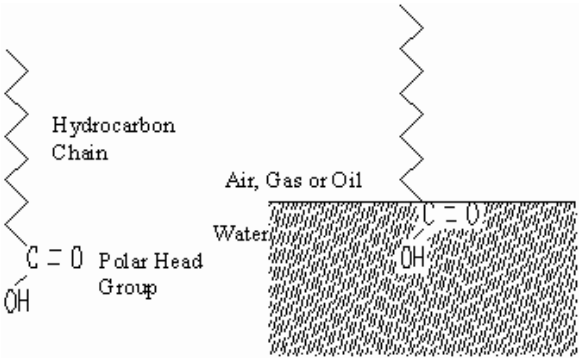

(b)

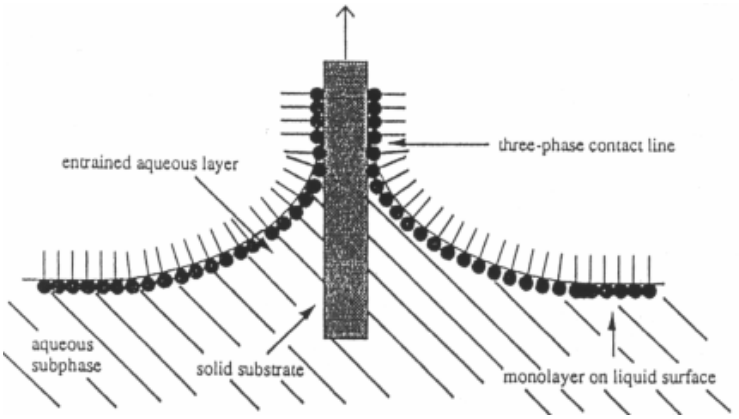

Figure 6-3. The scheme of Langmuir-Blodgett thin film. (a) A schematic illustration showed components of an amphiphile (left), and the orientation of an amphiphile adopted at an interface (right). (b) Deposition of a floating monolayer on a solid surface. [13]

Another substitute method is covalent binding such as the thiol-gold interaction [14]. For some solid state surfaces of sensors, such as quartz, silica, and conventional glass, which can be chemically modified by the type of $(RO)_3SiR$, with R (e.g. methyl or ethyl), and RO (e.g. aminopropyl, 3 chloro-propyl, 3 glycidyloxy, vinyl, or a long chain amine to easily react with protein/antibody. Covalent binding of antibodies to solid-state surfaces has been investigated as an alternative of physical adsorption to increase stability and control of protein binding site availability. The

covalent binding has two types, one is involved the modification the solid surface by using a hydroxyalkanethiol to introduce a functionality which may be coupled to the antibodies [8, 32-34], the other is by modified the antibody itself, which is described by Traut and co-workers [15-17]. Covalent binding exhibits high surface loading and low antibody loss. However, covalent binding might cause the higher antibody activity loss. But this loss relies on the antibody, the immobilization chemistry, and the solid-state surface [31]. Antibody modification, especially on antigen binding sites, is also one of several factors diminishing the antigen binding ability of a bound antibody. For example, several chemical crosslinkers that immobilize antibodies induce crosslinking of the antibody itself, which limits the availability of binding sites for antigen capture. Therefore, a cysteine residue was introduced into the antibody site specifically. For example, Hong et al. [18] introduced a single unique cysteine residue into cytochrome b5 and assembled the resulting antibody on a chemically modified SiO_2 surface. Vigmond et al. [19] assembled engineered dihydrofolate reductase onto a gold surface by introducing a cysteine residue at its C-terminus.

In addition to the immobilization techniques described above, the role of protein A in these attachment schemes was also investigated. The interaction schematic of protein A, antibody and solid-phase surface was described in Figure 6-2(c). One of the most common methods of immobilizing antibodies at the Fc fragment is through the utilization of protein A that is a 64 kDa bacterial surface protein extracted from the bacterium *Staphylococcus aureus*. Protein A binds specifically to the Fc region of immunoglobulin form many mammals [20-21]. In addition to protein A, other immunoglobulin-binding bacterial proteins such as protein G, protein A/G, and protein L are all commonly used to purify, immobilize or detect immunoglobulin. Each of these immunoglobulin-binding proteins has a different

antibody binding profile in terms of the portion of the antibody that is recognized and the species of antibodies it will bind. Since the binding does not interface with antigen-antibody reaction, antibody molecules on a protein A-assembled surface are expected to retain full antigen-binding activity. It has been shown that 2-8 times higher antigen-binding capacity when oriented coupling techniques (e.g. protein A) are used [22]. Protein A has been successfully applied in several groups. For example, Owaku et al. [23] used protein A modified with C18 fatty acid residues by chemical cross-linking to form in a stable monolayer on the air/water interface, then the monolayer was transferred onto a solid-surface to immobilize the antibody molecules. Lu et al. [24] constructed a protein A membrane on a solid-surface by combining an LB method and applied it for an optical immunosensing system. However, there are still some limitations for this method, such as this binding is weaker than the covalent binding, additional process for antibody-binding protein immobilization, not suitable for sandwich assays [25].

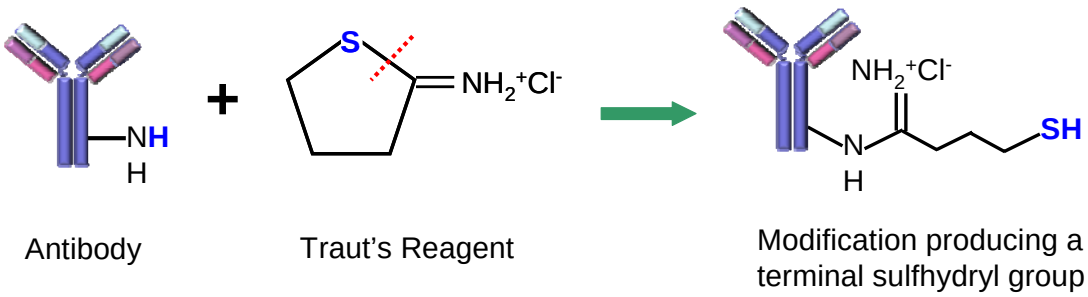

Figure 6-4. The schematic reaction of antibody and Traut's Reagent.

In this experiment, the covalent binding by functionality of the antibody with Traut's Reagent was used to immobilize antibody on the surface of magnetostrictive sensors. Traut's Reagent (2-Iminothiolane or 2-IT) is a cyclic thioimidate compound for thiolation (sulfhydryl addition). As shown in Figure 6-4, Traut's Reagent reacts with primary amines (-NH_2) to introduce sulfhydryl (-SH) groups while maintaining charge properties similar to the original amino group. Once added, sulfhydryls may be

specifically targeted for reaction in a variety of useful labeling, cross-linking, and immobilization procedures. The modified antibody was covalent bound on the gold-coated magnetostrictive sensors. The number of sulfhydryls for each antibody was determined by using Ellman's Reagent.

6.2 Experimental

6.2.1 Reagents

Traut's Reagent (2-Iminothiolane•HCl, Pierce, 26101) and Ellman Reagent (5, 5'-Dithio-bis-(2-nitrobenzoic acid, Pierce, 22582) were used to thiolate the antibody and measure the sulfhydryls after thiolation respectively. The molecular weight of Traut's Reagent is 137.63 g/mol. Purified rabbit anti - *S. aureus* polyclonal antibody was obtained from Accurate Chemical & Scientific Corp. (Westbury, NY 11590). The product number is YVS6881. The monoclonal anti-*aureus* IgG was provided by 3M Company. The polyclonal antibody, anti *E. coli* rabbit IgG, as the detector of *E. coli,* was obtained from GeneTex, Inc (GTX13626). Monoclonal antibodies C11E9 and Em10 used in this research were prepared and provided by Department of Agricultural and Biological Engineering at Purdue University. Phosphate buffered saline (PBS, 0.01M, pH=7.4, Sigma, P3813) adjusted to pH 8.0, was used for protein thiolation with Traut's Reagent.

6.2.2 Antibody thiolation and separation

0.25 ml antibody was dissolved into 0.25ml of PBS buffer (pH=8.0), and the 10-fold, 20-fold, and 40-fold molar excess of Traut's Reagent (14mM stock solution) were added to the solution. The according volumes of the stock solution were given in Table 6-1. Then, the mixed solution was incubated for 1 hour at room temperature.

Table 6-1. Traut's Reagent: 14mM stock solution.

Traut's Reagent	10-fold molar excess	20-fold	40-fold
Volume	5.35 µl	10.7 µl	21.4 µl

The excess Traut's Reagents in thiolation solution were removed by using a D-Salt^{TM} Dextran Desalting column (Pierce, 43233). D-Salt^{TM} Dextran Desalting columns are ready-to-use commons, which display excellent chromatographic properties and have good rigidity for easy handling and good flow properties. The principle of desalting common is that the molecules greater than 5,000 MW can emerge in the void volume, separating them from smaller molecular weight molecules. As shown in Figure 6-5, firstly, the top cap from the desalting common was removed and the storage solution (0.02% sodium azide) was decanted from the column. Then the bottom cap from the column was removed and the column was equilibrated with 50ml (5 column volumes) of PBS buffer containing the 2-5mM EDTA. The next step is that the tip of the column was placed in a test tube and thiolated antibody solution was applied into the column. For optimal separation, solution should be approximately 10% of the column volume. Allow the sample into the gel. The column will stop flowing when the sample has entered the gel. Add 0.5ml PBS buffer, and we can get 0.5ml solution in the test tube, repeat this step until the antibody has emerged from the column. For this experiment, we repeat 16 times and obtain 16 samples. Measure the absorbance of each sample at 280nm by using UV-Vis Spectroscopy. The blank sample is the PBS buffer. After measurement, 100ml of PBS (10 column volumes) buffer was used to regenerate the column. For storage, wash the column with 5 column volumes of ultrapure water containing 0.02 % sodium azide and cap the bottom then the top of the column when approximately 3ml of solution remains above the gel. The column should be stored at 4 °C.

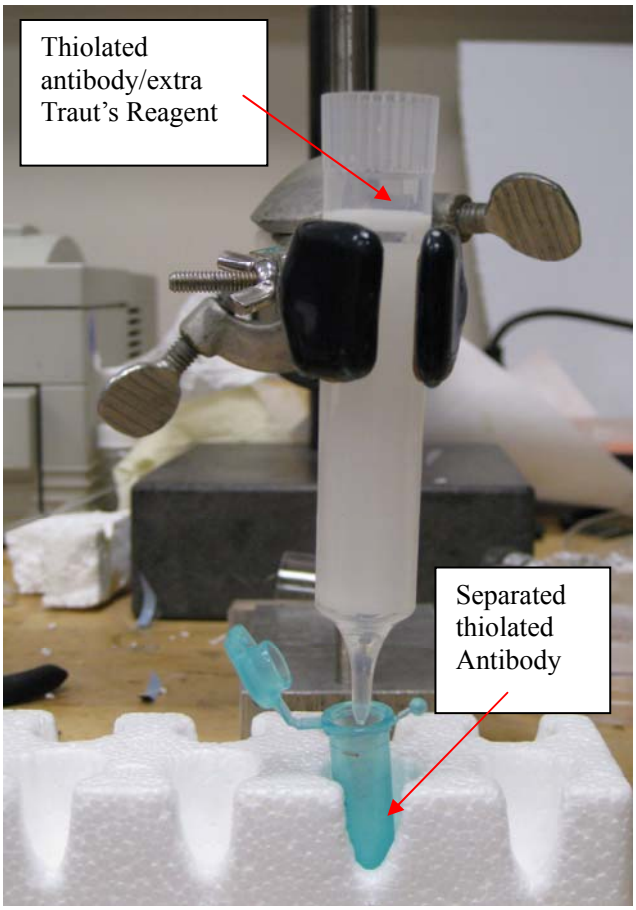

Figure 6-5. The schematic of desalting column used to separate thiolated antibody and extra Traut's Reagent.

6.2.3 Measurement of thiolated antibody – Bradford Dye Assay

Four spectroscopic methods are routinely used to determine the concentration of antibody in a solution, which include the measurement of the protein's intrinsic UV absorbance [26] and three methods which generate a protein-dependent color change; the Lowry assay [27], the Smith copper/bicinchoninic assay [28] and the Bradford dye assay [29]. Although one or more these methods are used routinely in almost every biochemical laboratory, none of the procedures are particularly convenient, for the reasons described below. The first one, UV absorbance, requires that a pure protein with known extinction coefficient be used, in a solution free of interfering substances. Usually the protein concentrations of a solution were measured at the 280 or 205 nm. However, different proteins have widely different extinction coefficients at the 280 or

205 nm, and concentration estimates obtained this way should be viewed with considerable skepticism. In this measurement, a quartz cuvette should be used.

The Lowry and copper/bicinchoninic assays are based on reduction of Cu^{2+} to Cu^{1+} by amides. Although this makes them potentially quite accurate, they require the preparation of several reagent solutions, which must be carefully measured and mixed during the assay. This is followed by lengthy, precisely timed incubations at closely controlled, elevated temperatures, and then immediate absorbance measurements of the unstable solutions. Both assays may be affected by other substances frequently present in biochemical solutions, including detergents, lipids, buffers and reducing agents. This requires that the assays also include a series of standard solutions, each with a different, known concentration of protein, otherwise having the same composition as the sample solutions.

In this experiment, Bradford dye assay was used to measure the concentration of thiolated antibody after separation. Standards and unknown samples should be prepared at the same time. Usually the concentration of the test sample should be diluted to less than 1 μg/μl. Run the duplicate preliminary standards and sample to find dilution point. The IgG with the concentration of 1.39mg/ml (IgG: 6mg and H_2O: 4.3ml) was used as the standard sample. Then the standard antibody was diluted twice by DI water (IgG : H_2O = 125μl : 125μl). The standard samples with various concentrations were prepared into test tubes and listed in Table 6-1. 100 μl of the unknown samples with different dilutions by DI water were also prepared. Then, 1 ml dye reagent (BioRad BradFord : H_2O = 1 : 4 solution) was added into each test tube. All the test tubes were vortex and incubated for 15 minutes. Read samples and standards on spectrophotometer at 595nm Vis. The standard curve for the standard samples was drawn of the measurement results.

Table 6-2. The experiment design of the standards.

IgG (μl)	0	5	10	15	20	25	30
H_2O (μl)	100	95	90	85	80	75	70
Dilution factor		x 20	x 10	x 6.7	x 5	x 4	x 3.3
Dilute Conc.	mg/ml	0.0695	0.139	0.207	0.278	0.3475	0.417
1/2 Dilute Conc.	mg/ml	0.035	0.07	0.105	0.14	0.175	0.21

6.2.4 Measurement of -SH group

The sulfhydryls was measured by using Ellman's Reagent. The reaction buffer was prepared to dissolve sodium phosphate, dibasic heptahydrate (Fisher Scientific, 7782-085-6) into water (0.1M), and pH was adjusted to 8.0 by using 1M HCl solution. The reaction buffer also was contained 1mM EDTA. The Ellman's Reagent solution was obtained to dissolve 4mg Ellman's Reagent in 1ml of reaction buffer. Prepare a set of test tubes, each containing 50μl of Ellman's Reagent solution and 0.5 ml of reaction buffer. 250 μl of each unknown samples with different dilutions, the same with the above thiolated antibody solution, were added into the each test tube. Each tube was mixed and incubated at room temperature for 15 minutes. Then the absorbances of the unknown samples were measured at 412 nm. The concentration (C) of sulfhydryls in the samples were calculated based on Beer's law $C = A/\varepsilon b$, where A, ε, and b represent the absorbance, the molar extinction coefficient ($14{,}150 M^{-1}cm^{-1}$), and the thickness of the cuvette (1cm).

6.3 Results and discussion

6.3.1 The collection of the thiolated antibody after separation

The thiolated protein/antibody concentrations of a solution were measured at 280 nm (UV). As we know, this method requires a pure protein with known extinction coefficient. Therefore, this method used here is for qualitative analysis, which means it was used to collect the test tubes containing thiolated antibody. According Beer law, the larger absorbance is proportional to the higher concentration. In Figure 6-4, we

can find the absorbances from test tubes 7 to 12 are much higher than the other samples. These six test tubes were collected and combined into one solution, which was used to measure the concentration of thiolated antibody, and sulfhydryls in each thiolated antibody.

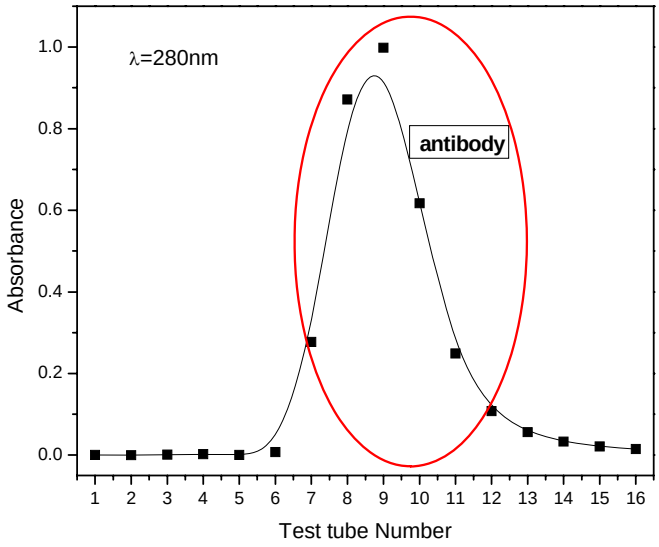

Figure 6-6. The UV absorbance of antibody at 280nm for the continuous thiolated antibody samples after separation. The test number represented the number of 0.5 ml of separated antibody solution.

6.3.2 The concentration of thiolated antibody

The absorbances for the standards at 595 nm were measured and listed in Table 6-3. The absorbance changes to higher value as the increasing of the content of IgG in the standards, which is in accordance with Beer's law.

Table 6-3. The results of the standards.

	Standard						
IgG (μl)	0	5	10	15	20	25	30
H_2O (μl)	100	95	90	85	80	75	70
A_1	-	0.0281	0.1542	0.2031	-	0.3362	0.4386
A_2	-	0.0656	0.1560	0.2158	0.3089	0.3476	0.4256
A_{avg}	Blank	0.0423	0.1551	0.2094	0.3089	0.3419	0.4321

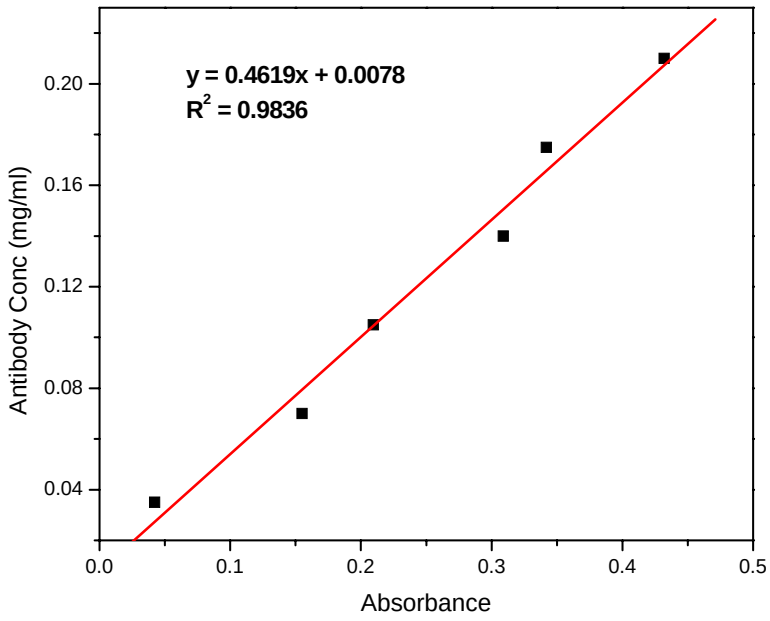

Figure 6-7. The standard curve of the antibody concentration with the absorbance at 595 nm.

Combined Tables 6-2 with Table 6-3, the standard curve can be drawn in Figure 6-5. The good linearity of the standards can be found in the absorbance range from 0.1 to 0.5. Therefore, we can obtain the concentration of the unknown sample through measuring its absorbance. Based on the method, the thiolated antibody was measured and the results were given in Table 6-4. For the same antibody content before thiolation, the different concentrations of thiolated antibody were obtained. The probable reason came from the different volumes of measured samples and the loss in the thiolation and separation.

6.3.3 Quantification of the sulfhydryls

The sulfhydryls in the original and thiolated anti-*aureus* antibody were measured by using Ellman's Reagent and the results were given in Table 6-4. The concentration of the antibody was obtained from the absorbance at 412 nm and Beer's law. Compared the concentrations with the sulfhydryls for the same antibody solution,

the sulfhydryls in each antibody can be calculated and shown in Table 6-4. The sulfhydryls number in the unmodified antibody is about 0.83, which mean there are free sulfhydryls for the antibody. After thiolation, the sulfhydryls number was increasing as the Traut's Reagent molar excess increased. The optimized molar excess is 20-fold for antibody, which can thiolate 2-3 sulfhydryls in each antibody.

Table 6-4. Results of polyclonal *anti-aureus* antibody modification by using Traut's Reagent. The concentrations of antibody and sulfhydryl group, the -SH number for each antibody molecular under different Traut's Reagent molar excess.

Traut's Reagent Molar excess	Antibody concentration	SH concentration	SH number
Blank	8.46×10^{-6}M	6.83×10^{-6}M	0.81
x 10	5.84×10^{-6}M	9.90×10^{-6}M	1.70
x 20	8.52×10^{-6}M	32.2×10^{-6}M	3.78
x 20	4.48×10^{-6}M	9.14×10^{-6}M	2.04
x 40	6.24×10^{-6}M	16.0×10^{-6}M	2.56

Additionally, several antibodies before and after thiolation were also measured the concentrations and sulfhydryls in this experiments. The results were listed in Table 6-5. Traut's Reagent with 20-fold molar excess was used here. These antibodies include monoclonal anti-*aureus* IgG, anti-*E. Coli* IgG, C11E9, and Em10. The concentration of the above modified antibodies and sulfhydryls were measured and the results were given in Table 6-5. The unmodified monoclonal anti-*aureus* IgG has 0.43 sulfhydryls for each protein/antibody molecular. For the anti-*E. coli* IgG, the free sulfhydryls is about 0.83 for each antibody. After thiolation by Traut's Reagent, the sulfhydryls are obviously increased for these two antibodies. C11E9 and Em10 is anti-*Listeria* antibody. Thiolated with 20-fold molar excess of Traut's Regents, the sulfhydryls per each antibody are 2.3 and 0.5.

Table 6-5. The concentrations of antibodies, and their sulfhydryls, and the -SH group per antibody molecular of several antibodies which modified by Traut's Reagent with the 20-fold molar excess.

antibody	Antibody Conc.	SH concentration	SH number
Thiolated monoclonal *anti-aureus* IgG	2.05 x 10^{-5}M	7.39 x 10^{-5}M	3.6
Monoclonal *anti-aureus* IgG	2.325 x 10^{-5}M	1.007 x 10^{-5}M	0.43
Thiolated anti-*E. coli* IgG	7.7 x 10^{-6}M	4.34 x 10^{-5}M	5.6
Anti-*E. coli* IgG	7.93 x 10^{-6}M	6.575 x 10^{-6}M	0.83
Thiolated C11E9	8.2 x 10^{-7}M	1.884 x 10^{-6}M	2.3
Thoilated Em10	4.45 x 10^{-5}M	2.188 x 10^{-5}M	0.5

6.4 Conclusions

In this work, to improve the antibody immobilization on the gold-coated magnetostrictive sensors, Traut's Reagent was used to introduce the sulfhydryls into the antibody, which can be covalent bond with gold. The results show that about 2-6 sulfhydryls per antibody were produced. In the typical IgG, usually ~20 available primary amines could be thoilated if extra Traut's Reagent was used, however, that would be more likely to adversely affect antibody function. Thus, 20-fold molar excess of Traut's Reagent is reasonable for thiolation of antibody.

References

1. Y. Jung, J.Y. Jeong, B.H. Chung, Recent advances in immobilization methods of antibodies on solid supports, The Analyst, 133 (2008) 697-701.
2. http://www.biology.arizona.edu/IMMUNOLOGY/tutorials/antibody/structure.html

3. S.S. Iqbal, M.W. Mayo, J.G. Bruno, B.V. Bronk, C.A. Batt, J.P. Chambers, A review of molecular recognition technologies for detection of biological threat agents, Biosensors and Bioelectronics 15 (11-12) (2000) 549-578.
4. J.S. Garvey, N.E. Cremer, D.H. Sussdorf, 1977. Methods in immunology, W.A. Benjamin, Inc., Reading, Massachusetts.
5. G. Köhler, C. Milstein, Continuous cultures of fused cells secreting antibody of predifined specificity, Nature 256 (1975) 495-197.
6. J.E. Herrmann, 1981. Methods in Enzymology 73, 224-239, Academic Press, New York.
7. J.E. Butler, L. Ni, W.R. Brown, K.S. Joshi, J. Change, B. Rosenberg, E.W. Jr. Voss, The immunochemistry of sandwich ELISAs. VI. Greater than 90% of monoclonal and 75% of polyclonal anti-fluorescyl capture antibodies (CAbs) are denatured by passive adsorption, Molecular Immunology 30 (1993) 1165-1175.
8. A. Ahuwalia, D. DeRossi, C. Ristori, A. Schirone, C. Serra, A comparative study of protein immobilization techniques for optical immunosensors. Biosensors and Bioelectronics 7 (1991) 207-214.
9. S.K. Bhatia, J.L. Teixeira, M. Anderson, L.C. Shriver-Lake, J.M. Calvert, J.H. Georger, J.J. Hickman, C.S. Dulcey, P.E. Schoen, F.S. Ligler, Fabrication of surfaces resistant to protein adsorption and application to two-dimensional protein patterning, Analytical Biochemistry 208 (1993) 197-205.
10. L.C. Shriver-lake, B. Donner, R. Edelstein, K. Breslin, S.K. Bhatia, F.S. Ligler, Antibody immobilization using heterobifunctional crosslinkers, Biosensors and Bioelectronics 12 (1997) 1101-1106.
11. M. Sriyudthsak, H. Yamagishi, M. Moriizumi, Enzyme immobilized Langmuir-Blodgett film for a biosensor, Thin Solid Films 160 (1988) 463-469.

12. A. Barraud, H. Perrot, V. Billard, C. Martelet, J. Therasse, Study of immunoglobulin G thin layers obtained by the Langmuir-Blodgett method: application to immunosensors, Biosensors and Bioelectronics 8 (1993) 39-48.
13. http://www.ksvinc.com/LB.htm
14. C. Duan, M.E. Meyerhoff, Separation-free sandwich enzyme immunoassays using microporous gold electrodes and self-assembled monolayer/immobilized capture antibodies, Analytical Chemistry 66 (1994) 1369-1377.
15. R. Jue, J.M. Lambert, L.R. Pierce, R.R. Traut, Addition of sulfhydryl groups to *Escherichia coli* ribosomes by protein modification with 2-iminothiolane (methyl 4-mercaptobutyrimidate), Biochemistry 17 (1978) 5399-5406.
16. J.M. Lambert, R. Jue, R.R. Traut, Disulfide crosslinking of *Escherichia coli* ribosomal proteins with 2-iminothiolane (methyl 4-mercaptobutyrimidate): evidence that the crosslinked protein pairs are formed in the intact ribosomal subunit, Biochemistry 17 (25) (1978) 5406-5416.
17. J.W. Kenny, T.G. Fanning, J.M. Lambert, R.R. Traut, The subunit interface of the *Escherichia coli* ribosome. Crosslinking of 30 S protein S9 to proteins of the 50 S subunit, Journal of Molecular Biology 135 (1) (1979) 151-170.
18. H.G.. Hong, M. Jiang, S.G.. Sligar, P.W. Bohn, Cysteine-specific surface tethering of genetically engineered cytochromes for fabrication of metalloprotein, Langmuir 10 (1994) 153-158.
19. S.J. Vigmond, M. Iwakura, F. Mizutani, T. Katsura, Site-specific immobilization of molecularly engineered dihydrofolate reductase to gold surface, Langmuir 10 (1994) 2860-2862.

20. H. Hjelm, K. Hjelm, J. Sjoquist, Protein A from *Staphylococcus aureus*: Its isolation by affinity chromatography and its use as an immunosorbent for isolation of immunoglobulin, FEBS Letters 28 (1972) 73-76.
21. J.W. Goding, Use of staphylococcal protein A as an immunological reagent, J. Immunol. Methods 20 (1978) 241-253.
22. B. Lu, M.R. Smyth, R. O'Kennedy, Oriented immobilization of antibodies and its applications in immunoassays and immunosensors, Analyst 121 (1996) 29R-32R.
23. K. Owaku, M. Goto, Y. Ikariyama, M. Aizawa, Protein A Langmuir-Blodgett film for antibody immobilization and its use in optical immunosensing, Analytical Chemistry 67 (1995) 1613-1616.
24. B. Lu, N. Yie, C.L. Lu, Y. Wei, Characterization of modified staphylococcal protein A containing phospholipid monolayer on both solution and slide surfaces, Biochemical and Biophysical Research Communications 200 (1994) 1463-1469.
25. http://www1.gelifesciences.com/aptrix/upp00919.nsf/Content/AC7760572A5CE500C125702800083FED/$file/11003558AA.pdf
26. C. Stoscheck, Quantification of Protein, Methods in Enzymology 182 (1990) 50-68.
27. O.H. Lowry, N.J. Rosebrough, A.L. Farr, R.J. Randall, Protein measurement with the Folin phenol reagent, Journal of Biological Chemistry 193 (1951) 265-275.
28. P.K. Smith, R.I. Krohn, G.T. Hermanson, A.K. Mallia, F.H. Gartner, M.D. Provenzano, E.K. Fujimoto, N.M. Goeke, B.J. Olsen, D.C. Klenk, Measurement of protein using bicinchoninic acid, Analytical Biochemistry 150 (1) (1985) 76-85.

29. M.M. Bradford, A rapid and sensitive method for the quantification of microgram quantities of protein utilizing the principle of protein-dye binding, Analytical Biochemistry 72 (1976) 248-254.
30. F.V. Bright, A.T. Betts, K.S. Litwiler, Regenerable fiber-optic-based immunosensor Analytical Chemistry 62 (1990) 1065-1069.
31. S.T. Pathirana, J. Barbaree, B.A. Chin, M.G. Hartell, W.C. Neely, V. Vodyanoy, Rapid and sensitive biosensor for *Salmonella*, Biosensors and Bioelectronics 15 (2000) 135-141.
32. R.A. Williams, H.W. Blanch, Covalent immobilization of protein monolayers for biosensors applications, Biosensors and Bioelectronics 9 (2) (1994) 159-167.
33. I. Moser, T. Schalkhammer, E. Mann-Buxbaum, G. Hawa, M. Rakohl, G. Urban, F. Pittner, Advance immobilization and protein techniques on thin film biosensors, Sensors and Actuators B: Chemical 7(1992) 356-362.
34. Y. Dong, C. Shannon, Heterogeneous immunosensing using antigen and antibody monolayers on gold surface with electrochemical and scanning probe detection, Analytical Chemistry 72 (2000) 2371-2376.

CHAPTER 7

ANTIBODY-IMMOBILIZED MAGNETOSTRICTIVE BIOSENSORS – BLOCKING NONSPECIFIC ADSORPTION

Nonspecific adsorption of antigen/antibody on to the solid surface is one of the most important issues for sensors in biological application. Biosensors, as fast detection methods, were widely developed in food safety, industrial application, environmental monitoring, clinical diagnostics, and public health. As we know, the mass sensitivity is an important parameter to evaluate the performance of biosensors. However, undesirable nonspecific binding may be minimized the specificity and sensitivity of biosensors by given error signals. The major work in this chapter is to evaluate the effectiveness of several common blocking agents against the nonspecific adsorption of *Staphylococcus aureus* on the gold surface of magnetostrictive biosensors using microscopic analysis (SEM) and ELISA (Enzyme-linked Immunosorbent Assay). The results showed that gelatin, bovine serum albumin (BSA), casein, nonfat dry milk, tween 20 and nonfat dry milk/tween 20 exhibited different abilities to resist the nonspecific binding. Casein and nonfat milk provided the better blocking abilities than other blocking agents used in this study. The best concentrations of casein and nonfat dry milk to block the nonspecific adsorption of *S. aureus* on gold surface were both 5 wt. % in this study. Gelatin and tween 20 may not be used as blocking agent in this study.

7.1 Introduction

Biosensors were widely used to detect all kinds of bacteria/antigen in real-time manner due to fast response, reliability, stability, high sensitivity and specificity in the last decades [1-3]. However, the nonspecific binding extensively lowered the specificity, and reliability of biosensor. Thus, it is necessary to efficient reduction of nonspecific absorption to develop biosensors and medical application. Blocking agents should stick strongly to the surface of sensor platform to resist the exchange reactions and not interfere with the further reactions such as the interaction of the antibody and antigen. Blocking agent is used to block possible excess solid surface after coating with one immuno-reactant to avoid unspecific adsorption of succeeding reactants. However, up to now, the detailed study on blocking the gold coated biosensor was not found in pervious literatures, although the applications of BSA [4-5], casein [6], and milk [7] on gold-coated biosensors have been studied. And the reported blocking performances were also different. Liu et al. [6] reported casein is more effective to block the nonspecific binding than BSA and myoglobin. Yakes et al. [8] reported the blocking agents of BSA, dry milk, and casein show low blocking ability because of their low surface tension. Thus, it is necessary to study the blocking performance of natural blocking agents on gold surface of biosensor.

In this paper, the blocking agents including BSA, casein, nonfat dry milk, gelatin, tween 20, and nonfat dry milk/tween 20 were chosen to prevent nonspecific binding of *Staphylococcus aureus* on the gold surface of magnetostrictive biosensors. These chemicals were selected because they commonly use as blocking agents in immunochemistry applications. Typically, the blocking agents were used at the concentrations of 1 to 5 wt. % in PBS buffer and the sensors were immersed into the blocking solutions for one hour. *S. aureus* used in this study was selected as the

targeted bacterium because of its pathogenic nature and its small size (~1μm in diameter). Furthermore, *S. aureus* possesses many adhesion proteins on its surface, but it is not known how they interact with each other to form stable interactions with the substrate [9]. To evaluate the resistance of nonspecific binding of *S. aureus* on gold surface, the magnetostrictive biosensors were used in this experiment. Magnetostrictive biosensors were developed and exhibited high potential applications in biological detection [10], environmental monitoring [11], and medical analysis [12] etc. The high sensitivity and fast response of gold-coated magnetostrictive biosensor have been demonstrated in real-time detection of foodborne pathogens such as *S. typhimurium* [10, 13] and biological threat agents (e.g. *B. anthracis* spores) [14-15].

The major protocol, the performance evaluation of blocking nonspecific binding is based on the immunoassay method, e.g. enzyme-linked immunosorbent assay (ELISA), using the microtiter plates [16-17]. However, for biosensors, it would produce some error signal from sensor itself, which lead to the inaccuracy of protocol. In this paper, we employ a new method, microscopic analysis of the number of the bacterial cells and its distribution based on Scanning Electron Microscopy (SEM), to evaluate the ability of blocking agents to prevent the nonspecific adsorption of *S. aureus* on the gold-coated biosensor.

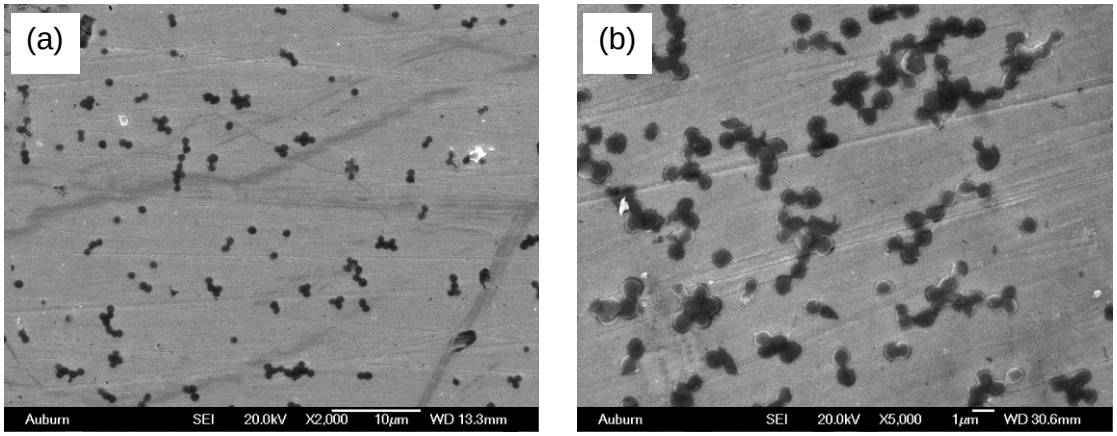

Figure 7-1. The typical SEM images of the reference magnetostrictive biosensors with different magnification of (a) x2000, and (b) x5000. The reference biosensors were absent of antibody immobilization and nonspecific blocking. The biosensors were exposed to the 5 x 10^8 cfu/ml of *S. aureus* culture for one hour.

7.2 Materials and methods

7.2.1 Sensor platform-Magnetostrictive particle

The fabrication of magnetostrictive biosensors used here was reported by a lot of literatures [10, 18]. Magnetostrictive biosensor is made of Metglas™ 2826 ribbon (Iron Nickel-based)obtained from Metglas®, Inc. (Conway, SC), which is an amorphous magnetostrictive alloy with low cost, large magnetostriction (12ppm) and high magnetostrictive coupling effect [19]. The ribbon was firstly polished down to 15 μm in thickness by #2000 polish paper for sensor's application. Sensor with the size of 2.0 x 2.0 x 0.015 mm was diced from the polished ribbon by microdicing saw. The surface of the sensor was ultrasonically cleaned by acetone for 30 minutes and dried in nitrogen. Then, the gold layer in thickness of 100 nm is employed to prevent the corrosion of the sensor and to promote the immobilization of the bio-recognition element. Prior to the gold deposition, a thin layer of chromium with a thickness of about 100 nm was sputtered on the sensor as the adhesion layer by Denton Sputtering System. Now the fresh gold-coated magnetostrictive sensor is ready for use.

7.2.2 Microorganisms

Purified rabbit anti - *S. aureus* polyclonal antibody were obtained from Accurate Chemical & Scientific Corporation (Westbury, NY 11590). The product number is YVS6881. The antigen *S. aureus* was provided by Department of Nutrition and Food Science at Auburn University, which was grown in Bacto^{TM} Tryptic Soy Broth (BD, 211825) at 37^{o}C overnight. *S. aureus* culture was washed 4 times using DI water by centrifuge with the speed of 8500 rpm for 3 minutes. Finally the bacteria sample was prepared by diluting the *S. aureus* culture into DI water.

7.2.3 Reagents

Round bottomed 96-well plates were used in all experiments. The blocking of nonspecific binding on pure gold surface was demonstrated using bovine serum albumin (BSA) (Equitech-Bio, Inc. BAH64-557), casein (Fisher Scientific, AC27607-1000), gelatin (Fisher Scientific, G8-500), nonfat dry milk (Walmart), tween 20 (Fisher Scientific, BP337-100), nonfat dry milk/tween 20. All the blocking agents were diluted by phosphate buffered saline (PBS, 0.01M, pH=7.4, Sigma, P3813) to prepare the various concentrations which were listed in Table 7-1. Casein is slightly soluble into PBS. To dissolve casein, 0.1 M NaOH was used to titrate to pH 7.0 with stirring. The performance of each agent to block nonspecific binding on gold surface of magnetostrictive biosensor was measured over a range of three different concentrations. For BSA, casein, and nonfat dry milk, 1.0, 2.0 and 5.0 wt. %, for gelatin, 0.1, 0.5 and 1.0 wt. %, and for tween 20, 0.05, 0.1, and 0.2 wt. % were used in this experiment. The combination of nonfat dry milk with tween 20 of 0.2 wt. % were also assayed for three different concentrations of 1.0, 2.0 and 5.0 wt. %.

Table 7-1. The blocking agents and its concentrations were used in this experiment.

Blocking agents	**Concentration (wt. %)**
Nonfat dry milk	1.0% 3.0% 5.0%
Nonfat dry milk /Tween 20 0.2%	1.0% 3.0% 5.0%
Tween 20	0.05% 0.1% 0.2%
BSA (Bovine Serum Albumin)	1.0% 3.0% 5.0%
Casein	1.0% 3.0% 5.0%
Gelatin (Porcine)	0.1% 0.5% 1.0%

7.2.4 Protocol for evaluating the ability of blocking agents

Microscopic analysis (SEM) of the distribution and number of bacteria on the gold surface of magnetostrictive biosensor were employed to evaluate the ability of blocking of nonspecific binding. Microlon microtiter plates, which contain 96 round-well (row x common: 8 x 12) were used in this research. To suppress the adsorption of antibody or antigen on the plate well, firstly 1 wt % BSA was coated on each well for 1 hour, as shown in Figure 7-2. Enzyme linked immunosorbent assay (ELISA) was used to double check the performance of blocking agents.

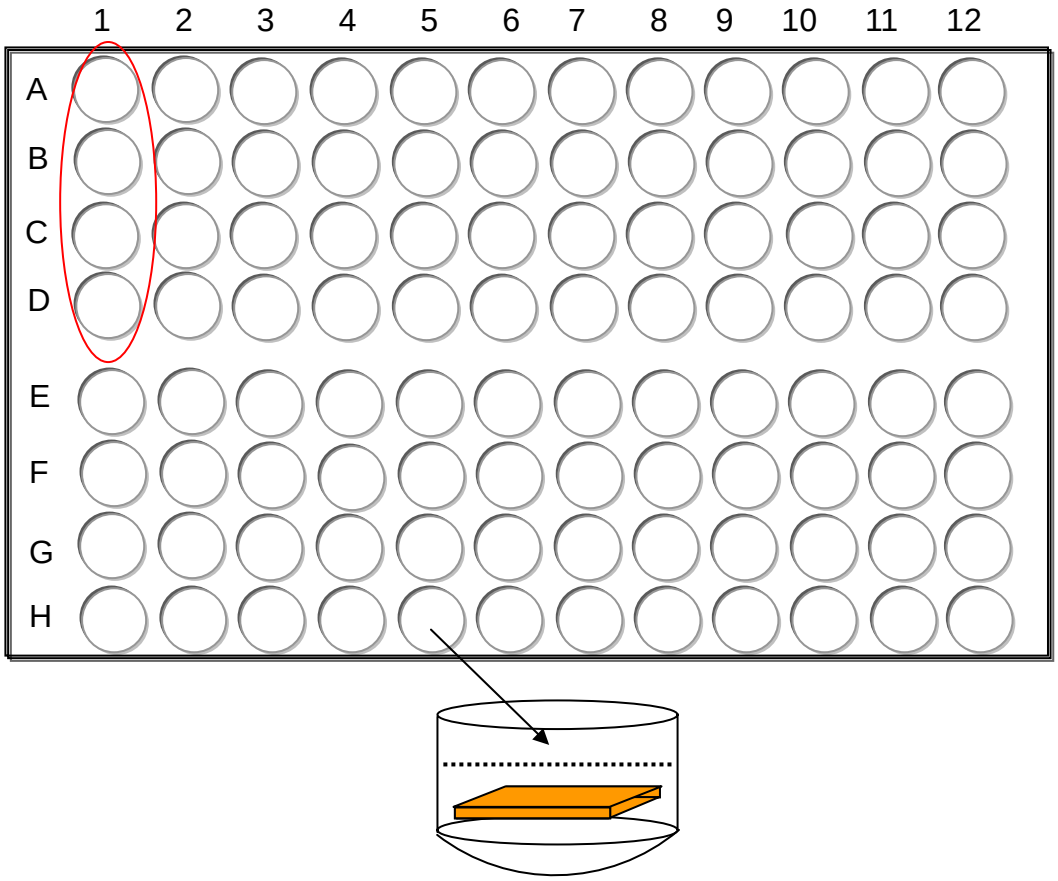

Figure 7-2. The schematic of microtiter plate (12 Columns x 8 Rows) and sensor in each well.

7.2.4.1 Microscopic analysis

The procedure of this protocol was illustrated in Figure 7-3. Figure 7-3(a) and Figure 7-3(b) represent the biosensors coated without antibody and with antibody respectively. In Figure 7-3(a), firstly the biosensors (the down side was marked) were put into the blocked plate by blocking agent, and the six blocking agents with three concentrations with the volume of 200 µl were added into the plate wells consequently. Each concentration was repeated 4 times (e.g. half column of A1-D1, or E1-H1 for convenience). Each sensor was incubated for 1 hour at room temperature. Meanwhile, one half column with 4 wells was incubated only with PBS buffer to characterize the nonspecific binding in the absence of blocking agent. After that, *S.*

aureus with the concentration of 5 x 10^8 cfu/ml was added into each well at room temperature incubating for 1 hour. Each sensor was rinsed 3 times by DI water after incubation steps. Finally, to observe the sensor surface by using SEM, the sample was exposed to OsO_4 vapor for one hour. The SEM observation of *S. aureus* on the gold surface of magnetostrictive sensor was performed using a JEOL-7000F SEM operated at 20 keV. For each sensor, five pictures were taken from the fixed positions of the sensor surface as shown in Figure 7-3(c) (①, ②, ③, ④, and ⑤). Compare to Figure 7-3(a), Figure 7-3(b) has one more step than that in Figure 7-1(a), that is, before coated blocking agents on the sensor surface, the sensors were incubated in antibody solution with the concentration of 50 μg/ml at room temperature for 2 hours. The volume of antibody in each well is 200 μl.

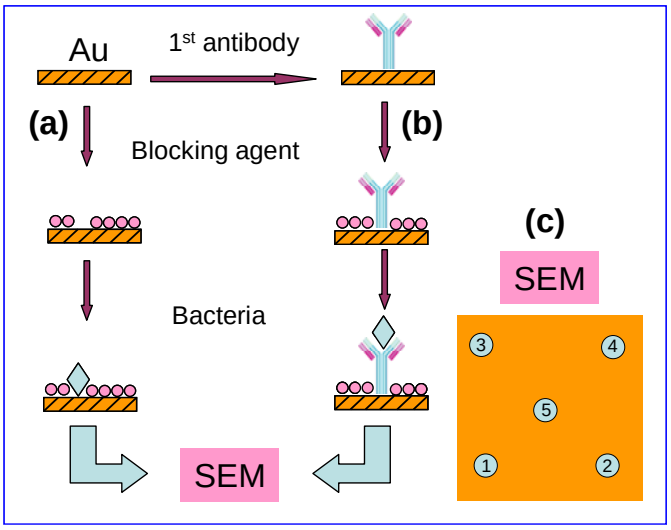

Figure 7-3. Schematic of the experiment design for evaluating the effectiveness of the blocking agents on the nonspecific adsorption in microscopic analysis without antibody (a) and with antibody (b).The symbols ①, ②, ③, ④, and ⑤ in the SEM images mean that these five regions (c) were taken SEM images in this experiment.

7.2.4.2 ELISA

The procedure was illustrated in Figure 7-4. The experiment design is the

same as in Section 2.4.1. The difference is that, instead of *S. aureus*, an alkaline phosphatase enzyme conjugated secondary antibody specific to rabbit IgG was accordingly added to the plate wells for 1 hour at room temperature. Each well was washed 3 times using DI water at the end of each incubation step. Finally, the chromogenic substrate (*p*-NPP, *p*-nitrophenyl phosphate) was added into each well at room temperature for color development and the absorbance was measured at $O.D._{405nm}$ using MultiSkan Ascent plate reader (Thermo Labsystems). To measure the absorbance accurately, the magnetostrictive sensors were removed from the plate wells after development 15 minutes. The blocking effectiveness should be reversal proportional to the color intensity.

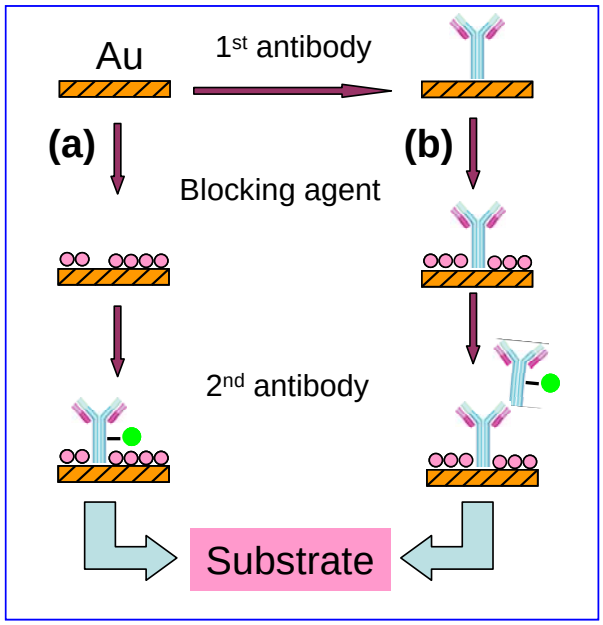

Figure 7-4. Schematic of the experiment design for evaluating the effectiveness of the blocking agents on the nonspecific adsorption in ELISA test without antibody (a) and with antibody (b).

7.2.5 Real time bacteria binding measurement

7.2.5.1 MSP sensor fabrication

Metglas alloy 2826MB ribbon was employed as the sensor platform. Firstly

the Metglas 2826MB thin film was polished to 15 μm in thickness. Then the polished thin film was cut into strips/rectangulars in the exact size of 1.0 mm x 0.3 mm by dicing saw. To remove the grease, the strips were cleaned in acetone by using ultrasonic cleaner for 30 min and dried in air. Followed, a chromium layer at the thickness of 100nm and a gold layer (125 nm in thickness) serially were deposited on the clean strips by using Denton sputtering system. The chromium layer was employed to enhance the adhesion between the gold layer and the sensor and resist corrosion. The gold layer provided a surface to immobilize the biomolecular recognition elements. Finally these particles were annealed at 220°C for 2 hours. These magnetostrictive particles (MSPs) are ready for antibody immobilization and bacterial testing.

7.2.5.2 Theory and principle

The strip-like MSP longitudinally vibrates under an external AC magnetic field. When the natural frequency of the particle is the same as that of the applied magnetic field, it reaches a resonance frequency (f_r) which is expressed as [20]

$$f_n = \frac{n}{2L}\sqrt{\frac{E}{\rho\left(1-\sigma^2\right)}} \qquad \text{n=1, 2, 3…} \qquad (7\text{-}1)$$

where f_n, and L are the n^{th} resonance frequency, and the length of the MSP sensor, E, σ, and ρ represent Young's modulus, Poisson's ratio, and the effective density of the sensor material.

For MSP sensor, the mass load on the sensor results in a shift in a resonance frequency of MSP sensor as shown in Figure 7-5. If an additional mass (*Δm)* is uniformly loaded on the sensor surface, the shift in the resonance frequency is given as [21]

$$\Delta f = -\frac{f_0}{2}\frac{\Delta m}{M} \qquad (7\text{-}2)$$

where f_0 is the fundamental resonance frequency of the MSP sensor, M, and Δm are the effective mass of the MSP sensor, and the additional mass load on sensor surface.

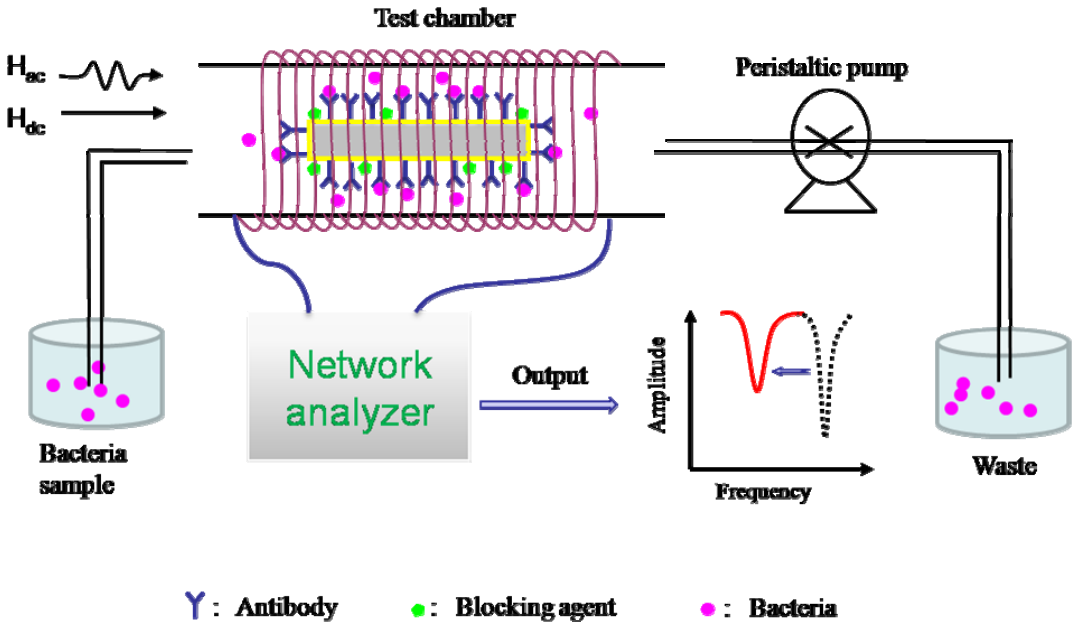

Figure 7-5. The schematic of measurement set-up and operation principle.

7.2.5.3 Measurement set-up

The set-up for the real time bacteria binding measurement was given in Figure 7-5. As shown in Figure 7-5, the set-up includes a test chamber, a permanent magnet, a peristaltic pump, and two reservoirs: one for bacteria sample and the other for bacteria waste. A test chamber was wounded by a magnetic copper wire which serve as the driving coil (ac magnetic field) and pick-up coil, and a permanent magnet provided DC magnetic field. The resonance frequency spectrum of the MSP sensor was measured by using an HP network analyzer 8751A with an S-parameter test set. The detail set-up based on network analyzer was given in Li's Ph.D. dissertation [22]. The network analyzer applied a RF signal sweeping over a certain frequency range to the driving coil and the driving coil would generate an AC magnetic field. The dimension is changed and the sensor mainly vibrates along the length dimension

while an ac magnetic field is applied. The permanent magnet as the source of DC magnetic bias was placed vertically to the test chamber so that the magnetic field direction is along the length direction of the sensor. In order to get an optimized signal, the DC magnetic field was adjusted by changing the distance between the test chamber and the magnet. Due to the magnetic effect, the sensor oscillating would generate a magnetic signal which can be received by pick-up coil. To eliminate the background from the instrument, the analyzer was calibrated to zero base-line by adjusting the intrinsic reflection signal of the coil to zero before the MSP was put into the test chamber. Therefore, the recording signal would only reflect the oscillating amplitude signal from the MSP. A personal computer was used to monitor and record resonance frequency. The experimental data analysis, calculations and graphs were all obtained by using OriginPro 7.0 (OriginLab Corporation, MA, USA) software.

7.2.5.4 Antibody immobilization

Purified rabbit anti - *S. aureus* polyclonal antibody (4.5mg/ml) was obtained from Accurate Chemical & Scientific Corp. (Westbury, NY 11590). The product number is YVS6881. Traut's Reagent (2-iminothiolane • HCl, Pierce, 26101) was used to introduce the sulfhydryl group of antibody, and Traut's Reagent was dissolved into the ultrapure water to obtain 2 mg/ml stock solution (14mM). The polyclonal antibody with the volume of 0.25 ml was dissolved into 0.25 ml PBS buffer (Sigma, P3813, 0.01M, pH=8.0, 3mM EDTA). For thiolation, a 20-fold molar excess of Traut's Reagent stocking solution (10.7 μl) was added into the antibody solution and this mixture was incubated for 1 hour at room temperature. Extra Traut's Reagent was immediately removed to form the concentrated antibody solution by using Centricon YM-30 (Millipore, 10,000 MWCO, Cat. # 4205), and the concentrated antibody solution was diluted with PBS (0.01 M, pH=7.4) to form 50 μg/ml solution. The

introduced sulfhydryl groups were determined by using Ellman's reagent (Pierce, 22582). Each anti IgG molecule can be modified with 3-5 sulfhydryls. The MSP sensor was immediately added into the thiolated polyclonal antibody for 2 hours at room temperature. After immobilization, the MSP sensor was rinsed with DI water for 3 times. Now the MSP sensor is ready for detecting *S. aureus*.

7.2.5.5 Real time measurement

The *S. aureus* suspension was serially diluted by using DI water for preparing the test bacterial solution with the concentration ranging from 5×10^1 to 5×10^8 cfu/ml. All the test solutions were prepared at the same day for biosensor detection and stored at 4 °C. The sensor was put into the test chamber as shown in Figure 7-1. In order to detect *S. aureus* by direct assay, the water and the above eight concentrations of *S. aureus* suspensions were serially passed over the prepared sensor at a flow rate of 30 μl/min for 20 minutes. The characteristic frequency was monitored and recorded with 30-second intervals.

7.3 Results and discussion

7.3.1 Blocking efficiency of nonspecific binding from SEM analysis

A variety of blocking agents ranging from BSA or milk to purified proteins such as casein have been used to block nonspecific binding sites on the solid surface of biosensors. The ideal blocking agent can bind to all nonspecific sites, eliminating background altogether without changing the epitope for antibody binding. BSA is commonly used as a blocking agent to block nonspecific binding in ELISA assays, Western blot, immunohistochemistry and biosensors since it is low cost, and most importantly has a large hydrophobic pocket which can bind to nonspecific sites. To verify this result, we use BSA to block several antigens including *Salmonella typhimurmium*, *Staphylococcus aureus* and *Escherichia coli* on gold surface of

magnetostrictive biosensor, and it works well when the targeted antigens are *E. coli* and *S. typhimurium* (results not shown). However, when the targeted antigen is *S. aureus*, the nonspecific binding is very severe on gold surface even blocked with BSA (see Figure 7-6 (a) and (b)). The reason for this is probably *S. aureus* has smaller size than other two antigens and BSA has a relatively large molecular size. Thus, five more molecules and combinations of molecules were investigated as blocking agents, gelatin, casein, nonfat dry milk, tween 20 and nonfat dry milk/tween 20 to prevent the nonspecific binding of *S. aureus* on magnetostrictive biosensor and the results were shown in Figure 7-7 (a). We can find two blocking agents, casein and nonfat dry milk work much better than BSA. Especially for casein, when the concentration is up to 3 wt. %, compare to control sample (devoid of blocking agent) (shown in Figure 7-7 (a)), it can block up to 90% nonspecific binding of *S. aureus* on gold surface. Nonfat dry milk also exhibited the ability to block close to 85% the nonspecific binding while the concentration is up to 5 wt.%. BSA is better than tween 20 and gelatin. But the efficiency of nonspecific binding is not obvious.

Figure 7-7 (b) shows the ability of each blocking agent to prevent the nonspecific binding of *S. aureus* on gold surface of magnetostrictive biosensor. Signal to noise ratio (SNR) as another most important parameter was used to evaluate the efficiency of blocking agent. Signal to noise ratio in this study is the bacterial number measured as the signal obtained with a sensor immobilized with antibody as compared to that obtained with a sensor devoid of antibody treated with various blocking agents. Adequate concentration for each blocking agent is required since inadequate concentration would lead to excessive background binding and a reduced signal to noise ratio. Of course, excess blocking agent would prevent the antibody/antigen interaction and still result in a reduced signal to noise ratio. For each blocking agent,

the adequate concentration shown in Figure 7-7 (b) is different. For BSA, 3% is the best concentration, while 5% is for casein and nonfat dry milk, and tween 20 is 0.02%. Casein with 5% took superior advantage over other blocking agents in blocking the nonspecific binding of *S. aureus* on gold surface and the SEM images were shown in Figure 7-6 (c) and (d). Next is nonfat dry milk, and the worst is gelatin, which are consistent with the results obtained from Figure 7-7 (a). Compare to casein, BSA contain relatively large molecular weight components so that random closepacking of these molecules leaves bare batches of unblocked Au surface to which antigen can bind, leading to higher background characteristics of the blocking agent (MW ~ 60-70kDa). Casein appears to be an effective blocking agent due to its content of small protein species (MW ~ 20-30kDa).

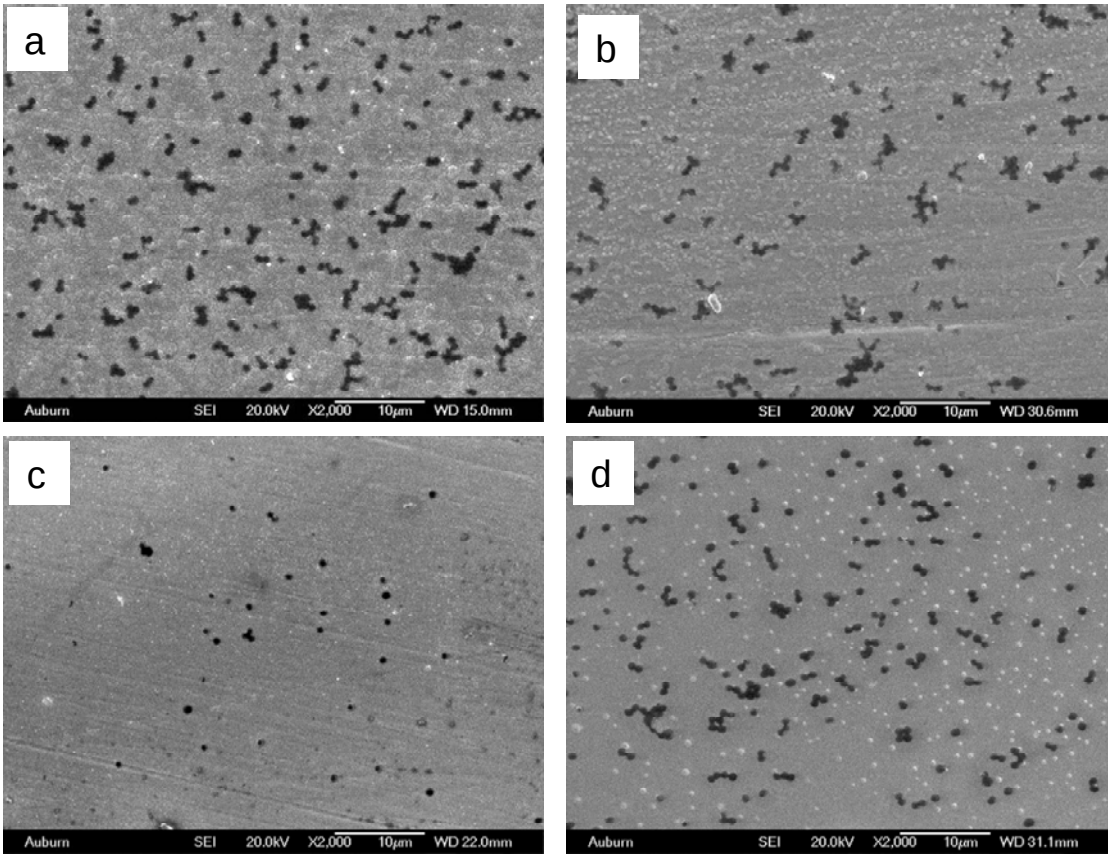

Figure 7-6. SEM images of bacterial adsorption on magnetostrictive biosensors. Negative control (devoid of antibody immobilization): (a) *S. aureus* adsorption directly to non-blocking gold surface, (b) 5% BSA blocking surface, (c) 5% casein blocking surface. (d) Antibody-immobilized biosensor: *S. aureus* adsorption to 5% casein blocking surface.

Tween 20 is a nonionic detergent used to wash loose/unspecific bound reactants (e.g. antibody, antigen and other molecules). It may also be used for blocking possible excess solid surface after coating with one reactant (e.g. antibody) to avoid nonspecific immobilization of subsequent reactants (e.g. antigen). Batterger et.al [23] reported tween 20 exhibited higher performance as a blocking agent to block the nonspecific binding sites on nitrocellulose membranes than other protein. However, in this study, just like gelatin (shown in Figure 7-7 (a)), it is one of the least effective blocking agents: it did not reduce nonspecific binding more than 60% even

at its highest concentration (0.2 wt. %), its blocking ability fell rapidly with dilution; and it was almost useless as a blocking agent. But in Figure 7-7 (b), for tween 20 0.02%, signal to noise ratio (SNR) is relatively high like nonfat dry milk. The results seem conflict. The reason is, just like Bird et al. reported, that tween 20 used as blocking agent alone in immunoblotting would cause artifactual results by nonspecific antigen/antibody reaction [24]. One of the possible solutions is using tween 20 together with other molecules, e.g. nonfat dry milk. The nonspecific binding shown in Figure 7-7 (a) was suppressed using nonfat dry milk/tween 20. However, Figure 7-7 (b) listed opposite results for tween 20 and nonfat dry milk/tween 20. One reason, as mentioned above, is tween 20 produced wrong signals. The other one, as Esser [25] described, came from the competition of nonfat dry milk and tween 20 resulted in the counteraction each other which also can be illustrated by the decreasing trend of blocking efficiency in Figure 7-7 (b) for nonfat dry milk/tween 20.

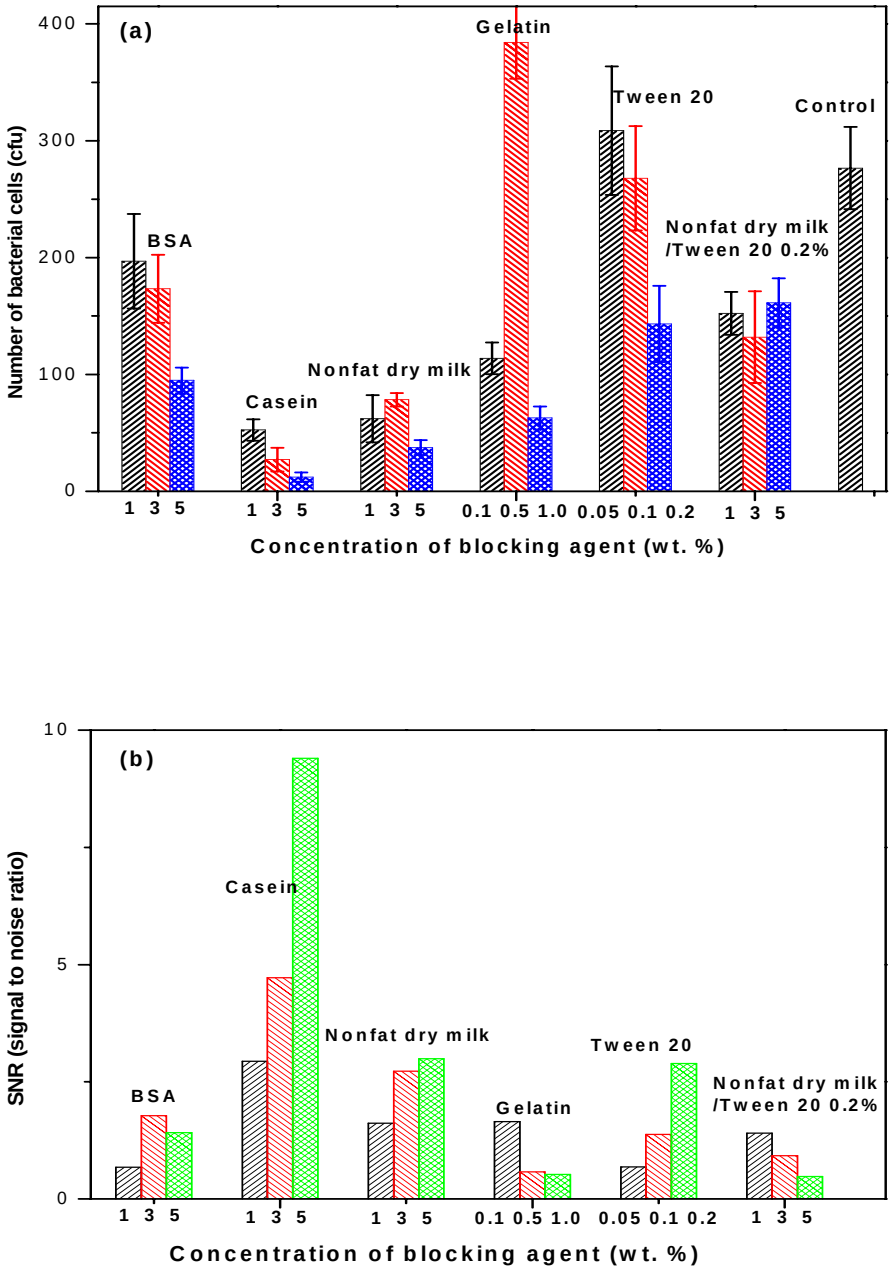

Figure 7-7. Efficiency of six blocking agents with three different concentrations evaluated by SEM. (a). Number of bacterial cells means the average number adsorbed on various surfaces in a 48 μm x 60 μm (2880 μm^2) area of magnetostrictive sensor treated only with blocking agent (devoid of antibody). Each sensor was taken five pictures. Each blocking agent with various concentrations was repeated 4 times. Control means the sensor devoid of blocking agent.

(b). SNR means the average number of bacterial cells obtained from the sensor treated with antibody as compared to that obtained with sensor treated without antibody under different blocking agents with its concentration. Each blocking was done on 4 sensors, and each sensor was taken 5 pictures in the area of 48 μm x 60 μm (2880 μm^2) of the biosensor.

7.3.2 Blocking efficiency of nonspecific binding from ELISA test

The results from the ELISA test were given in Figure 7-8. As we know, the absorbance reflects the number of secondary antibody/primary antibody absorbance on the sensor surface. In Figure 7-8 (a), the absorbance represented the 2^{nd} antibody sticking on the blocked sensor's surface. We can find casein, nonfat dry milk and nonfat dry milk/tween 20 exhibited the similar blocking ability. And these three blocking agents possessed the better blocking ability than these other three including BSA, tween 20 and gelatin.

In Figure 7-8 (b), the absorbance represented the specific absorption and nonspecific absorption of 2^{nd} antibody. Since the nonspecific blocking ability for casein, nonfat dry milk and nonfat dry milk/tween 20 were similar as shown in Figure 7-7 (a), the performance of nonfat dry milk/tween 20 is better than that of casein and nonfat dry milk in immunoassay application as shown in Figure 7-9.

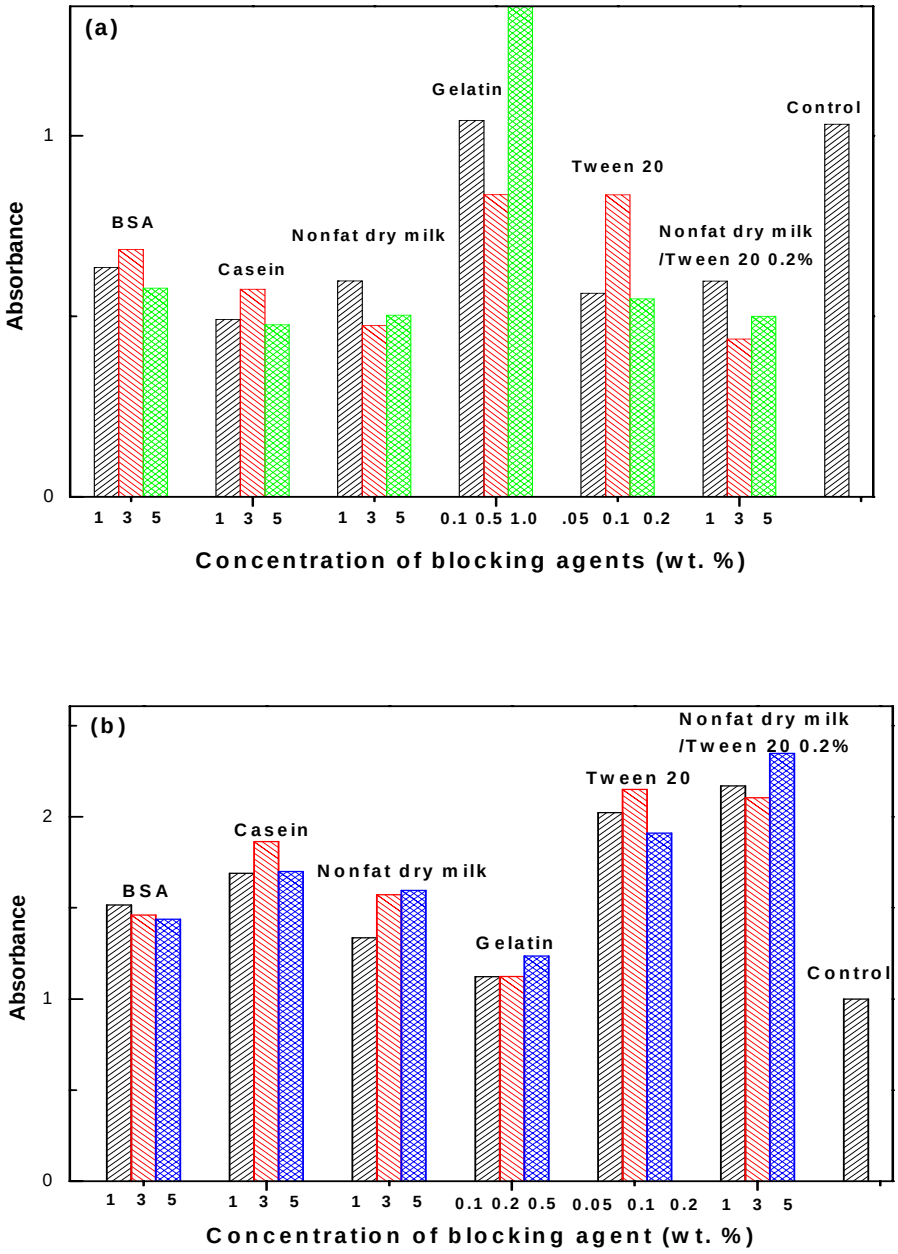

Figure 7-8. The absorbances ($O.D._{405}$) in ELISA for the magnetostrictive biosensor immobilized without antibody (a) and with antibody (b). Each data were the average values of 5 samples. The concentration of each blocking agent was listed in the X-axis.

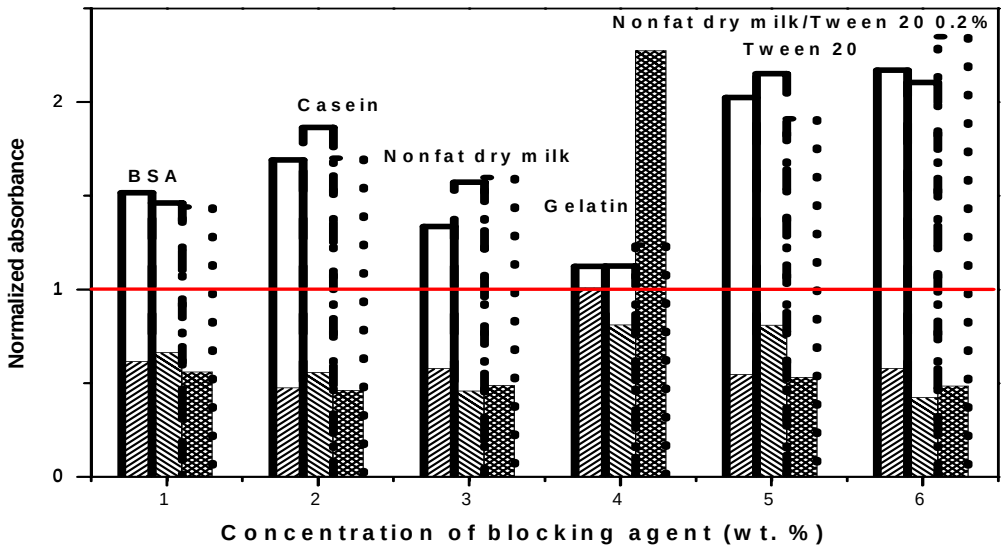

Figure 7-9. The result was combined the absorbance from the sensor treated with antibody and without antibody in ELISA test. The solid column represents the absorbance obtained from the sensor devoid of antibody immobilization. The blank columns represent the absorbance obtained from the antibody-coated sensors.

Six blocking agents exhibited various abilities to block the nonspecific binding of *S. aureus* on gold-coated magnetostrictive biosensor. Some blocking agents (e.g. casein) seem to block non-specific binding to solid sites on biosensor, primarily through protein-surface interactions, while others (e.g. gelatin) block primarily through protein-protein interactions. Moreover, some blocking agents have intrinsic antigenic properties and participate directly in antibody-antigen interactions, sharing parts of the epitope.

In conclusion, the blocking abilities of these blocking agents to bacteria/antigens (e.g. *S. aureus*) and to 2nd antibody were a little bit different. To *S. aureus*, the best are casein and nonfat dry milk. To 2nd antibody, the best are nonfat dry milk/tween 20, and casein. Thus, casein would be selected as the blocking agent

in the sensor's application.

7.3.3 Dose response of reference sensors

To further confirm the performance of casein as the blocking agent, the dose response of the reference MSP sensors treated with 5 wt% casein was conducted and the results were given in Figure 7-10 (a). The reference sensor was the sensor without antibody immobilization, and the size was 1.0 x 0.3 x 0.015 mm. Clearly, compare to the reference sensor without blocking, the nonspecific binding for the reference sensor with casein blocking is decreased in a large scale as shown in Figure 7-10 (a). For example, the resonance frequency shift reduced from 4200 Hz to1800 Hz while the reference sensor was exposed into the *S. aureus* suspension of 5×10^8 cfu/ml.

The dose response of the antibody immobilized MSP sensor while exposed into the various concentrations of *S. aureus* suspensions was also measured in this experiment. The dose response of the antibody-immobilized MSP sensor and the reference sensor both blocked with casein were shown in Figure 7-10 (b). The antibody immobilized MSP sensor exhibited much higher dose response than that of reference sensor. As shown in Figure 7-10 (b), the response curve exhibited a good linear relationship between 5×10^3 and 5×10^7 cfu/ml. The slope of the response curve in the linear region was defined as the sensitivity and its value is about 600 Hz ($R^2 = 0.998$). For the antibody-immobilized MSP sensor in size of 1.0 x 0.3 x 0.015 mm, the detection of limitation was 10^2 cfu/ml.

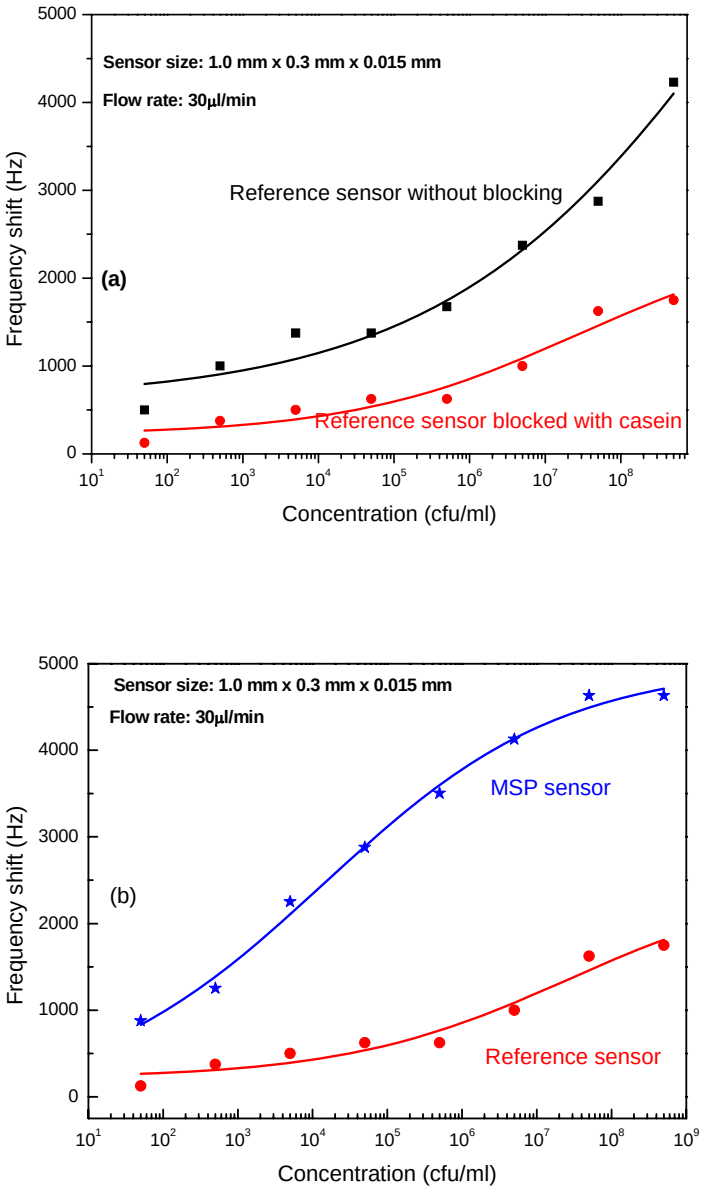

Figure 7-10. The dose response of (a) the reference sensor without and with casein blocking and (b) of the antibody-immobilized MSP sensor via dynamic system. The size of MSP sensor was 1.0 x 0.3 x 0.015 mm. The flow rate was 30 µl/min.

7.4 Conclusions

The sensitivity and specificity of magnetostrictive biosensor for detecting the antigen is strongly determined by the ability of the blocking agent to prevent the

nonspecific binding sites on its gold surface. In this study, the best results were obtained using casein or nonfat dry milk as the blocking agent to block the nonspecific binding of *S. aureus*. The results suggested that some proteins such as casein block nonspecific binding through protein-solid surface interactions while others such as gelatin prevent through protein-protein interactions. We found casein and nonfat dry milk provided the best results to block *S. aureus* on the gold surface of magnetostrictive biosensor. However, each biosensor with various solid surfaces requires the testing of different blocking agents to determine which blocking agent is the most effective prevention. No only one blocking agent is ideal for various biosensors with various solid surfaces to detect various antibody/antigen pair. It would be strongly suggested the interactions between blocking agent, the solid surface of biosensors and targeted antigen under investigation before detection or assay.

References

1. D. Ivnitski, I. Abdel-Hamid, P. Atanasov, E. Wilkins, Biosensors for detection of pathogenic bacteria, Biosensors & Bioelectronics 14 (1999) 599-624.
2. K. Lange, B.E. Rapp, M. Rapp, Surface acoustic wave biosensors: a review, Analytical and Bioanalytical Chemistry 391 (5) (2008) 1509-1519.
3. L.D. Mello, L.T. Kubota, Review of the use of biosensors as analytical tools in the food and drink industries, Food Chemistry 77 (2001) 237-256.
4. http://www.springerlink.com/content/a25484v2q3u8801q/fulltext.pdf
5. A.H. Schmid, S.E. Stanca, M.S. Thakur, K.R. Thampi, C.R. Suri, Site-directed antibody immobilization on gold substrate for surface Plasmon resonance sensors, Sensors and Actuators, B: Chemical 113 (1) (2006) 297-303.

6. L. Liu, J.G. Ghosh, J.I. Clark, S. Jiang, Studies of αB crystalline subunit dynamics by surface Plasmon resonance, Analytical Biochemistry 350 (2006) 186–195.
7. T. Akimoto, K. Ikebukuro, I. Karube, A surface Plasmon resonance probe with a novel integrated reference sensor surface, Biosensors and Bioelectronics 18 (12) (2003) 1447-1453.
8. B.J. Yakes, R.J. Lipert, J.P. Bannantine, M.D. Porter, Detection of mycobacterium avium subsp. Paratuberculosis by a sonicate immunoassay based on surface-enhanced Raman scattering, Clinical and Vaccine Immunology 15 (2) (2008) 227–234.
9. L.G. Harris, S.J. Foster, R.G. Richards, An introduction to *Staphylococcus aureus*, and techniques for identifying and quantifying *S. aureus* adhesions in relation to adhesion to biomaterials: review, European Cells and Materials 4 (2002) 39-60.
10. R. Guntupalli, J. Hu, R.S. Lakshmanan, T.S. Huang, J.M. Barbaree, B.A. Chin, A magnetoelastic resonance biosensor immobilized with polyclonal antibody for the detection of *Salmonella typhimurium*, Biosensors and Bioelectronics 22 (7) (2007) 1474-1479.
11. C.A. Grimes, K.G. Ong, K. Loiselle, P.G. Stoyanov, D. Kouzoudis, Y. Liu, C. Tong, F. Tefiku, Magnetostrictive sensors for remote query environmental monitoring, Smart Materials and Structures 8(5) (1999) (639-646).
12. G. Ong, X. Yang, K. Zeng, C.A. Grimes, Magnetoelastic sensors for biomedical monitoring, Sensor Letters 3(2) (2005) 108-116.

13. R.S. Lakshmanan, R. Guntupalli, J. Hu, D.-J. Kim, V.A. Petrenko, J.M. Barbaree and B.A. Chin, Phage immobilized magnetoelastic sensor for the detection of *Salmonella typhimurium*, J. Microbiol. Methods 71 (2007) 55–60.
14. M.L. Johnson, J. Wan, S. Huang, Z. Cheng, V.A. Petrenko, D.-J. Kim, I.-H. Chen, J.M. Barbaree, J.W. Hong and B.A. Chin, A wireless biosensor using microfabricated phage-interfaced magnetoelastic particles, Sens. Actuators A 144/1 (2008) 38–47.
15. J. Wan, M. Johnson, R. Guntupalli, V.A. Petrenko and B.A. Chin, Detection of *Bacillus anthracis* spores in liquid using phage-based magnetoelastic micro-resonators, Sens. Actuators B 127 (2007) 559-566.
16. R.F. Vogt, D.L. Phillips, L.O. Henderson, W. Whitfield, F.W. Spierto, Quantitative differences among various proteins as blocking agents for ELISA microtiter plates, J. Immunol. Methods 101 (1) (1987) 43-50.
17. M.A. Sentandreu, L. Aubry, F. Toldrá, A. Ouali, Blocking agents for ELISA quantification of compounds coming from bovine muscle crude extracts, Eur. Food Res. Technol. 224 (5) (2007) 623-628.
18. S. Huang, J. Hu, J. Wan, M.L. Johnson, H. Shu, B.A. Chin, The effect of annealing and gold deposition on the performance of magnetoelastic biosensors, Materials Science and Engineering C 28(3) (2008) 380-386.
19. http://www.metglas.com/downloads/2826mb.pdf
20. L.D. Landau, E.M. Lifshitz, Theory of elasticity, Pergamon Press 1986.
21. C.A. Grimes, C.S. Mungle, K. Zeng, M.K. Jain, W.R. Dreschel, M. Paulose, K.G. Ong, Wireless magnetoelastic resonance sensors: A critical review, Sensors 2 (2002) 294-313.

22. Li, S., 2007. PhD Dissertation: Development of Novel Acoustic Wave Biosensor Platform Based on Magnetostriction and Fabrication of Magnetostrictive Nanowires. Auburn University.
23. B. Batteiger, W.J. Newhall 5th, R.B. Jones, The use of tween 20 as a blocking agent in the immunological detection of proteins transferred to nitrocellulose membranes, J Immunol. Methods 55(3) (1982) 297-307.
24. C.R. Bird, A.J. Gearing, R. Thorpe, The use of tween 20 alone as a blocking agent for immunoblotting can cause artefactual results, J Immunol. Methods 106(2) (1988) 175-179.
25. P. Esser, Blocking agent and detergent in ELISA, Nunc Bulletin 9, 337-340.

CHAPTER 8

CONCLUSIONS AND FUTURE RECOMMENDATIONS

8.1 Conclusions

(1) The resonance behaviors of MSMCs in various viscous media were characterized. The influence of density and viscosity of viscous media on the frequency and Q value of MSMCs was studied. The frequencies of MSMCs in various liquid media are density dependent, and Q values of MSMCs are viscosity dependent. The optimal ratio of length-to-width is between 2-3 (close to 2).

(2) The fundamental study of MSMCs in air and reduced air was also conducted. The Q value of MSMCs in air and reduced air is pressure dependent and harmonic mode dependent. Higher pressure, lower Q value, and higher harmonic mode, higher Q value. It is also found that the viscous damping effect of MSMCs is negligible while compared to the intrinsic damping and support loss of the holder, which is the obvious difference from Si-based MCs.

(3) The phage-immobilized MSMCs as biosensors were demonstrated. The size effect of MSMCs on the sensor's performance was studied. The limit of detection is 10^5 cfu/ml for the MSMCs with the size of 2.8 x 1.0 x 0.035 mm, and 10^4 cfu/ml for the MSMCs with the size of 1.4 x 0.8 x 0.035 mm respectively in static system. It indicates that the mass sensitivity and limit of detection of MSMCs can be improved by using smaller size.

(4) Antibody was covalent immobilized on the magnetostrictive biosensor by using Traut's Reagent which can introduce sulfhydryls into antibody. It is found that 20-fold

molar excess of Traut's Reagent can thiolate antibody with 2-4 sulfhydryls.

(5) The blocking abilities of various blocking agents were studied to resist the nonspecific adsorption of *S. aureus* on the gold surface of magnetostrictive biosensors. Casein exhibits high performance to block the nonspecific adsorption of *S. aureus*. Furthermore, the mass sensitivity of magnetostrictive biosensors can be improved.

8.2 Future recommendations

(1) MSMC was demonstrated as a high performance sensor platform in this research. By considering the mass sensitivity and limit of detection we obtained, there is still large space to improve the sensor's performance. As the theoretical and experimental analysis of mass sensitivity, a smaller size of MSMC results in a higher mass sensitivity. Thus, it is possible to achieve high mass sensitivity for detecting small number bacteria/cells or even single cell by reducing the size of MSMC.

Table 8-1. The design of MSMC dimension using micro-fabrication technique.

Sample	Length mm	Width mm	Thickness μm
1	1.5	0.8	2/5/10
2	1.0	0.6	2/5/10
3	0.5	0.3	2/5/10
4	0.3	0.1	2/5/10

Also, according to Eq. (3-12), the resonance frequency of a cantilever is determined by the properties of the cantilever beam materials. However, the selection of other beam materials will influence the Q value and output signal strength of the MSMC device. Thus, it is much easier to reduce the dimension/size of the MSMC devices.

While the MSMC size is reduced, challenges arise in fabrication which requires new technique. As we know, microfabrication technique was popularly employed to fabricate the micro, or even nano-scale device. In the future work, microfabrication technique will be used to obtain the smaller MSMCs.

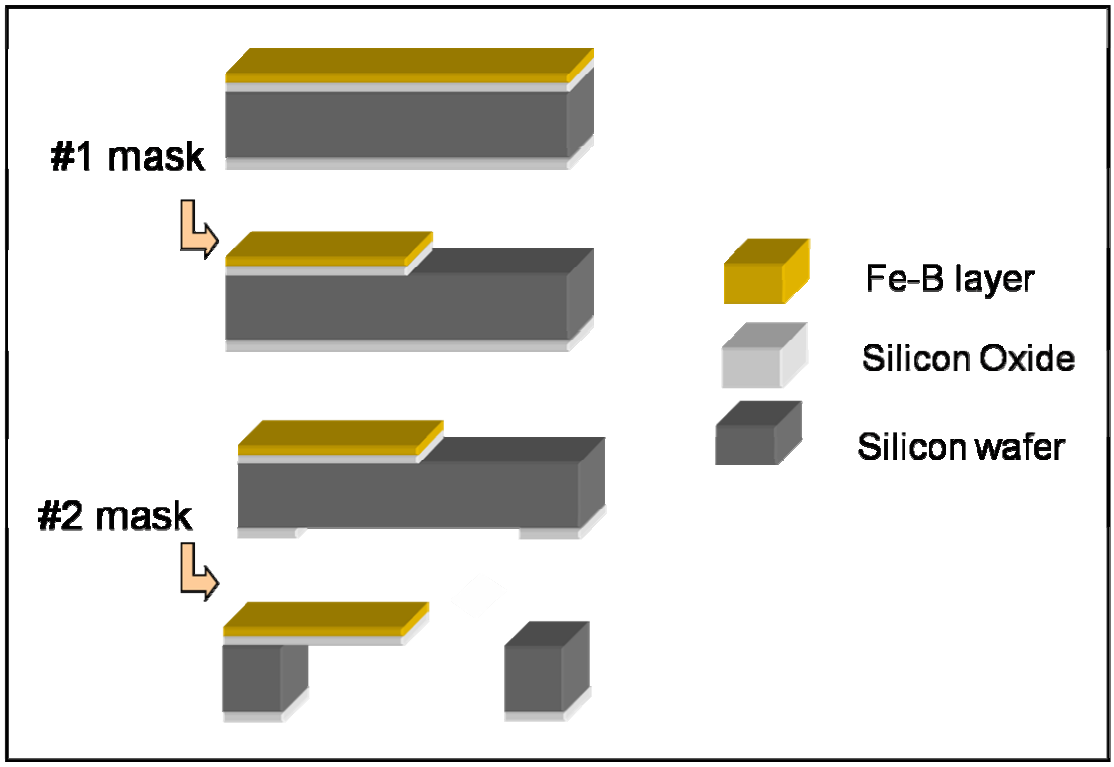

Figure 8-1. The microfabrication process of MSMC.

A possible microfabrication process of MSMCs is shown in Figure 8-1. To make MSMC sensors, amorphous Fe-B thin film would be deposited on the silicon wafer by using sputtering system. That is, the bilayer structure of MSMC, Metglas^{TM} 2826MB and copper thin film would be substituted by the amorphous Fe-B thin film and silicon wafer. A principle advantage of microfabrication technique is that MSMCs with different sizes can be obtained in a same batch. The possible size dimension of the MSMCs is given in Table 8-1. Furthermore, to match the microcantilever and increase the signal from the MSMCs, the pick-up coil will also be made by using the microfabrication technique and the schematic mask was given in Figure 8-2.

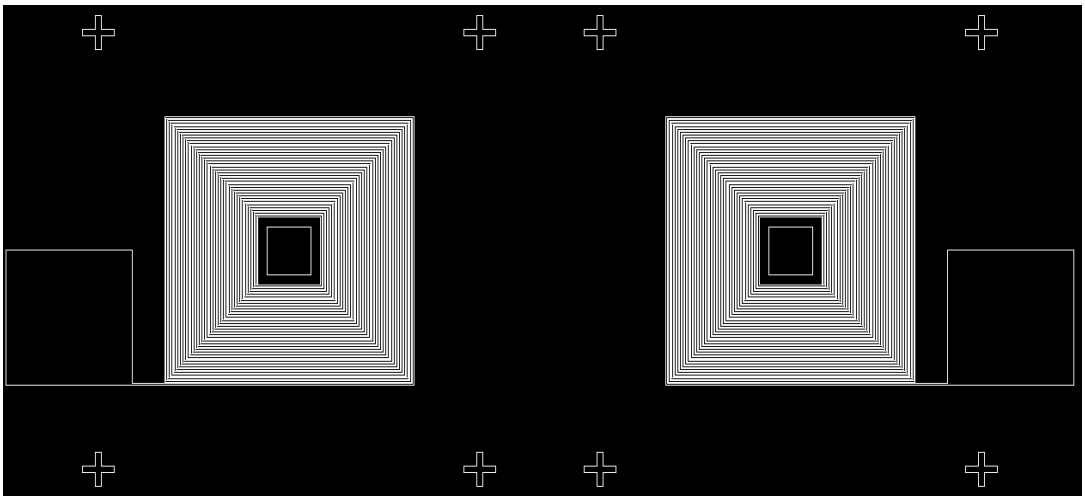

Figure 8-2. The schematic of the microfabricated pick-up coil.

By combining the microfabricated MSMC sensors and pick-up coil, we can reduce the dimension of sensor device, and the amount of bacteria sample in the dynamic system. This type of MSMC based biosensors for detection of *B. anthracis* spores or *S. typhimurium* will be demonstrated via dynamic system and the mass sensitivity and the limit of detection of MSMC biosensors might be improved.

(2) The antibody immobilization on the magnetostrictive sensor still can be improved due to the random orientation. Protein A/G，which can provide mediate orientation, might be introduced to improve the interface between the sensor surface and antibody. For the magnetostrictive sensors, the sensor surfaces coated with gold and polymers would be studied and compared. Polystyrene (PS) and Polymethyl methacrylate (PMMA) were selected to study Protein A/G interfaced magnetostrictive sensors. The preliminary results indicated that PS is better than PMMA for antibody immobilization through Protein A. Polyethyleneimine (PEI) and Poly (styrene/maleic anhydride) (PSMA) were selected to covalently bind antibody due to -NH_2 and –COOH respectively in the polymer structure.